Radio Wave Propagation Measurements and Modeling for Land Mobile Satellite Systems

Laure Mousselon

Thesis submitted to the Faculty of the
Virginia Polytechnic Institute and State University
in partial fulfillment of the requirements for the degree of

Master of Science
in
Electrical Engineering

Warren L. Stutzman, Chair
William A. Davis
Timothy Pratt

November 20, 2002
Blacksburg, Virginia

Keywords: LMSS, DARS, S-band, Propagation Model, Propagation Simulator, Rayleigh, Ricean, Lognormal, Shadowing, Cumulative Fade Distribution, Average Fade Duration, Level Crossing Rate, Measurements, Dual satellites

Radio Wave Propagation Measurements and Modeling for Land Mobile Satellite Systems

Laure Mousselon

(ABSTRACT)

The performance of a mobile satellite communications link is conditioned by the characteristics of the propagation path between a satellite and mobile users. The most important propagation effect in land mobile satellite system is roadside attenuation of the signals due to vegetation or urban structures. System designers should have the most reliable information about the statistics of the propagation channel to build reliable systems that can compensate for bad propagation conditions.

In 1998, the Virginia Tech Antenna Group developed a simulator, PROSIM, to simulate a propagation channel in the case of roadside tree attenuation in land mobile satellite systems. This thesis describes some improvements to PROSIM, and the adaptation and validation of PROSIM for Digital Audio Radio Satellite systems operating at S-band frequencies. The performance of the simulator for S-band frequencies was evaluated through a measurement campaign conducted with the XM Radio signals at 2.33 GHz in various propagation environments. Finally, additional results on dual satellite systems and fade correlation are described.

Acknowledgements

I would like to thank all the people who helped for finishing my thesis research. I would especially like to thank my advisor, Dr. Warren Stutzman, for his continuous supervision and his helpful suggestions. I would also like to thank the other members of my committee, Dr. Davis and Dr. Pratt for their sincere advice.

In addition, I would like to thank Dr. Seong-Youp Suh for letting me use the PROSIM simulator, R. Michael Barts for sharing his ideas and correcting my work, and the members of the Virginia Tech Antenna Group who worked on the XM Radio project for their contribution to my work. Also, I would like to thank the other VTAG members for their concern about my thesis, and the general work atmosphere in the group.

Finally, I would like to thank my family, and my friends in the United States and in France, for their continuous encouragement and support.

Table of Contents

Table of Figures

Chapter 1

Introduction

A Land Mobile Satellite System LMSS is a satellite-based communications system that provides voice and data communications to terrestrial mobile users. The first mobile satellite experiment program, called MSAT-X, was initiated by the National Aeronautics and Space Administration (NASA) in 1984 and was managed by the Jet Propulsion Laboratory (JPL). The goal of MSAT-X propagation research was to characterize the land mobile satellite channel between a satellite and a mobile user. The MSAT-X program demonstrated that mobile satellite communications is feasible and was followed by many other experimental mobile satellites worldwide. In January 1985, the US Federal Communications Commission (FCC) proposed to allocate spectrum in both the UHF band (806 to 890 MHz) and L-band (1.53 to 1.6606 GHz) for a North American Mobile Satellite Service. In 1986, the proposed allocation spectrum was modified to only L-band. Then, in 1997, the FCC allocated 25 MHz of S-band spectrum (between 2320 and 2345 MHz) to Digital Audio Radio Satellite communication system [19] to provide nationwide radio services to the North American continent via satellite.

Channel characteristics determine the modulation and the coding scheme that can be used in the communication system. The channel characteristics depend on the propagation effects through the channel, and, for LMSS systems, the main propagation effect is fading caused by road side vegetation and structures.

The Virginia Tech Antenna Group has been active in propagation modeling and simulation of LMSS systems since its early development. Several versions of a VT simulator were developed to predict propagation effects [9] [13] [14]. However, this VT simulator was restricted to the UHF and L-bands. The simulator used a measured data set, called the universal data set, and scaling factors to generate the simulated signals. It was found that the simulated results were not the same when different universal data sets were

used and the secondary statistics of the simulated signals did not match the secondary statistics of the measured data. To solve these problems, a new simulator, called PROSIM, was developed in 1998 by Suh and Stutzman [15]. PROSIM uses a random number generator and phasor sum theory, rather than universal data sets, to generate the simulated output data set. PROSIM was validated with an analytical model and measured data at 870 MHz from Goldhirsh and Vogel [18]. Good statistical results were obtained for both primary and secondary statistics of the signals. This report presents results from a research program that further improved PROSIM, and adapted it to S-band and to Digital Audio Radio Satellite (DARS) system. Also a measurement campaign using the XM Radio signals at 2.33 GHz was conducted to validate PROSIM simulations for DARS applications in various environments and shadowing conditions.

Chapter 2 describes the physics and statistics of mobile satellite propagation. Chapter 3 presents a review of PROSIM, and the validation and improvement efforts of the simulator. Chapter 4 and 5 describes the XM Radio measurement campaign and the analysis of the measurement data. Then, Chapter 6 presents the validation of PROSIM for S-band frequencies based on the measurement data, and exposes results on dual satellite systems and fading correlation. Finally, the conclusions and recommendations for future work are discussed in Chapter 7.

Chapter 2

The Physics and Statistics of Mobile Satellite Propagation

2.1 Introduction

This chapter describes the physics of propagation along the path between a satellite and land mobile vehicles. Land mobile systems experience multipath fading and signal blockage by terrain obstacles. This is quite different from fixed satellite systems (i.e. fixed earth terminals), where multipath fading does not occur, and where the terrain obstacles are fixed and well known. The signal at the land mobile receiver can be classified into two different signals: the shadowed signal, and the unshadowed signal. The unshadowed signal consists of the direct component, the specular component, and the diffuse component. The shadowed signal consists of the shadowed direct component and the diffuse component. The following sections describe the details of each component and the statistics used to model the propagation effects. This study focused on the downlink of the satellite communication link. However, the results are also valid for the uplink.

2.2 The Physics of Mobile Satellite Propagation

2.2.1 *Unshadowed Propagation*

Unshadowed propagation occurs for land-mobile satellite links when the path between the satellite and the mobile vehicle is a clear line-of-sight (LOS). The propagation with a clear LOS has been extensively studied and is well understood. In this section, each signal component and their associated propagation will be detailed. There are three components in the unshadowed signal: the direct component, the specular component, and the diffuse component, as illustrated in Figure 2.2-1.

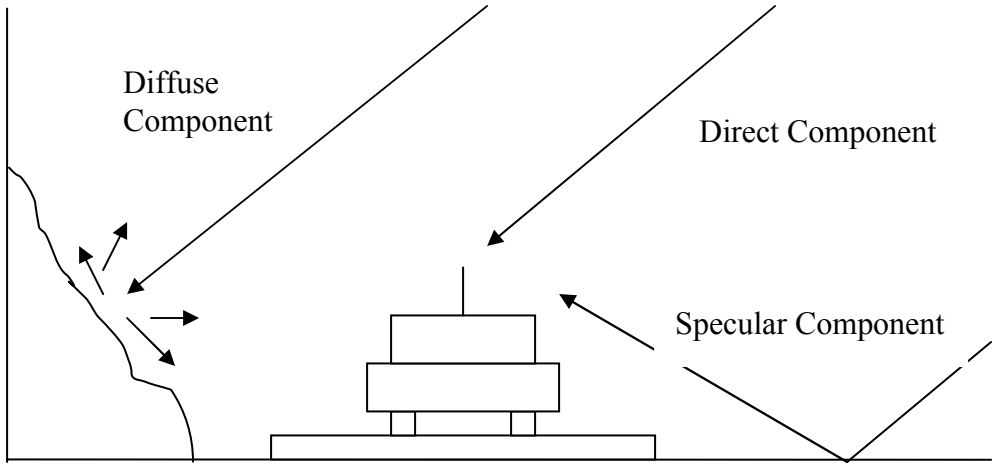

Figure 2.2-1 Illustration of signal components for unshadowed propagation.

2.2.1.1 The Direct Component

The unshadowed direct component arrives via the clear LOS; however, it is affected by atmospheric effects.

The first of these effects is the Faraday rotation which is the rotation of the polarization angle of the electric field. The rotation angle is inversely proportional to the frequency squared, and is significant at UHF and L-band, which are widely used in LMSS systems. Circular polarization, however, does not experience Faraday rotation effects. Since circular polarization is used for LMSS systems, we will ignore the effects of Faraday rotation [1].

Another direct path effect is ionospheric scintillation resulting from the variation of the electron density as a wave passes through the ionosphere. These effects are most severe at low latitudes (about 9 degrees North to 21 degrees South) and at auroral latitudes (> 59 degrees North of North America) [2]. Since the regions of primary interest fall between these latitudes, scintillation effects will be ignored.

Absorption by atmospheric gases is of particular importance for earth terminals with extremely low elevation angles to the satellite and at high frequencies. However, the elevation angle is relatively large for most North American mobile satellite users. Coupled with the relatively low frequency allocated to the mobile satellite service, the

amount of atmospheric absorption is expected to be very small [3]. Hence, we will not include atmospheric absorption in our model.

Other loss mechanisms such as rain and ice attenuation should be considered when determining overall system reliability. They are ignored in this analysis since their effects have been well studied and account for a very small percentage of the overall time of system degradation at S-band frequencies.

2.2.1.2 The Specular Component

The specular component is a phase coherent ground reflected wave coming from points on the first Fresnel zone of the mobile vehicle. It can cause deep fades of the received signal if its amplitude is comparable to the direct component, and its phase is opposite to the phase of the direct wave at the terminal. Beckmann [4] and Jamnejad [3] analyzed the Fresnel zone ellipses and specular reflection of a circularly polarized wave. The polarization state of the ground reflected wave for a circularly polarized incident wave is illustrated in Figure 2.2-2 for several incident angles. Except for grazing angles 0° and 90°, the reflected wave is elliptically polarized. Reflected waves incident below the Brewster angle are polarized with the same sense as the incident wave. But, reflected waves incident at angles greater than the Brewster angle are polarized with the opposite sense. This reversal of polarization sense is important to system performance. The Brewster angle is between 6° and 27° for a rough surface, whereas the elevation angle for most LMSS applications is typically between 20° and 60°. Hence, the specular component will arrive at the terminal in an opposite sense to the direct wave, resulting in considerable multipath rejection at the antenna.

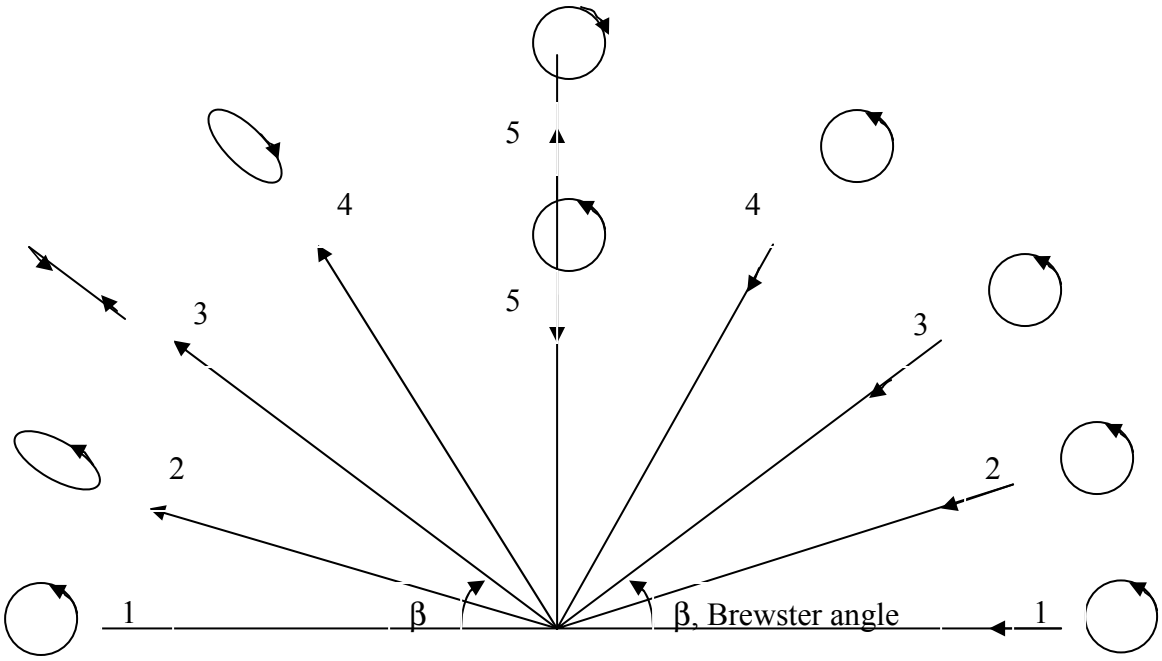

Figure 2.2-2 Illustration of polarizations of waves reflected from the ground for an incident circularly polarized wave for several incident angles [3].

2.2.1.3 The Diffuse Component

The diffuse component is a phase incoherent multipath wave due to reflections and scattering from outside the first Fresnel zone of the vehicle [4]. Experiments by Campbell [5] indicate that the diffuse component has little variation with the direction of arrival. The diffuse component is the phasor sum of a number of individual signals scattered from the terrain surrounding the mobile vehicle. The magnitude of the component is assumed to be Rayleigh distributed while its phase is uniformly distributed. The statistics of the diffuse component are explained in Section 2.3. Interference with the direct component causes rapid fading of the received signal.

2.2.1.4 The Total Unshadowed Signal

The total received signal for unshadowed propagation is the phasor the three components discussed above:

$$R_{\text{total unshadowed}} = R_{\text{direct}} + R_{\text{specular}} + R_{\text{diffuse}} \quad (2.2\text{-}1)$$

For the reasons explained in Section 2.2.1.2, the specular component is considered to be negligible. Thus, the total unshadowed signal expression simplifies to

$$R_{\text{total unshadowed}} \cong R_{\text{direct}} + R_{\text{diffuse}} \quad (2.2\text{-}2)$$

The direct component is essentially constant for purposes of the analysis of propagation effects.

The total unshadowed signal has a Ricean distribution, which is a sum of constant and Rayleigh phasors. The statistics of the total unshadowed signal are explained in Section 2.3.

2.2.2 *Vegetatively Shadowed Propagation*

Shadowed propagation occurs when the direct path between a stationary source and a mobile vehicle is not clear line-of-sight (NLOS). In some cases, the shadowing is so severe that the signal is lost, such as with tall buildings in the path. This situation is often referred to as blocked LOS. Another common source of shadowing is trees along the roadside. In this case, the situation is referred to as vegetatively shadowed propagation, and there are two components to the signal: the shadowed direct component, and the diffuse component. These two components are illustrated Figure 2.2-3.

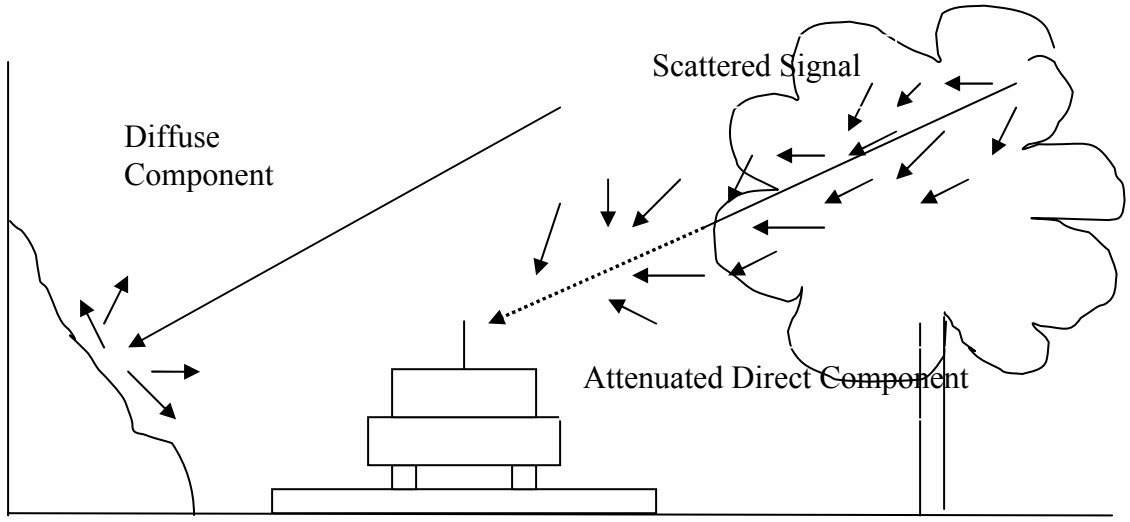

Figure 2.2-3 Illustration of signal components for vegetatively shadowed propagation.

2.2.2.1 The Shadowed Direct Component

When there are trees along the roadside, the direct component from the satellite passes through the roadside vegetation where it is attenuated and scattered by the leaves, branches and limbs. The amount of the vegetation along the path depends on the path length through the vegetation which depends on the stand of trees and the angle to the satellite. Scattering by the vegetation generates a random scattered field that interferes with the direct component causing it to fade and degrade its phase coherency. Thus, the shadowed direct component can be modeled as the phasor sum of the attenuated LOS signal and a random scattered field:

$$R_{\text{shadowed direct}} = A^* R_{\text{direct}} + R_{\text{scattered}} \qquad (2.2\text{-}3)$$

where A is the attenuation factor of the direct component caused by the vegetation and $R_{\text{scattered}}$ represents the signal forward scattered from the vegetation.

The shadowed direct component can be modeled by a lognormally distributed signal, the statistics of which are explained in Section 2.3.

2.2.2.2 The Diffuse Component

The diffuse component for vegetatively shadowed propagation is identical in form to the diffuse component for unshadowed propagation. It is an incoherent ground scattered signal and is Rayleigh distributed in amplitude. The carrier-to-multipath ratio $\overline{K}$ for shadowed propagation tends to be lower than for unshadowed propagation. One explanation for this may be that when a vehicle is vegetatively shadowed, there tends to be more scatterers closer to the vehicle than when it is unshadowed.

There is also diffuse scattering along the direct path resulting from vegetation in the path. The vegetatively forward-scattered signal is assumed to be received from approximately the angular direction of the direct component, whereas the diffuse component arising from terrain scattering arrives at the receiver from many angular directions. While both may behave similarly, this analysis assumes that the effects of the vegetatively forward scattered signal are included in the shadowed direct component whereas the diffuse component includes the effects of all the other scatterers.

2.2.2.3 The Total Shadowed Signal

The total received signal for vegetatively shadowed propagation is the phasor sum of the shadowed direct component and the diffuse component:

$$R_{\text{total shadowed}} = R_{\text{shadowed direct}} + R_{\text{diffuse}} \quad (2.2\text{-}4)$$

The total signal can be modeled by a Vegetatively Shadowed (VS) distribution, which is the sum of a lognormally distributed signal and Rayleigh distributed signal, the statistics of which are explained in the next section.

2.3 Statistical Propagation Models Description, Propagation Constants and Statistics

The physics of mobile satellite propagation can be modeled by four statistical distributions: Rayleigh, Rician, lognormal and the vegetatively shadowed (VS) distribution. To study a propagation link, two different types of statistics are used: primary statistics, quantified with the Probability Density Function (PDF) and Cumulative Distribution Function (CDF), and the secondary statistics, quantified using the Average Fade Duration (AFD), and Level Crossing Rate (LCR). The analytical models used to describe each distribution are described in this section.

2.3.1 *Primary Statistics*

2.3.1.1 The Rayleigh Distribution

The diffuse signal is the sum of the scattered fields from the surrounding terrain. It is expressed as a sum of a large number of scattering point sources:

$$R_{diffuse} = r \cdot e^{j\theta} = \sum_{j=1}^{n} A_j \cdot e^{j\varphi_j} \quad (2.3\text{-}1)$$

where r is the amplitude of the diffuse component, θ is the phase of the diffuse component, φ_j is the phase of the j^{th} diffuse component with respect to the direct component, and A_j is the random amplitude of the j^{th} scattered wave with respect to the direct component. For the case of scattered signals that are sufficiently random with

phases uniformly distributed over 2π, Beckmann [6] showed that the diffuse component can be modeled by the Rayleigh density function defined by

$$p(r) = \frac{2r}{\alpha} e^{-r^2/\alpha} \qquad , \mathrm{r} \geq 0 \tag{2.3-2}$$

$$p(r) = 0 \qquad , \mathrm{r} < 0$$

where α is the mean square value of the signal r. Beckmann also showed that a Rayleigh quantity can be composed of real and imaginary components

$$\mathrm{R=X+\ jY} \tag{2.3-3}$$

where X and Y are normally distributed with zero mean and equal variance σ. It can then be shown that the mean square value of R is [6]

$$\left\langle R^2 \right\rangle = \left\langle r^2 \right\rangle = 2\sigma^2 = \alpha \tag{2.3-4}$$

In the literature, the Rayleigh distribution is usually specified by the parameter $\overline{K}$, in dB, which is given by

$$\overline{K} = 10 \log \frac{1}{\alpha} \quad [\mathrm{dB}] \tag{2.3-5}$$

$\overline{K}$ is physically interpreted to be the ratio of carrier-to-multipath power with unity carrier power assumed. If we express the Rayleigh density function in terms of $\overline{K}$, (2.3-2) becomes

$$p(r) = \frac{2r}{10^{-\overline{K}/10}} \exp\left[-\frac{r^2}{10^{-\overline{K}/10}} \right], \qquad \mathrm{r} \geq 0$$

$$p(r) = 0 \ , \quad \mathrm{r} < 0 \tag{2.3-6}$$

The probability that the Rayleigh distributed signal amplitude is greater than R is given by [6]

$$P_{Rayleigh}(R) = \int_R^\infty p_{Rayleigh}(r) dr = e^{-R^2/\alpha} = \exp\left[-\frac{R^2}{10^{-\overline{K}/10}} \right] \tag{2.3-7}$$

2.3.1.2 The Ricean Distribution

The Ricean distribution is a model used to describe the unshadowed component. It can be expressed as a phasor sum of a constant and a large number of scattering point sources. Hence, the unshadowed signal can be written as

$$R_{unshadowed} = r \cdot e^{j\theta} = C + \sum_{j=1}^{n} A_j \cdot e^{j\varphi_j} \tag{2.3-8}$$

where C represents a constant coherent signal with clear LOS, n is the number of scatterers and the remaining symbols are as defined for the Rayleigh distribution. Beckmann [6] showed that the unshadowed component can be modeled by a Ricean probability density function defined by

$$p(r) = \frac{2r}{\beta} \exp\left[-\frac{(r^2 + C^2)}{\beta} \right] I_0\left(\frac{2rC}{\beta} \right), \quad r \geq 0$$

$$p(r) = 0, \quad r < 0 \tag{2.3-9}$$

where β is the mean square value of the Rayleigh distributed component of r and I_0 is the modified Bessel function of order zero. The Ricean quantity β is analogous to the Rayleigh α. It is a measure of the multipath power. The literature commonly refers to the Ricean parameter K, given by

$$K = 10 \log\left(\frac{C^2}{\beta} \right) \qquad \text{[dB]} \tag{2.3-10}$$

K is interpreted to be the carrier-to-multipath power. C is assumed to be unity in PROSIM. Hence (2.3-9) can be rewritten in terms of K as

$$p(r) = 2r \exp\left[-10^{-K/10} (r^2 + 1) \right] I_0\left(2r^{-K/10} \right) \tag{2.3-11}$$

The probability that the Ricean distributed unshadowed signal amplitude is greater than R is given by [6]

$$G\left(R \mid \overline{VS}\right) = \int_{R}^{\infty} p_{unshadowed}(r) dr \tag{2.3-12}$$

where $\overline{VS}$ indicates no vegetative shadowing.

2.3.1.3 The Lognormal Distribution

The fading caused by vegetative shadowing of a mobile satellite signal is described by the lognormal density function [7]. The lognormal density is the result of combining independent random variables in a multiplicative process just as the normal distribution is the result of combining independent variables in an additive process [8]. Hence, the lognormal signal can be described as

$$R_{\log normal} = r \cdot e^{j\theta} = \prod_{j=1}^{n} B_j \exp\left[j \sum_{j=1}^{n} \Phi_j \right] \tag{2.3-13}$$

where the B_j are a sequence of independent positive random variables and the phases Φ_j are uniformly distributed between 0 and 2π. The lognormal probability density function is given by [6]

$$p(r) = \frac{1}{\sqrt{2\pi}\sigma r} \exp\left[-\frac{(\ln r - \mu)^2}{2\sigma^2} \right], \quad r > 0$$

$$p(r) = 0, \quad r \le 0 \tag{2.3-14}$$

where r is the signal amplitude, μ is the mean of ln(r), and σ is the standard deviation of ln(r). The lognormal density function is completely specified by μ_{dB} and σ_{dB} in dB which are given by

$$\begin{aligned} \log r &= (\log e) \ln r \\ \mu_{dB} &= (20 \log e)\mu \\ \sigma_{dB} &= (20 \log e)\sigma \end{aligned} \tag{2.3-15}$$

Hence (2.3-14) can be rewritten in terms of log(r), μ_{dB} and σ_{dB}:

$$p(r) = \frac{20 \log e}{\sqrt{2\pi}\sigma_{dB} r} \exp\left[-\frac{(20 \log r - \mu_{dB})^2}{2\sigma^2{}_{dB}} \right], \quad r > 0 \tag{2.3-16}$$

The probability that the signal amplitude of the lognormally distributed shadowed direct component is greater than R is given by [6]

$$G(R) = \int_{R}^{\infty} p_{\log normal}(r) dr \tag{2.3-17}$$

2.3.1.4 The Vegetatively Shadowed (VS) Distribution

When vegetatively shadowed, the received satellite signal is the sum of a lognormally distributed direct component and a Rayleigh distributed diffuse component. The distribution function for the sum is referred to as the VS distribution, for Vegetatively Shadowed. The expression for the VS function was derived by Loo [7] and is given by

$$p(r) = \frac{2r}{\sqrt{2\pi}\alpha\sigma}\int_0^\infty \frac{1}{z} I_0\left(\frac{2rz}{\alpha}\right)\exp\left[-\frac{(\ln z - \mu)^2}{2\sigma^2} - \frac{(r^2+z^2)}{\alpha}\right]dz \qquad (2.3\text{-}18)$$

The symbols used in (2.3-18) are the same as defined for the previous sections. The VS cumulative distribution function is given by

$$G(R\,|\,VS) = \int_R^\infty p_{VS}(r)\,dr \qquad (2.3\text{-}19)$$

where VS indicates vegetative shadowing and $G(R\,|\,VS)$ is the probability that the signal amplitude is greater than R under the conditions of vegetative shadowing. The evaluation of (2.3-19) can be achieved only by numerical calculation.

2.3.1.5 The Total Distribution

The propagation path is composed of two separate parts: an unshadowed part that can be modeled by the Ricean distribution presented in Section 2.3.1.2, and a shadowed part that can be modeled by the VS distribution presented in Section 2.3.1.4. On a time series basis, a typical mobile path will include both unshadowed and shadowed propagation conditions in some mixture. On a statistical basis, the total distribution that describes a mixed path is the sum of a shadowed and unshadowed distribution weighted by the fraction of shadowing and unshadowing and is given by

$$G(R) = G(R\,|\,VS)\cdot S + G\left(R\,|\,\overline{VS}\right)\cdot(1-S) \qquad (2.3\text{-}20)$$

which is the probability that the total signal amplitude is greater than R. This approach was developed by Smith and Stutzman [9], but was apparently developed by Lutz, et al. [10] independently as well.

It is often more convenient to work with fade exceedance distributions than signal exceedance distributions. And the total signal distribution (2.3-20) can be rewritten as a cumulative fade distribution (CFD)

$$\begin{aligned} CFD(R) &= 1 - G(R) \\ F &= -R \\ CFD(F) &= 1 - G(F) \end{aligned} \tag{2.3-21}$$

where signal and fade quantities R and F are in dB. Referencing R and F to clear line-of-sight LOS power level, positive signal levels correspond to negative fade levels. CFD(F) is the probability that the fade is greater than F dB while G(F) is the probability that the fade will be less than F dB. The fade exceedance distribution, CFD(F) will be used as a primary statistic in evaluating the satellite propagation link. Figure 2.3-1 illustrates the concept of the CFD. As an example of how to read this plot, the fading equals or exceeds 5 dB for 10% of the time.

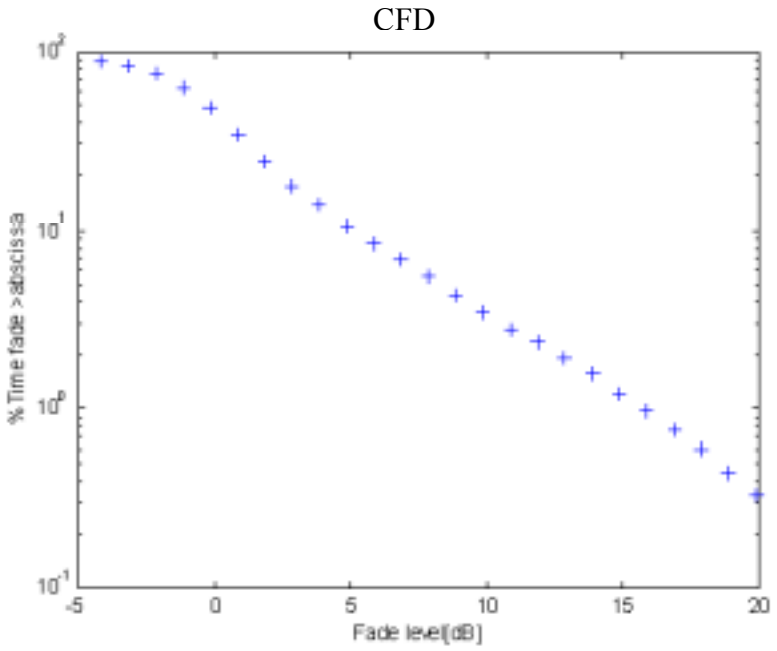

Figure 2.3-1 An example of cumulative fade duration (CFD) found from the PROSIM simulator

2.3.2 *Secondary Statistics: Level Crossing Rate, LCR, and Average Fade Duration, AFD*

The secondary statistics of Level Crossing Rate, LCR, and Average Fade Duration, AFD, are used to represent dynamic, time-varying characteristics of the propagation channel. They depend on the presence of shadowing, speed of the mobile vehicle, relative direction of the source, and antenna pattern. Obtaining good agreement for the secondary statistics between simulated and experimental data is a big challenge in actual propagation models.

The level crossing rate is the expected rate at which the envelope crosses a specified level R with a positive slope in a given period of time. The LCR can be normalized by maximum Doppler-shift frequency to eliminate the dependence on vehicle speed. The normalized LCR, in crossings per wavelength, is given by

$$LCR'(R) = \frac{LCR(R)}{f_m} \text{ [crossings per wavelength]} \qquad (2.3\text{-}22)$$

where the maximum Doppler-shift frequency f_m is defined by

$$f_m = \frac{V}{\lambda} \qquad \text{[Hz]} \qquad (2.3\text{-}23)$$

where V is the vehicle speed and λ is the wavelength of the transmitted signal.

The average fade duration is the average length of a fade for a given threshold. The AFD can also be normalized to eliminate the vehicle speed dependence. The normalized AFD is given by

$$AFD'(R) = AFD(R) \cdot f_m \qquad \text{[wavelength]} \qquad (2.3\text{-}24)$$

where f_m is as defined as above.

Figures 2.3-2 illustrates the concept of LCR and Figure 2.3-3 is an example of an AFD both found using PROSIM simulation. As an example of how to read Figure 2.3-2, the signal envelope crosses the 20 dB fade level with a positive slope approximately 0.1 time per wavelength. As an example of how to read Figure 2.3-3, every time the signal undergoes a fade level of 5 dB, the fading event lasts 0.03 wavelength on average.

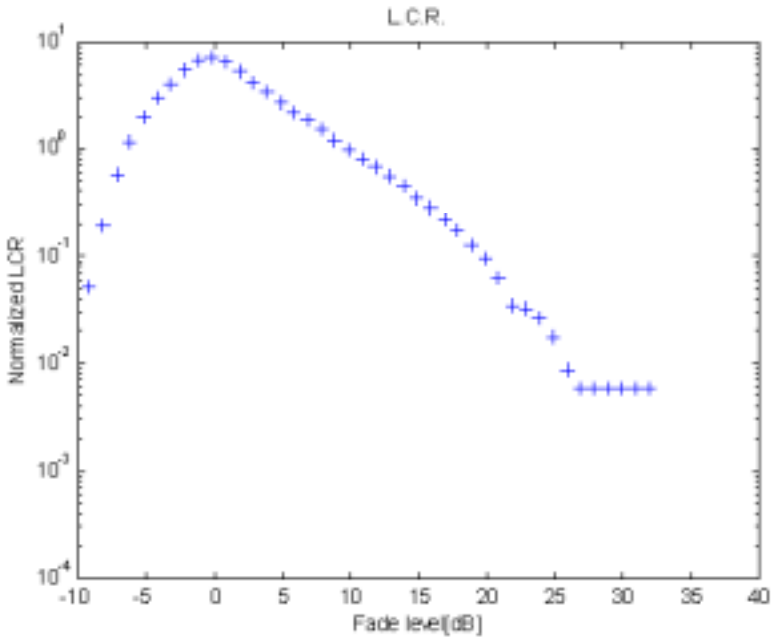

Figure 2.3-2 An example of level crossing rate (LCR) found from the PROSIM simulator

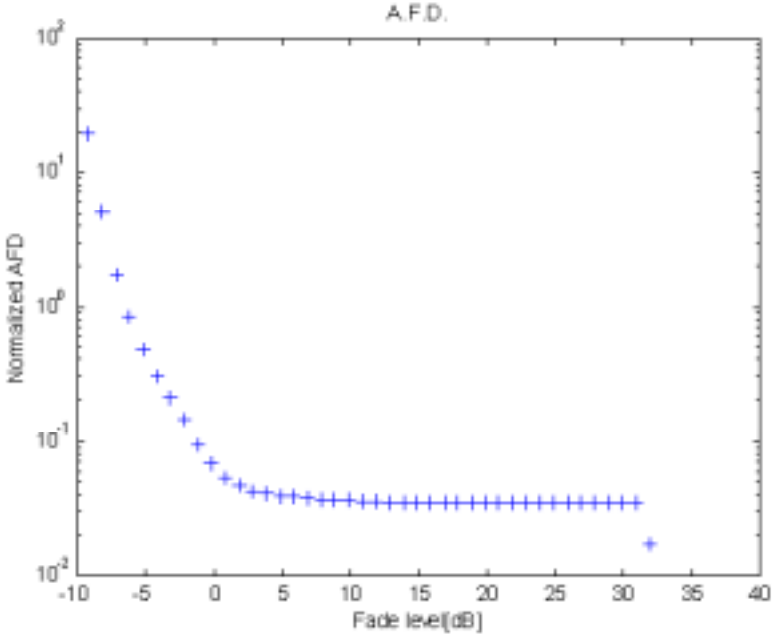

Figure 2.3-3 An example of average fade duration (AFD) found from the PROSIM simulator

Chapter 3

The PROSIM Simulator Overview

3.1 Historical Background of PROSIM

The Virginia Tech Antenna Group, and its sister organization the Satellite Communications Group, have been involved in modeling and simulation of the propagation effects of land mobile satellite systems (LMSS) channels for over 15 years. Several versions of propagation simulators have been developed over the years to predict propagation effects [9] [13] [14]. Previous versions of the propagation simulators had issues that needed to be resolved in order to apply them to the S-band case. First, the previous simulators were built using propagation measurements performed at UHF and L-band, whereas our interest is to study S-band (2.3 GHz) propagation. Fading behavior due to vegetation is a function of frequency, so we needed to quantify the differences between the fading characteristics at S-band and the lower frequencies used in the past. Secondly, previous simulation results were based on universal data sets derived from measured data, and were different depending on the data sets used. This dependency on variations in measured data needed to be corrected. Thirdly, the secondary statistics from the previous VT simulators did not provide a good match with the secondary statistics of the measured signals.

These problems in the earlier VT simulator were resolved by Suh and Stutzman [15] through the development of a new propagation simulator, called PROSIM. PROSIM is based on a random number generator to create the simulated output data with the correct statistical properties. Previous simulators used measured data as the basis for its simulation, which produced the problems mentioned previously. PROSIM is based on the fundamentals of random phasor sum theory and its performance has been evaluated using analytical and measured data at UHF and L-band. For this effort, PROSIM was updated and enhanced to address the specifications of S-band signals. This chapter gives an overview of PROSIM. Section 3.2 describes the generation of the propagation distributions and Section 3.3 presents improvements to the first version of PROSIM. Then, Section 3.4 sums up the PROSIM functions.

3.2 Generation of the Statistical Distributions

The originality of this simulator is that it is based on a random number generator that generates data sets to compute statistics of the propagation channel for geostationary satellites. The simulator is a two state simulator; it assumes that the propagation environment is either vegetatively shadowed, or completely unshadowed. This section describes how random phasors are used to build the propagation distributions.

3.2.1 *Generation of Rayleigh Data Set*

3.2.1.1 The Fundamentals

A Rayleigh data set can be generated using Rayleigh random phasor sum, according to the expression (2.3-1) given in Section 2.3.1. Figure 3.2-1 illustrates the random phasor sum in the complex plane. The Rayleigh complex-value data can be decomposed in a real and an imaginary part, both having a normal distribution with zero mean and one variance. This can be written as follows:

$$X = \mathrm{Re}(R_{Rayleigh}) = r\cos\theta = \sum_{j=1}^{n} A_j \cos\Phi_j = \sum_{j=1}^{n} X_j \tag{3.2-1}$$

$$Y = \mathrm{Im}(R_{Rayleigh}) = r\sin\theta = \sum_{j=1}^{n} A_j \sin\Phi_j = \sum_{j=1}^{n} Y_j \tag{3.2-2}$$

where A_j is the amplitude of the j^{th} random phasor, and Φ_j its phase. If n is large enough, then both X and Y will be normally distributed, according to the Central Limit Theorem. The mean and variance values are derived by Beckmann [6]

$$\langle X\rangle = \sum_{j=1}^{n}\langle A_j\cos\Phi_j\rangle = \sum_{j=1}^{n}\langle A_j\rangle\langle\cos\Phi_j\rangle = \sum_{j=1}^{n}\langle A_j\rangle\frac{1}{2\pi}\int_{c}^{c+2\pi}\cos\varphi_j\,d\varphi_j = 0 \tag{3.2-3}$$

and in the same way

$$\langle Y\rangle = \sum_{j=1}^{n}\langle A_j\rangle\langle\sin\Phi_j\rangle = 0 \tag{3.2-4}$$

$$\left\langle X^2 - \langle X\rangle^2\right\rangle = \langle X^2\rangle = \sum_{j=1}^{n}\langle A_j^2\rangle\langle\cos^2\Phi_j\rangle = \frac{1}{2}n\langle A_j^2\rangle = \sigma^2 \tag{3.2-5}$$

$$\left\langle Y^2 - \langle Y\rangle^2\right\rangle = \langle Y^2\rangle = \sum_{j=1}^{n}\langle A_j^2\rangle\langle\sin^2\Phi_j\rangle = \frac{1}{2}n\langle A_j^2\rangle = \sigma^2 \tag{3.2-6}$$

$$\left\langle A_j^{\,2} \right\rangle = \frac{2\sigma^2}{n} = \frac{\alpha}{n} \tag{3.2-7}$$

We can also determine the mean-square value of r given by [6]

$$\left\langle r^2 \right\rangle = \sum_{j=1}^{n} \left\langle A_j^{\,2} \right\rangle = n\left\langle A_j^{\,2} \right\rangle = \left\langle X^2 \right\rangle + \left\langle Y^2 \right\rangle = 2\sigma^2 \equiv \alpha = 10^{-\overline{K}/10} \tag{3.2-8}$$

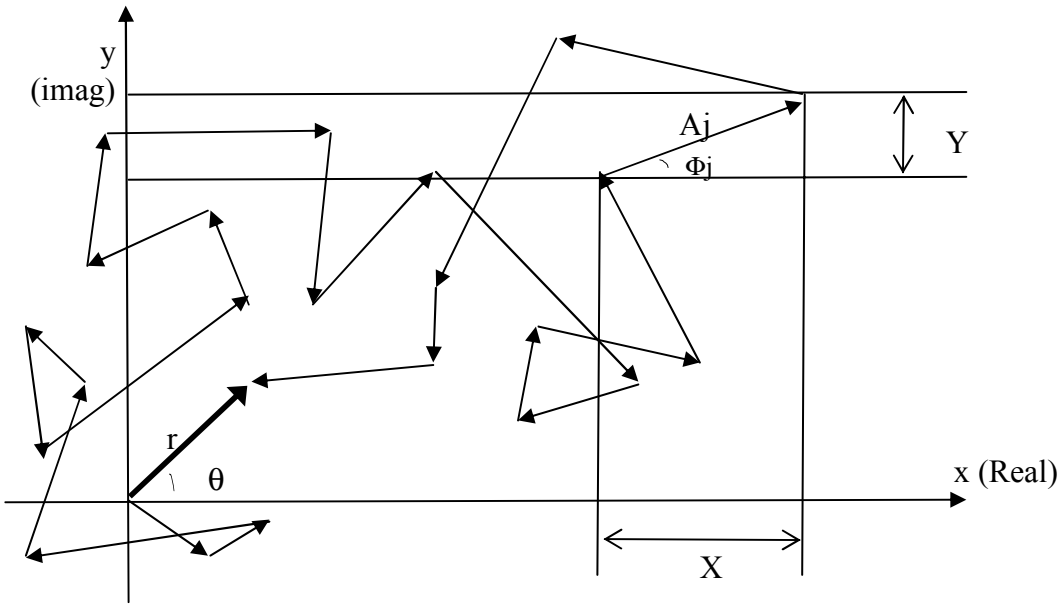

Figure 3.2-1 Illustration of a Random phasor sum in the complex plane [6] [15].

3.2.1.2 Generating the Rayleigh Data Set

The Rayleigh data set was generated using the Random Number Generator (RNG) of MATLAB. MATLAB has two different random number generator functions: rand(n,m) and randn(n,m). The first one (rand(n,m)) generates a uniform distribution of 1s, with a mean value of 0.5 and a variance of 1/12, whereas the second function (randn(n,m)) generates a normal distribution with zero mean and variance of unity. The parameter, n, represents the number of scattered phasors, and m is the number of points to be represented in time or distance. The value of n should be sufficiently large to obtain a normal distribution, and as low as n=5 based on the Central Limit Theorem. The fade distribution is a statistical distribution in terms of time or distance and to obtain a 0.1%

statistical accuracy, we need at least 10,000 samples. Consequently, m should be chosen to be at least equal to 10,000 points. Increasing values of m and n increase the accuracy of the simulation, but also increase the computation time. To avoid a time-consuming simulation, values of n between 5 and 15, and m between 10,000 and 15,000 are recommended.

Using the functions in MATLAB, the random amplitude A_j can be produced according to a normal distribution with zero mean and variance of unity. However, a variance of 1 does not fit well to the Rayleigh distribution. The variance indeed depends on the carrier-to-multipath ratio $\overline{K}$. The relation between $\overline{K}$ and the Rayleigh distribution mean-square value, α is given (2.3-5). The scaling factor, α can be obtained from (2.3-4), which relates the mean-square value of A_j to $\frac{\alpha}{n}$. Hence, the desired data set, having the carrier-to-multipath ratio $\overline{K}$, can be generated using the following relationships:

$$A_j = \sqrt{\frac{\alpha}{n}} randn(j,m) \tag{3.2-9}$$

$$\Phi_j = 2\pi \cdot rand(j,m) \tag{3.2-10}$$

where the function 'randn' generates the normally distributed random vector amplitude and the function 'rand' generates the uniformly distributed random vector phase.

Then it can be shown that the scaling factor $\sqrt{\frac{\alpha}{n}}$ gives a mean-square value of the signal r with the desired value α.

$$\left\langle r^2 \right\rangle = \sum_{j=1}^{n} \left\langle A_j^{\,2} \right\rangle = n \left\langle \left(\sqrt{\frac{\alpha}{n}} randn(j,m) \right)^2 \right\rangle = n \cdot \frac{\alpha}{n} = \alpha \tag{3.2-11}$$

Here, the following relationship between the scaling factor and the function 'randn' was used [16]:

$$\mathrm{var}\left[k \cdot randn(1,m)\right] = k^2 \tag{3.2-12}$$

where k is an arbitrary scaling factor. Hence, the Rayleigh data set can be generated using (3.2-9) and (3.2-10) as

$$R_{Rayleigh} = r \cdot e^{j\theta} = \sum_{j=1}^{n} A_j \cdot e^{j\Phi_j} \tag{3.2-13}$$

3.2.2 *Generation of the Ricean Data Set*

The Ricean data set is generated in the same way as the Rayleigh data set except for the adding of a constant LOS component. In PROSIM, this LOS signal is assumed to be unity. The Ricean data set is used to model the unshadowed signal, as explained in Section 2.3.1. The phasor plot in Figure 3.2-2 illustrates the phasor plot of a Ricean model in the complex plane. As one can notice, the LOS component, C, is much larger than the Rayleigh component ρ. Consequently, the phase of the Rayleigh component, ψ, has little effect on the phase of the total Ricean signal, θ. The Ricean distribution is completely defined by its carrier-to-multipath power ratio K in dB. The relation between K and the Ricean signal mean square value, β is derived according to the following relationship:

$$\beta = C^2 \cdot 10^{-K/10} = 10^{-K/10} \tag{3.2-14}$$

(since C is assumed to be unity).

As for the Rayleigh data set, the scaling factor is

$$Scaling\ \ factor = \sqrt{\frac{\beta}{n}} \tag{3.2-15}$$

$$A_j = \sqrt{\frac{\beta}{n}} randn(1, m) \tag{3.2-16}$$

$$\Phi_j = 2\pi \cdot rand(1, m) \tag{3.2-17}$$

Hence, the Ricean data set can be generated using (3.2-16) and (3.2-17) as

$$R_{Ricean} = r \cdot e^{j\theta} = C + \rho \cdot e^{j\psi} = C + \sum_{j=1}^{n} A_j \cdot ej^{\Phi_j} = 1 + \sum_{j=1}^{n} A_j \cdot ej^{\Phi_j} \tag{3.2-18}$$

where r is the amplitude of the Ricean distribution and θ is its phase.

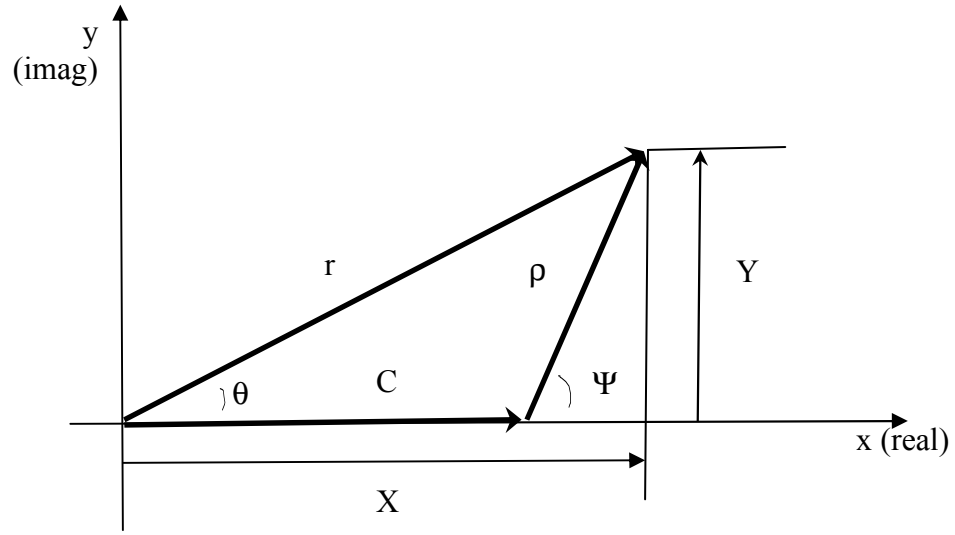

Figure 3.2-2 Illustration of a Ricean phasor plot in the complex plane [6] [15].

3.2.3 *Generation of the Shadowed Data Set*

3.2.3.1 Generation of the Lognormal Data Set

The lognormal data set is quite different from the Rayleigh and the Ricean data sets. Whereas the Ricean and Rayleigh data sets are based on an addition of random phasors, a multiplicative process of random variables develops the lognormal distribution. The lognormal data set is generated with a lognormally distributed amplitude and a uniformly distributed phase between 0 and 2π. Suh [15] developed the following expression for a phasor plot of the lognormal model:

$$R_{\log normal} = r \cdot e^{j\theta} = \prod_{j=1}^{n} B_j \cdot \exp\left[j \sum_{j=1}^{n} \Phi_j \right] \tag{3.2-19}$$

$$\ln(R_{\log normal}) = \ln r + j\theta = \sum_{j=1}^{n} \ln B_j + j \sum_{j=1}^{n} \Phi_j = \sum_{j=1}^{n} \left(\ln B_j + j\Phi_j \right) = \sum_{j=1}^{n} H_j \cdot e^{j\Psi_j} = h \cdot e^{j\varphi} \tag{3.2-20}$$

where $H_j = \sqrt{\left(\ln B_j\right)^2 + \Phi_j{}^2}$, $\Psi_j = \tan^{-1}\left(\dfrac{\Phi_j}{\ln B_j} \right)$ and h and φ are the amplitude and the phase

of $\ln(R_{lognormal})$. When we take the natural log of the expression (3.2-19), it becomes clear that the log amplitude of the signal, $\ln(R_{lognormal})$, can be decomposed into a real part which is the natural log of the amplitude of the signal ln(r), and an imaginary part which is the phase of the lognormal distribution (3.2-20). Figure 3.2-3 illustrates the phasor plot in the complex plane of the lognormal model derived by Suh [15].

The lognormal model is completely defined by the mean of the signal μ_{dB}, and its standard deviation σ_{dB}, in dB. As for the Ricean and the Rayleigh distribution, the signal is scaled to obtain the desired mean and variance. First, the MATLAB 'randn' function generates negative values, which is not appropriate here when the log of these random values is required. Hence, these values are first shifted to the positive region. Then, the natural log function is applied. We now need to find the scaling factor K. This scaling factor is different for each n^{th} run of the total sum, and depends on the variance of each data set run. Hence, K is evaluated for each run as

$$K = \sqrt{\frac{\sigma^2}{c \cdot n}} \tag{3.2-21}$$

where σ^2 is the desired variance of our final distribution. c is a slope factor and is determined for each run as

$$c = \frac{\mathrm{var}\,iance\left\{s \cdot \ln\left[randn_{positive}(j,k)\right]\right\}}{n \cdot s^2} \tag{3.2-22}$$

where s is arbitrary set to 100. Then, the total distribution can be described as

$$\sum_{j=1}^{n} K(j) \cdot \ln\left[randn_{positive}(j,m)\right] \tag{3.2-23}$$

According to (3.2-22), the variance of this distribution is

$$\mathrm{var}\,iance\left\{\sum_{j=1}^{n} K(j) \cdot \ln\left[randn_{positive}(j,m)\right]\right\} = \mathrm{var}\,iance\left\{K \cdot \sum_{j=1}^{n} \ln\left[randn_{positive}(j,m)\right]\right\} = n \cdot c \cdot K^2 = \sigma^2 \tag{3.2-24}$$

and its mean is

$$M = mean\left\{\sum_{j=1}^{n} K(j) \cdot \ln\left[randn_{positive}(j,m)\right]\right\} \tag{3.2-25}$$

Next, consider the distribution B defined as

$$\mathrm{B} = \sum_{j=1}^{n} B_j = \sum_{j=1}^{n} \left(K(j) \cdot \ln\left[randn_{positive}(j,m) \right] - M(j) + \mu / n \right) \tag{3.2-26}$$

where μ is the desired mean of the final distribution. This distribution seems to have the desired mean μ

$$mean\left\{ \sum_{j=1}^{n} K(j) \cdot \ln\left[randn_{positive}(j,m) \right] - M + \mu \right\} \approx \mu \tag{3.2-27}$$

and the desired variance σ^2

$$\mathrm{var}\,iance\left\{ \sum_{j=1}^{n} K(j) \cdot \ln\left[randn_{positive}(j,m) \right] - M + \mu \right\} = \mathrm{var}\,iance\left\{ \sum_{j=1}^{n} K(j) \cdot \ln\left[randn_{positive}(j,m) \right] \right\} = \sigma^2 \tag{3.2-28}$$

Finally, the lognormal distribution will be produced according to (3.2-19) and (3.2-20) as

$$R_{\log normal} = \exp\left(\sum_{j=1}^{n} \left(B_j + j \cdot \Phi_j \right) \right) \tag{3.2-29}$$

.

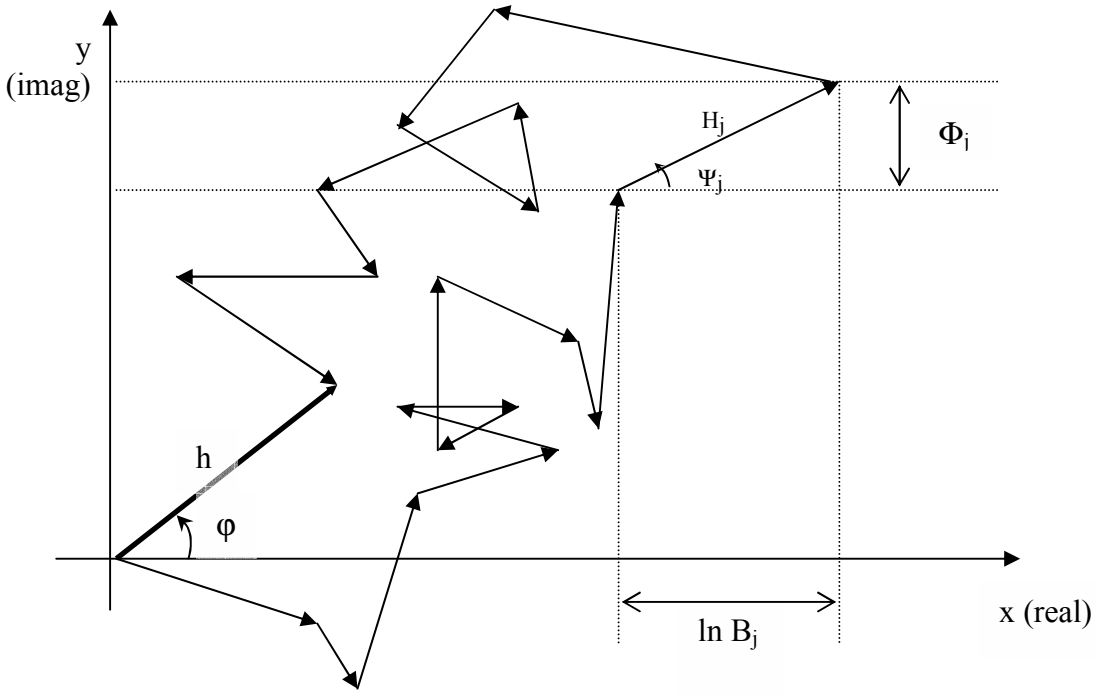

Figure 3.2-3 Illustration of the lognormal phasor plot in the complex plane [15].

3.2.3.2 Generation of the Shadowed Data Set

The shadowed data set is the phasor sum of a Rayleigh data set and a lognormal data set, both developed in Sections 3.2.1 and 3.2.3.1. The total shadowed signal can be written as

$$R_{shadowed} = R_{\log normal} + R_{Rayleigh} = r \cdot e^{j\theta} = z \cdot e^{j\phi} + w \cdot e^{j\varphi} \qquad (3.2\text{-}30)$$

where the phase φ and ϕ are uniformly distributed, z is lognormally distributed, and w has a Rayleigh distribution.

3.2.4 *Generation of the Total Data Set*

The total data set is generated as a combination of the Ricean and the shadowed data set, according to the percentage of shadowing S. In the first version of PROSIM [15], the total signal is a simple concatenation of shadowed and unshadowed data points, with respect to S:

$$R_{total} = S * R_{shadowed} + (1 - S) * R_{unshadowed} \qquad (3.2.31)$$

A new combination of the shadowed and unshadowed data points, based on a Gaussian distribution, gives more realistic simulated results, since it takes into account the correlation of the successive shadowing events. This new combination will be extensively detailed in Section 3.3.2.

3.3 Improvements to PROSIM

3.3.1 *Test of PROSIM Robustness: New Random Algorithms*

Because PROSIM is based on a random number generator, it is unexpected that it should provide results that compare favorably with measured secondary statistics. Thus, it became necessary to test the robustness of the simulator: with another random number generator, will the secondary statistics still match? Basically, two different distributions of random numbers are created: a Gaussian distribution, for the amplitude of the signals, and a uniform distribution for the phases.

3.3.1.1 Uniform Distribution

Usually, PROSIM generates uniform distributions in the unit interval with the MATLAB function 'rand'. A new distribution is created by randomizing the output numbers of the function 'rand': the output of the new function is a number randomly chosen among a set of numbers generated by the 'rand' function. The different steps of the new random number generator are (see also Figure 3.3-1):

- Step1: creation of the initial set of 100 random numbers with the 'rand' function of MATLAB
- Step2: one of the numbers of the set is randomly picked (with the 'rand' function) → output number
- Step3: replace the number picked by another random one ('rand' function), so that the set remains random and not restricted to 100 values (we have a sort of dynamic set)
- Step4: go back to step 2 to have a new number

Etc….

The loop {step2 to step4} is repeated each time a new random number is needed. For PROSIM, a distribution is typically 10000 points.

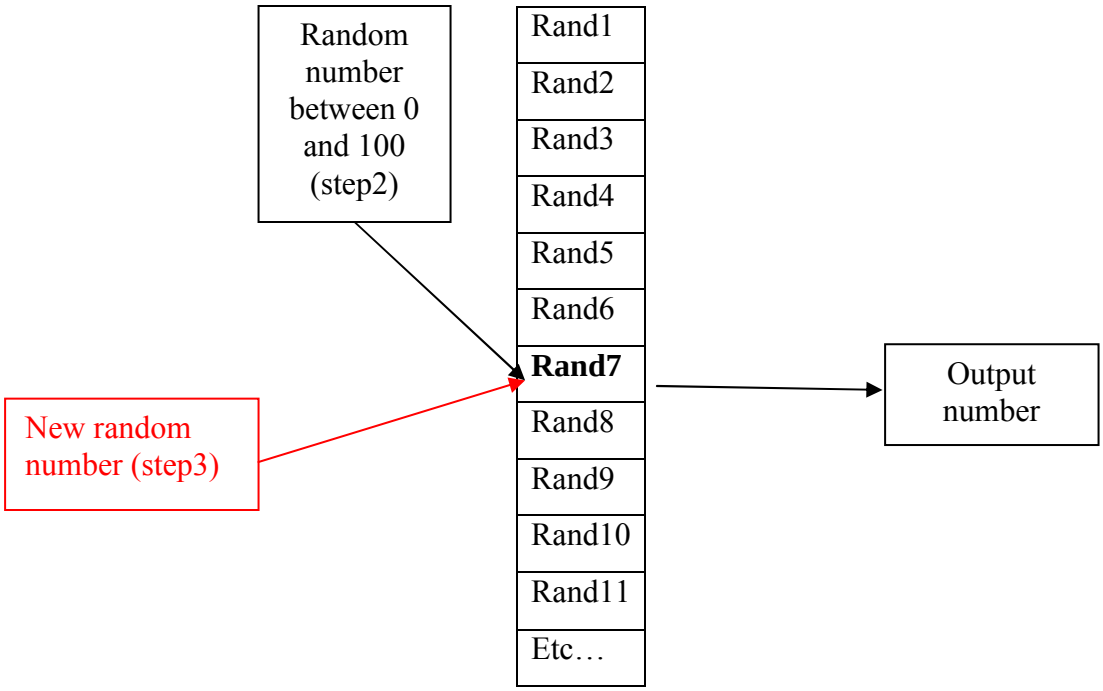

Figure 3.3-1 Algorithm of the new uniform distribution generator used in PROSIM.

3.3.1.2 Gaussian Distribution

PROSIM uses the MATLAB function 'randn' to generate Gaussian numbers with mean zero and variance one. To replace this function, the Box-Müller method is used: if U_1 and U_2 are two independent variables uniformly distributed in the unit interval, then it is shown [17] that

$$X = \left(-2\ln(U_1)\right)^{1/2} \cdot \cos(2\pi U_2) \tag{3.3-1}$$

is a Gaussian variable with mean zero and variance one. The uniformly distributed variables U_1 and U_2 are generated with the uniform distribution algorithm presented in Section 3.3.1.2.

3.3.1.3 Results of the Robustness Test: Comparison of MATLAB and New Random Number Generators

PROSIM is run with the new uniform and Gaussian distribution generators presented in Sections 3.3.1.1 and 3.3.1.2. In particular, we compared the propagation distributions generated by the MATLAB random number generator using 'rand' and 'randn' function with the distribution generated using the new uniform and Gaussian distributions described above. We also compare the statistical behavior of signals simulated with both methods.

3.3.1.3.1 Generation of the Different Data Sets

First, the Ricean, Rayleigh and lognormal data sets generated using the new uniform and Gaussian distribution ("new random generator") described in Sections 3.3.1.1 and 3.3.1.2 are compared with the corresponding data sets generated with the classic 'rand' and 'randn' MATLAB functions. Figures 3.3-2, 3.3-3 and 3.3-4 give a simultaneous plot of the PDF of the simulated distributions for both old and new random number generators, along with the analytical model PDF. It can be observed that the PDF of each data set are very similar in every case presented, and present a good match with the analytical model.

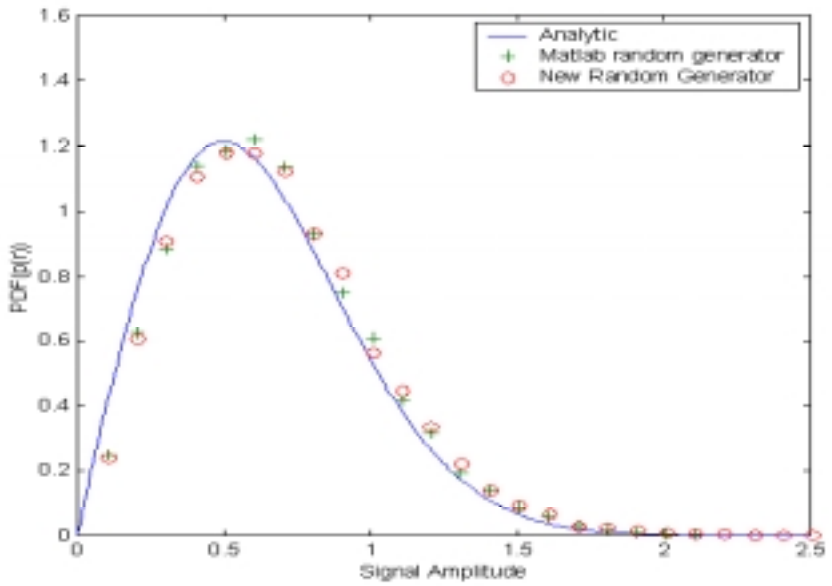

Figure 3.3-2 Comparison of Rayleigh magnitude PDF for Analytical model, MATLAB random generator and new random generator ($\overline{K}$ =3 dB) [15].

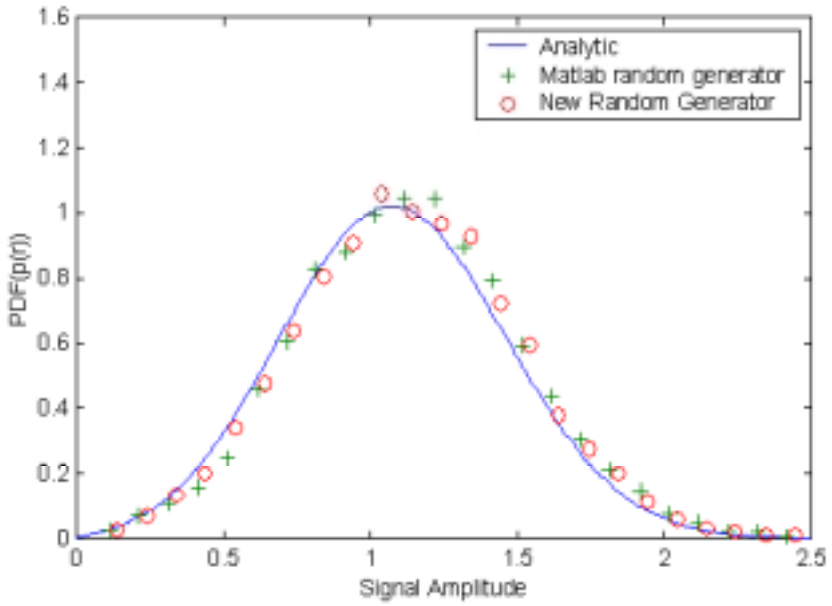

Figure 3.3-3 Comparison of Ricean magnitude PDF for Analytical model, MATLAB random generator and new random generator (K=5 dB) [15].

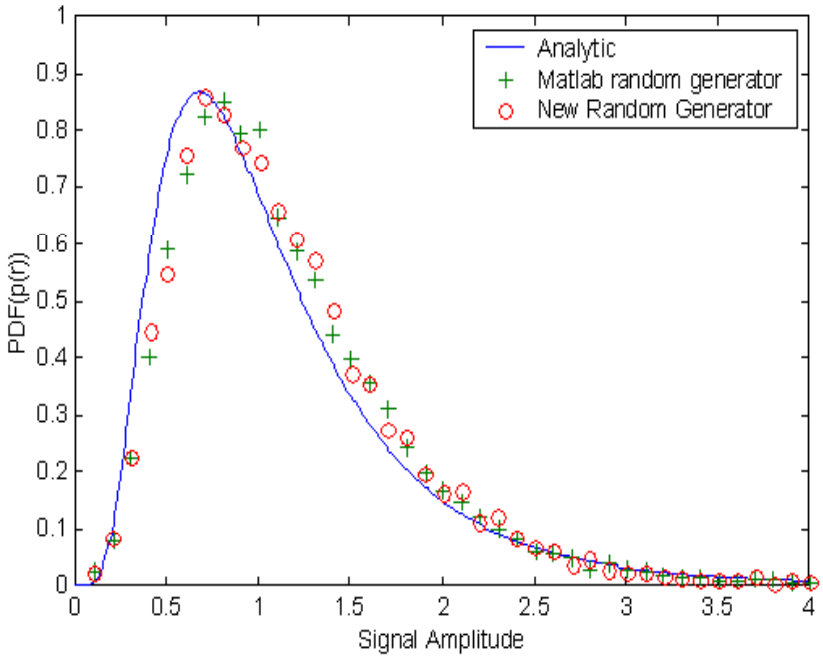

Figure 3.3-4 Comparison of lognormal magnitude PDF for Analytical model, MATLAB random generator and new random generator (μ_{dB} = -0.5 dB, σ_{dB} = 5 dB) [15].

3.3.1.3.2 Running PROSIM with both Random Numbers Generators

To test the random number generators, the simulated signals are compared to Goldhirsh and Vogel [18] measured data set BA181556. In fact, at the time when the robustness tests were conducted, no XM Radio data were available, because the VTAG receiver for XM Radio signals was not ready. That is why the PROSIM designers used previous Vogel measurements to test the robustness, instead of XM Radio measurements.

The propagation constants of the Vogel signal, extracted by Barts [13], are chosen as inputs to PROSIM, and the following two signals are simulated: one using the MATLAB random generator and the other one using the new random number generator. Figure 3.3-5 presents the propagation constants corresponding to each measured or generated signal. Figure 3.3-6 is a plot of the signals envelopes in the time domain, assuming that the samples points are one millisecond apart. And Figures 3.3-7 to 3.3-9 present the statistics of the signals.

The parameters, [K, Kbar, u, sigma] of INPUT, SIMULATION, and SIMULATIONRNG are
INPUT =
 13.0000 4.4000 -4.0000 4.9000
SIMULATION =
12.9733 4.4177 -4.0000 4.9199
SIMULATIONNRG =
12.9446 4.3979 -4.0000 4.8613

Figure 3.3-5 Measured and Simulated propagation constants for both MATLAB (simulation) and New Random number Generator (SimulationNRG) signals (BA181556 data set).

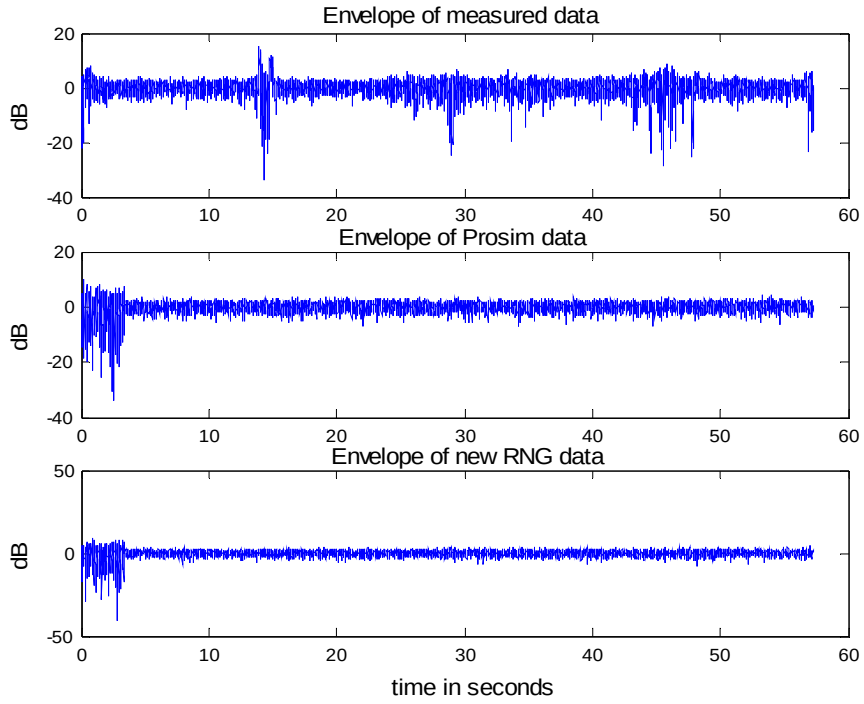

Figure 3.3-6 Envelopes of measured data BA181556 and corresponding simulated PROSIM data, and PROSIM data with new Random Number Generator (RNG data).

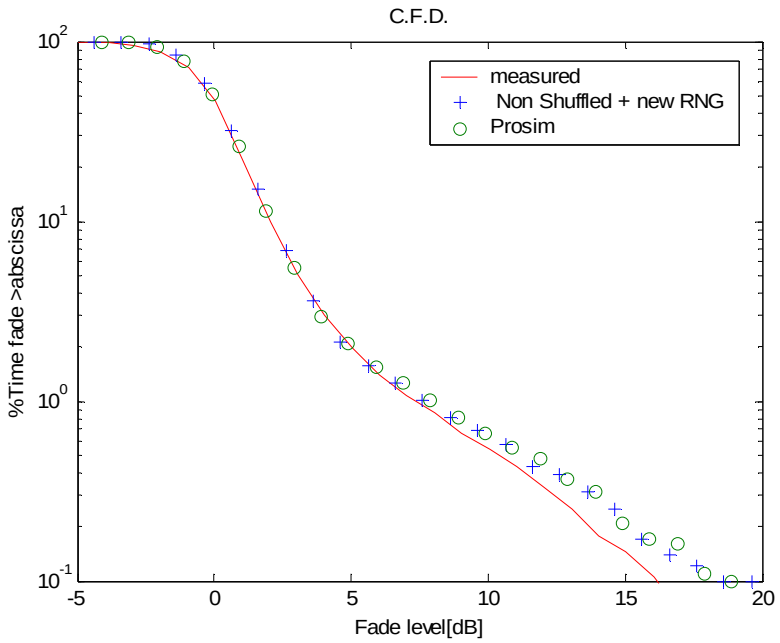

Figure 3.3-7 CFD of measured data BA181556 and corresponding simulated PROSIM data, and PROSIM data with new Random Number Generator.

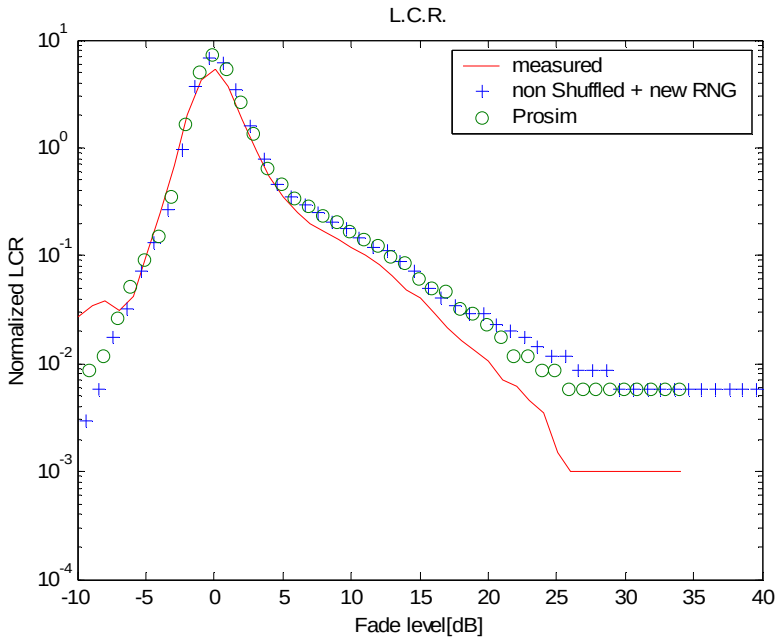

Figure 3.3-8 LCR of measured data BA181556 and corresponding PROSIM data, and PROSIM data with new Random Number Generator.

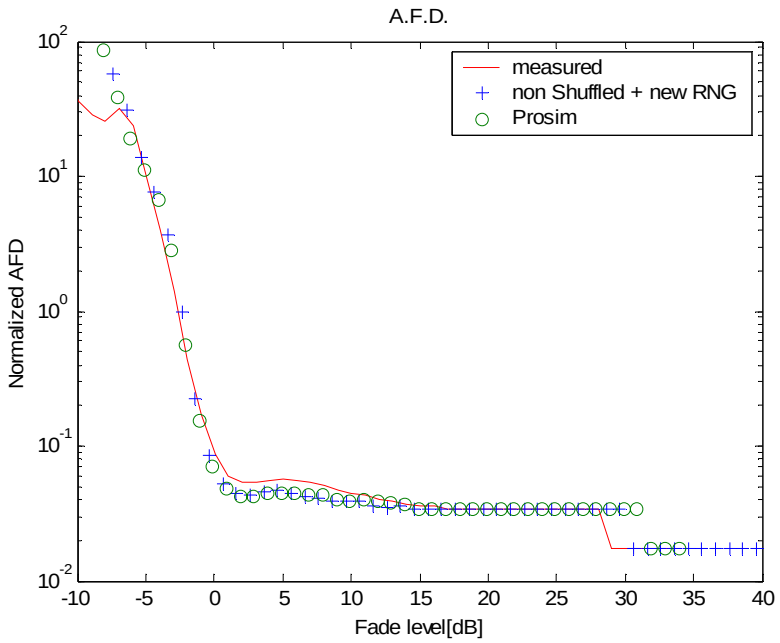

Figure 3.3-9 AFD of measured data BA181556 and corresponding PROSIM data, and PROSIM data with new Random Number Generator.

Based on the good agreement between the statistics of both MATLAB and new random number generator simulated signals from Figures 3.3-5 to 3.3-9, it can be said that PROSIM is a robust simulator, and that the simulated signal statistics do not depend on the way the variables are generated within MATLAB. For the rest of the simulation, and for the particular study of the XM Radio signals, the MATLAB random number generator is used because it saves a lot of computation time.

3.3.2 *New Combination of the Shadowed and Unshadowed Data Sets*

The original version of PROSIM processes the unshadowed and shadowed data points very simply, according to the percentage of shadowing S: for example, if there is 80% of shadowing, PROSIM will generate 80%*(total number of samples) of shadowed points, and concatenate them with 20%*(total number of samples) of unshadowed points. This does not reflect what happens in real propagation channels: a totally shadowed then totally unshadowed propagation signal is never observed. The shadowing is always more

balanced and random. Hence, next, the sorting of PROSIM simulated samples is modified and the statistics of both concatenated and new signals are compared.

3.3.2.1 The First Improvement: Random Shuffling of the Signal

In a first attempt to improve the combination of the data points, a new shuffling algorithm was developed. That assumes that for a total number of required samples of N, an array of the corresponding length N is created. Then, PROSIM generates a shadowed and an unshadowed data set, according to the percentage of shadowing. If the percentage of shadowing is S, PROSIM simulates S*N shadowed points and (1-S)*N unshadowed points. Then, instead of concatenating both sets, the two shadowed and unshadowed data sets are mixed. The shuffling algorithm is based on the probability of shadowing S, which is one of the inputs of the simulator. For each point of the final signal, a point from the shadowed or unshadowed data set is picked up with a probability of respectively S% and (1-S)%, and inserted in the final signal array. Figure 3.3-10 presents a simple graphic explanation of the shuffling algorithm.

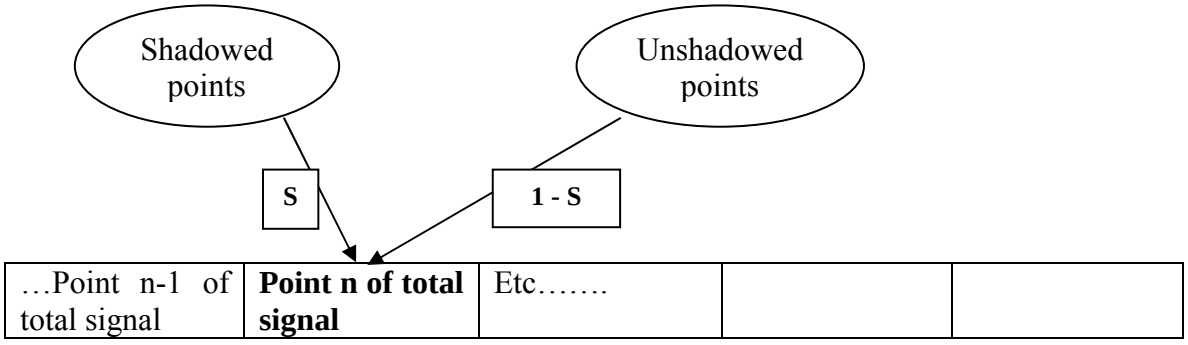

Figure 3.3-10 Illustration of the time sequence of data points using the new shuffling algorithm.

This new shuffling of the signal gives more realistic looking signals. Moreover, it does not affect the statistics of the signal, and there is still a good agreement between the statistics of the measured and simulated data points. However, this shuffling procedure is still based on artificial randomness, so that the signal is a succession of shadowed and

unshadowed independent data points. The possible correlation between successive points, resulting from the continuity of the shadowing event, is considered next.

3.3.2.2 New Combination of the Simulated Data Points: Gaussian Model

In a real environment, the shadowing events are partially correlated; each shadowing event lasts more than one sample point. Therefore, when a point is shadowed, its neighbor is likely to be also shadowed, as part of the same shadowing event. And a succession of randomly shadowed and unshadowed data points does not represent reality.

Hence, a new space series of the simulated data points is created, with correlation between points. The combination of the data points is based on a routine that generates curves with Gaussian correlated values. For each simulation run, a curve is generated. This curve has the length of the final simulated signal, and its successive points are correlated according to a Gaussian correlation function with the desired value of correlation length Lc. In fact, the power spectral density of the curve is Gaussian, according to

$$y = h^2 L_c \frac{e^{-\left(\frac{kx*Lc}{2}\right)^2}}{2\sqrt{\pi}} \tag{3.3-1}$$

where y contains the values of the power spectral density, h is the mean square value of the signal strength, Lc is the correlation length, and

$$k_x = \frac{2\pi N}{r_l} \tag{3.3-2}$$

where N contains the indexes of the points, and r_l is the total length of the curve in meters.

The correlation length Lc indicates for how long the value (or signal strength) of the curve at a given point can be considered to be correlated with the values of its predecessors. For example, when the correlation length is 2 meters (corresponding to approximately 15.5 wavelengths when working at 2.33 GHz), the signal strength for one point will depend on the value of the signal strength for its predecessors within 2 meters.

And the closer the neighbor, the larger the dependence. Following this idea, the new point is independent from its predecessors generated more than 2 meters before.

Once the curve is generated according to the correlation length, the shadowed and unshadowed data points are combined, with respect to the percentage of shadowing S. When the curve is below a certain signal strength L, the corresponding data points are considered shadowed. So, the total signal array is filled with points from the shadowed data set. Then, when the curve is above L, the total signal array is filled with unshadowed data points. The value of L is determined by the percentage of shadowing S; that is, S % of the total curve has to be under L. Thus, a simple CFD is run to determine L before filling the total signal array. Figure 3.3-11 illustrates the combination of the shadowed and unshadowed data points into the total signal according to the Gaussian correlated curve. There is no link between the signal strength of the Gaussian curve at a point, and the value of the total simulated signal amplitude for this point: the signal strength is used only to determine whether the total signal point will be shadowed or unshadowed. Typical values of the correlation length Lc for the XM Radio measurements are given in Section 6.2.2.

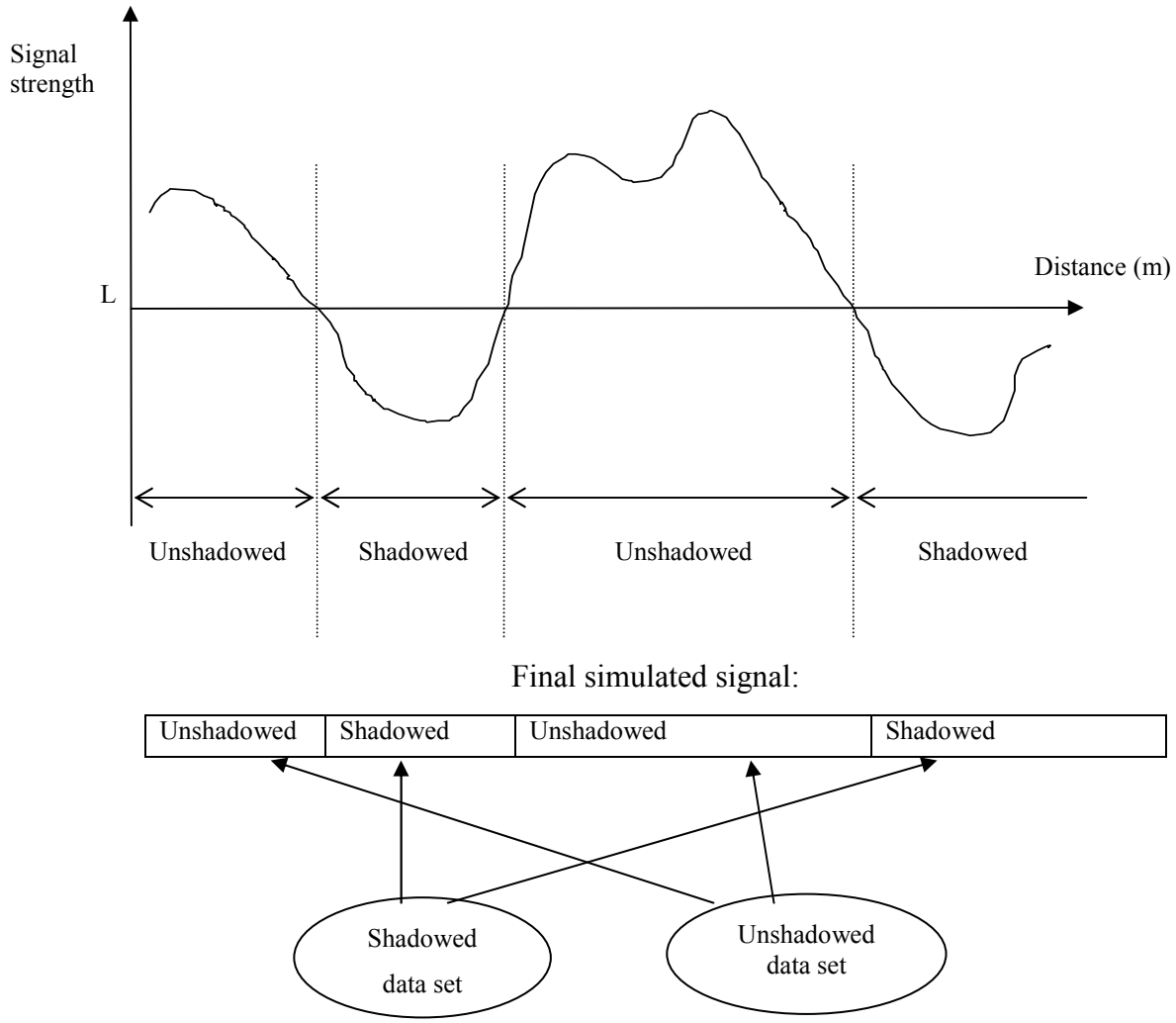

Figure 3.3-11 Conceptual illustration of the time sequence of the data points using a Gaussian correlated curve.

3.3.2.3 Results of the New Gaussian Combination

This new combination of the shadowed and unshadowed data sets in the final signal, based on a curve with Gaussian correlated successive heights, gives good results. First, the simulated signals seem more realistic than the previously randomly distributed signals. Then, the statistics of the simulated signal using the new Gaussian method match well with the statistics of the measured signals, at least as well as the statistics of the 'Shuffling' simulated signal. And in some cases, the 'Gaussian' statistics fit the measured statistics better than the 'Shuffling' statistics. A comparison of the 'Shuffling' and

'Gaussian' combination methods is presented Figure 3.3-12 to 3.3-13. The comparison was performed using 2.33 GHz signals measured on Route 114 West, on September 1, 2002. For this scenario, named 'Route114WEST3', two signals are acquired simultaneously: one is received from satellite Roll, and the other one from satellite Rock. Also, the AGC of the receiver was not removed. Further details about the measurements campaign are given in Chapter 4.

Since the 'Gaussian' method gives realistic signals with good statistical results, it is selected and implemented into PROSIM. Hence, the user will have to enter a correlation length Lc for each simulation. In case of the comparison with the measured signals, the correlation lengths of the simulated signals were set experimentally, by trial and error, as explained in Section 6.2.2.

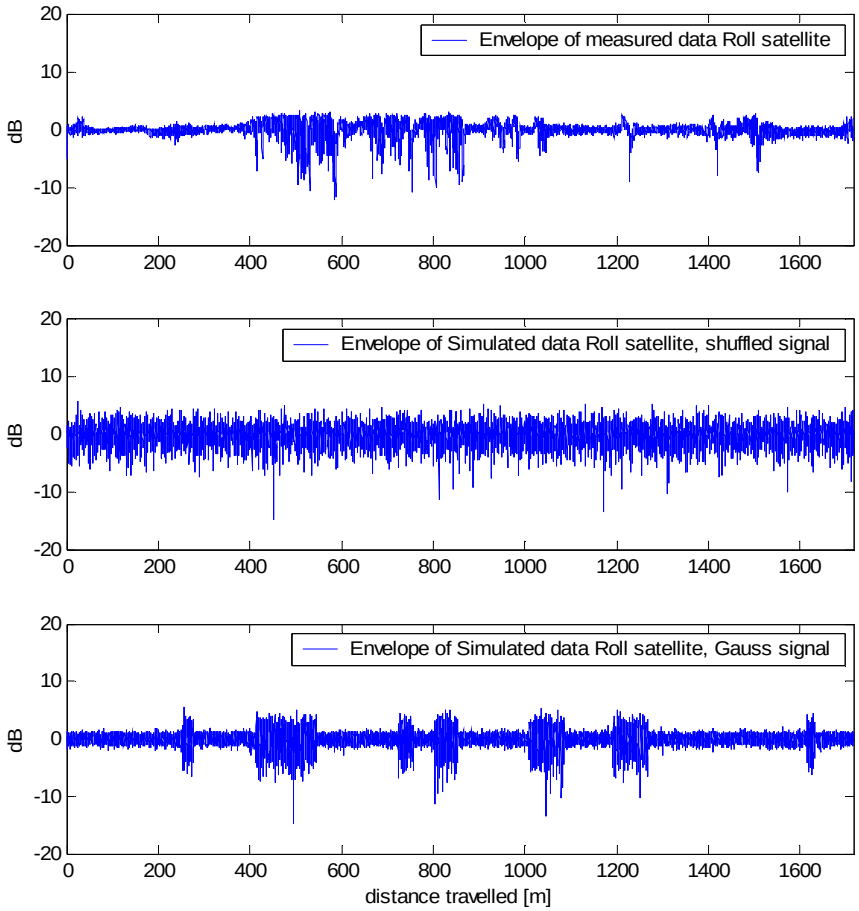

Figure 3.3-12 Measured and simulated signal received from Roll satellite for Route114WEST3 scenario: (a) Measured signal received from Roll satellite, (b) Corresponding simulated signal, using the 'Shuffling' method, (c) Corresponding simulated signal, using the 'Gaussian' method.

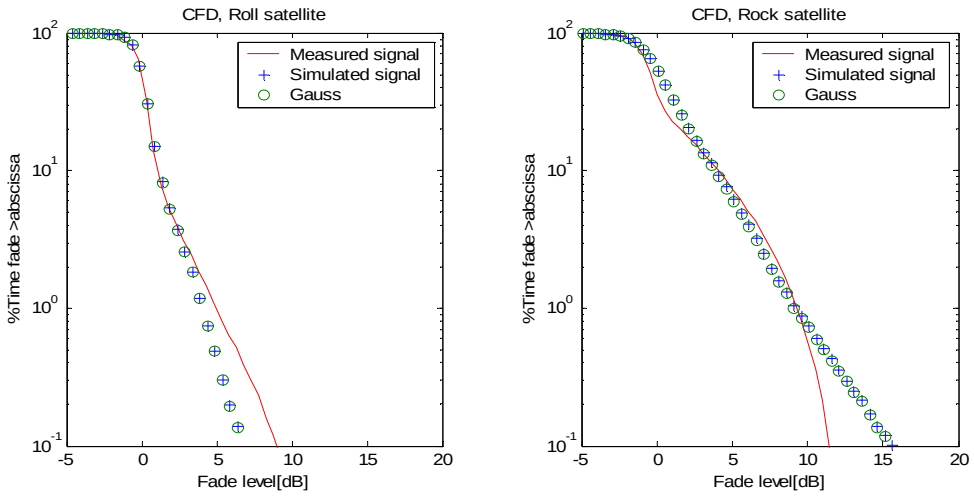

Figure 3.3-13 CFD of measured and simulated signal for Route114WEST3 scenario. For each satellite, the CFD of the measured signal, the CFD of the corresponding simulated signal using the 'Shuffling' method ('Simulated signal'), and the CFD of the corresponding simulated signal using the 'Gaussian' method ('Gauss') are shown.

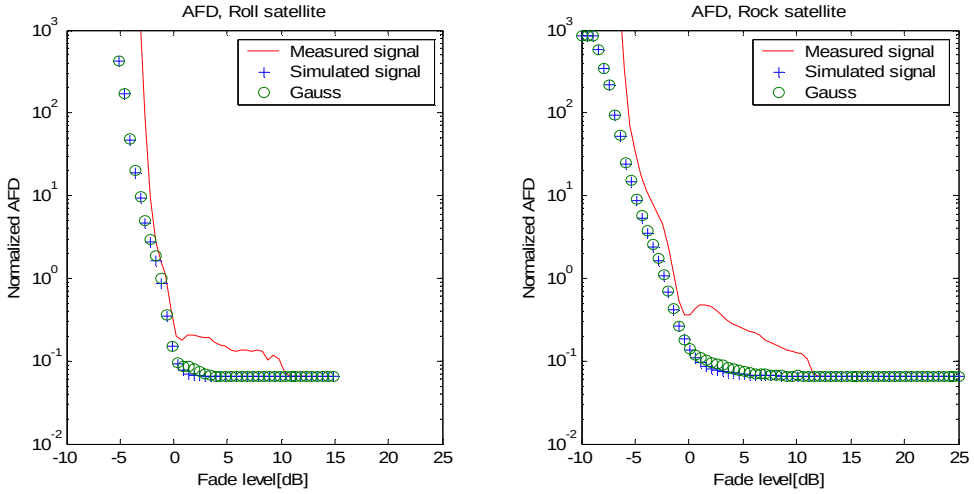

Figure 3.3-14 AFD of measured and simulated signal for Route114WEST3 scenario. For each satellite, the AFD of the measured signal, the AFD of the corresponding simulated signal using the 'Shuffling' method ('Simulated signal'), and the AFD of the corresponding simulated signal using the 'Gaussian' method ('Gauss') are shown.

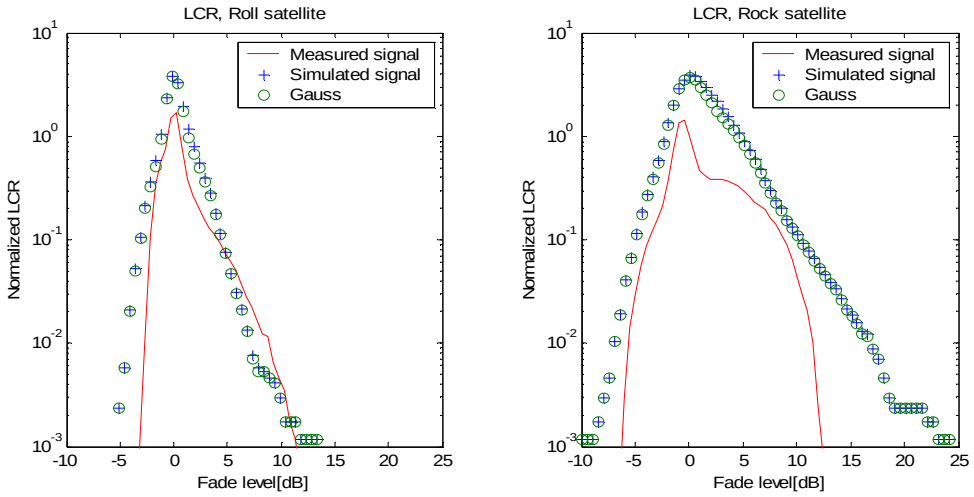

Figure 3.3-15 LCR of measured and simulated signal for Route114WEST3 scenario.For each satellite, the LCR of the measured signal, the LCR of the corresponding simulated signal using the 'Shuffling' method ('Simulated signal'), and the LCR of the corresponding simulated signal using the 'Gaussian' method ('Gauss') are shown.

3.4 Description of the PROSIM Simulator

PROSIM is used to simulate a set of shadowed data points and a set of unshadowed data points. It estimates the propagation constants of these simulated distributions, constructs the total signal, and computes the primary and secondary statistics for this total signal. The block diagram is the simulator is given Figure 3.4-1. PROSIM has the following user-specified options:

- Simple simulation
- Comparison of simulation with analytical model
- Comparison of simulation with simple model
- Comparison of simulated data with XM Radio scenario, with or without AGC

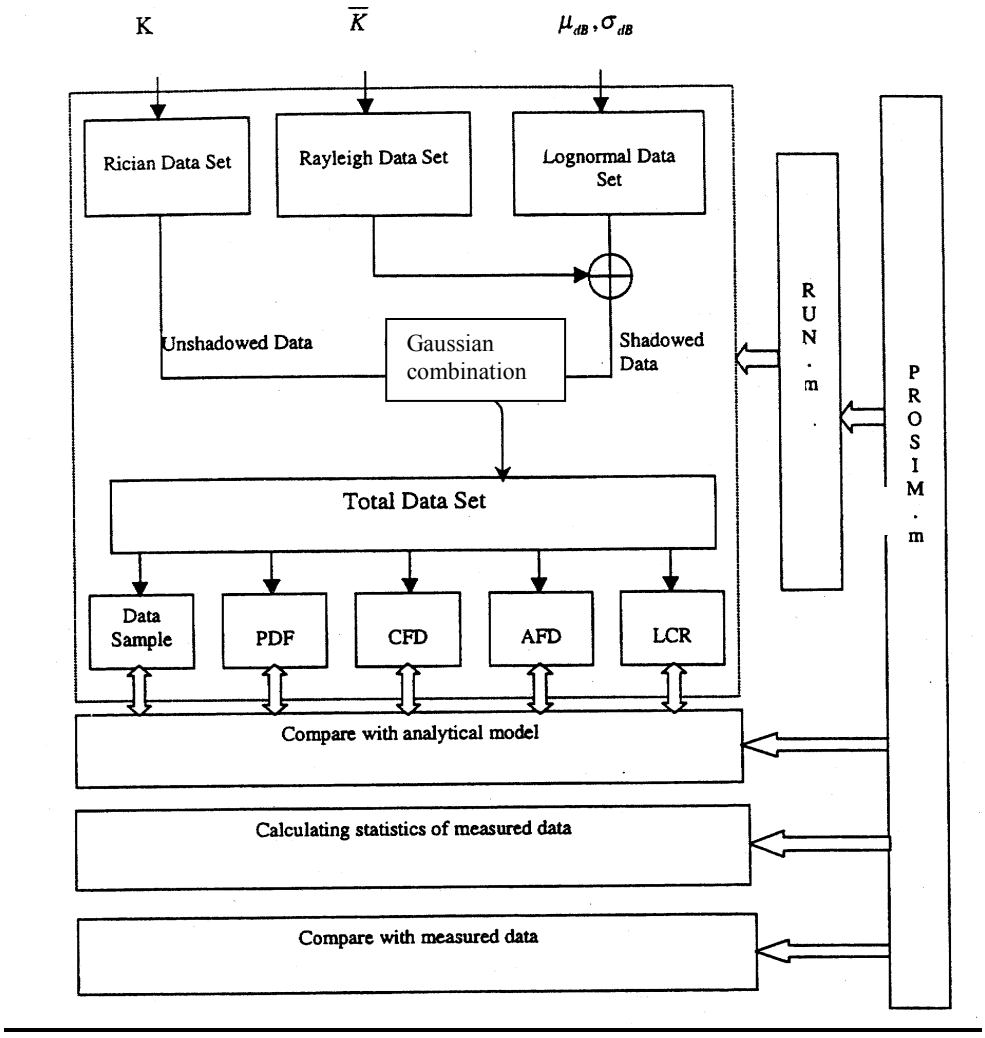

Figure 3.4-1 Block diagram of the PROSIM propagation simulator.

3.4.1 *The Simple Simulation Option*

Inputs to the simple simulation

- Percentage of shadowing, S
- Carrier-to-multipath ratio for the Ricean distribution, K, in dB
- Carrier-to-multipath ratio for the Rayleigh distribution, $\overline{K}$, in dB
- Mean of the lognormal distribution, μ, in dB
- Standard deviation of the lognormal distribution, σ, in dB
- Frequency of the signal, in MHz
- Number of samples, N
- Correlation length, Lc, in meters

All the simulation results are given as a function of the distance traveled, so that the impact of the speed of the vehicle is removed. An example of the PROSIM inputs is Figure 3.4-2.

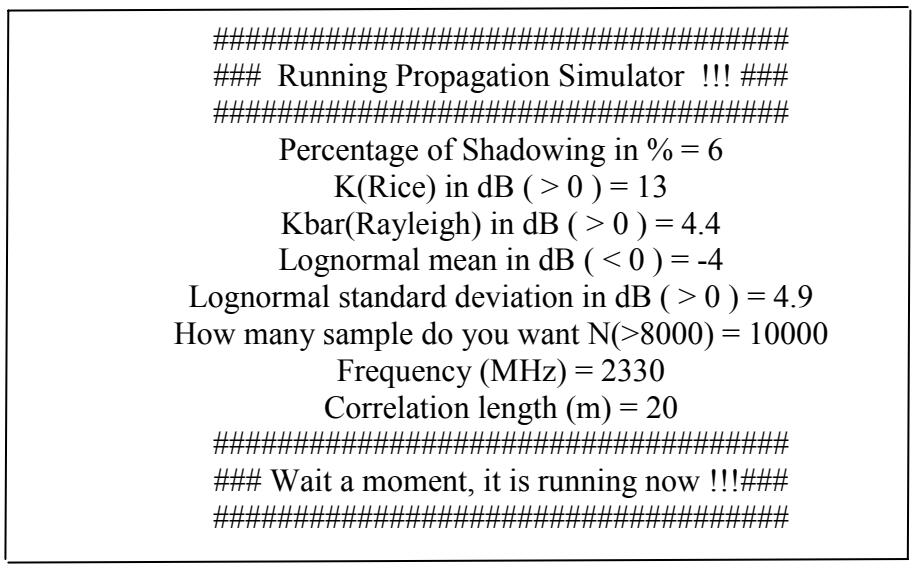

Figure 3.4-2 Example of PROSIM inputs for the simple simulation option.

The propagation constants, and other PROSIM inputs are used to simulate a signal based on different routines created by the designer of PROSIM [15]:

- 'Sim_ray' creates a Rayleigh distribution from $\overline{K}$ and calculates the new $\overline{K}$ value for this simulated distribution
- 'Sim_log' creates a lognormal distribution from the input lognormal mean μ and standard deviation σ and calculates its new experimental mean and standard deviation
- 'Shad_run' creates a set of shadowed data points, combining the lognormal distribution and the Rayleigh distribution of parameter $\overline{K}$
- 'Unsh_run' creates a set of unshadowed data points, with a Ricean distribution of parameter K and estimates the new K for these points
- 'tot_gen3' combines the shadowed and unshadowed simulated data sets in a total signal, according to the 'Gaussian' distribution method presented in Section 3.3.2.2

After executing these routines, PROSIM estimates the primary and secondary statistics of the total signal, using the function 'cdf_run', which gives the CDF of the signal, and 'afd_run', which calculates the AFD and LCR of the signal.

Output of the simulator

After computation, PROSIM yields the propagation constants extracted from the simulated data. An example of PROSIM outputs is shown Figure 3.4-3. PROSIM also gives several curves: envelope of the total simulated signal, CDF, AFD, LCR, lognormal and Rayleigh signals with their PDF, shadowed and unshadowed signals with their PDF. Examples of such curves are given at various points in this report.

```
The parameters, [K, Kbar, u, sigma] of INPUT and SIMULATION are
                        INPUT =
   12.0000    0.2000   -2.0000    1.0000
                     SIMULATION =
   11.9822    0.1955   -2.0000    0.9933
```

Figure 3.4-3 Example of PROSIM outputs for the simple simulation option.

3.4.2 *Comparison with Analytical Model Option*

The user also has the possibility to compare the signal simulated with PROSIM with its corresponding analytical model. The input interface of PROSIM in this case is very similar to the Simulation option. The user enters the following parameter values:

- Percentage of shadowing, S
- Carrier-to-multipath ratio for the Ricean distribution, K, in dB
- Carrier-to-multipath ratio for the Rayleigh distribution, $\overline{K}$, in dB
- Mean of the lognormal distribution, μ, in dB
- Standard deviation of the lognormal distribution, σ, in dB
- Frequency of the signal, in MHz
- Number of samples, N
- Correlation length, Lc, in meters

Then, PROSIM simulates the corresponding signal. At the same time, it computes the analytical CDF corresponding to the propagation constants entered by the user. After computation, PROSIM gives several curves:

- Envelope of the simulated lognormal distribution, comparison of simulated and analytical PDF

- Envelope of the simulated Rayleigh distribution, comparison of simulated and analytical PDF

- Envelope of the simulated unshadowed distribution, comparison of simulated and analytical PDF

- Envelope of the simulated shadowed distribution, comparison of simulated and analytical PDF

- Envelope of the total simulated signal

- Comparison of the analytical and simulated CDF for the total signal

- LCR and AFD of the simulated signal

The MATLAB routine designed to run the comparison with the analytical comparison is 'cha_run'. The MATLAB routine designed to compute the CDF of the analytical signal is 'channelf'.

3.4.3 *Comparison with Simple Model Option*

3.4.3.1 Description of the Simple Model

The simple propagation model presented by Barts [13] has the same structure as the analytical model option; that is, the shadowed and unshadowed fade distributions are modeled separately and combined to form the total signal. It uses the LMSSMOD [13] simulator to generate fade distributions for purely shadowed and purely unshadowed propagation conditions. Then, the fade distributions were curve fitted using common mathematical equation forms. The equation form giving the best curve fit to the distribution over a range of "typical" model parameters was chosen for the simple model. Best fit was defined as the equation form having the smallest average error and the smallest maximum error fitting to the fade distribution.

For the Ricean distribution, the fraction of time the fade will be greater than F dB is

$$C_u(F) = e^{-(F+U_1)/U_2} \tag{3.4-1}$$

where

$$\begin{aligned} U_1 &= 0.01K^2 - 0.378K + 3.98 \\ U_2 &= 331.35K^{-2.29} \end{aligned} \tag{3.4-2}$$

and K is the Ricean carrier-to-multipath ratio in dB.

For the vegetatively shadowed (VS) signal, the fade distribution can be approximated by

$$C_s(F) = \left[\frac{50-F}{V_1}\right]^{V_2} \tag{3.4-3}$$

where

$$\begin{aligned} V_1 &= -0.275\overline{K} + 0.723\mu + 0.336\sigma + 56.979 \\ V_2 &= \left[-0.006\overline{K} - 0.008\mu + 0.013\sigma + 0.121\right]^{-1} \end{aligned} \tag{3.4-4}$$

where $\overline{K}$ is the carrier-to-multipath ratio for the Rayleigh distribution, and μ and σ are the mean and standard deviation of the lognormal distribution. Finally, the fade distribution for the total signal is obtained by combining the shadowed and unshadowed fade distributions according to the percentage of shadowing S:

$$\text{CDF\_total}=(\text{Cs}*\text{S} + \text{Cu}*(1-\text{S}))*100 \tag{3.4-5}$$

As mentioned above, the simple model is valid only for a range of "typical" propagation parameters, as summarized in Table 3.4-1.

Table 3.4-1 Simple Model propagation parameters range [13].

	Minimum valid value (dB)	Maximum valid value (dB)
K	10	22
$\overline{K}$	10	18
μ	-10	-1
σ	0.5	3.5

3.4.3.2 Comparison with the Simple Model Option

The user can compare a PROSIM simulated signal with the simple model, by entering the following parameter values:

- Percentage of shadowing, S
- Carrier-to-multipath ratio for the Ricean distribution, K, in dB
- Carrier-to-multipath ratio for the Rayleigh distribution, $\overline{K}$, in dB
- Mean of the lognormal distribution, μ, in dB
- Standard deviation of the lognormal distribution, σ, in dB
- Frequency of the signal, in MHz
- Number of samples, N
- Correlation length, Lc, in meters

Then, PROSIM simulates the signal. At the same time, it computes the CDF of the simple model corresponding to the propagation constants entered by the user. After computation, PROSIM outputs several curves:

- Envelope of the simulated lognormal distribution, and its PDF
- Envelope of the simulated Rayleigh distribution, and its PDF
- Envelope of the simulated unshadowed distribution, and its PDF
- Envelope of the simulated shadowed distribution, and its PDF
- Comparison of simple model and simulated CDF for the total signal

The MATLAB routine designed to run the analytical comparison is 'sim_run'. The MATLAB routine designed to compute the simple model CDF is 'simplef'. Figure 3.4-4 is a comparative plot of the CDF of a PROSIM simulated signal, and the CDF of the corresponding simple model.

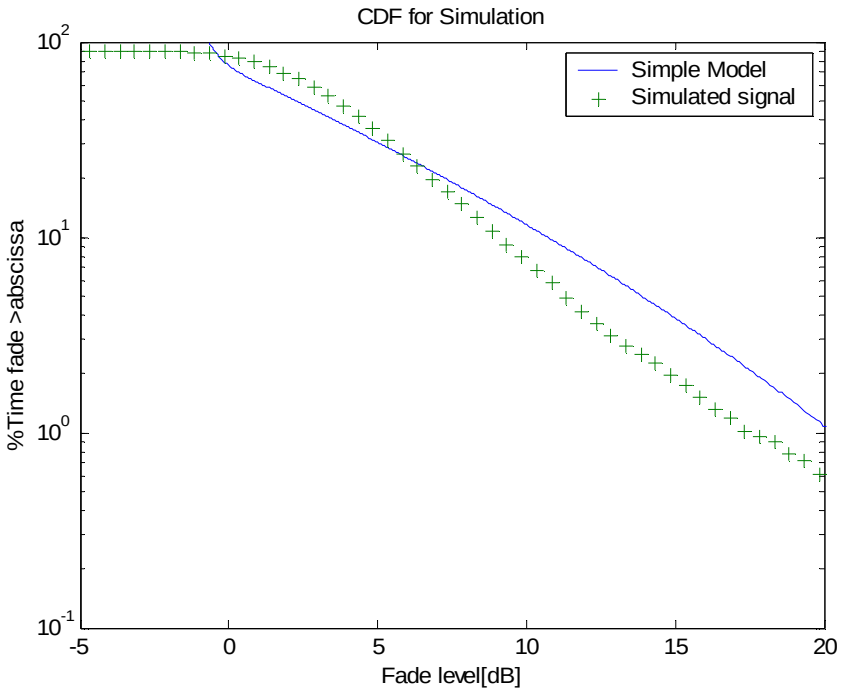

Figure 3.4-4 Example of comparison of the CDF of a PROSIM simulated signal with the CDF of the corresponding Simple model for S = 90%, K = 21 dB, $\overline{K}$ = 10 dB, μ = -4.8 dB, σ = 1.7 dB and Lc = 20 m

3.4.4 *Comparison with Measured XM Radio Signals Option*

PROSIM has an option customized for the simulation of XM Radio signals. The user can choose between 19 different propagation scenarios, with or without AGC, as discussed below.

3.4.4.1 AGC XM Radio Scenarios

In the case of an AGC scenario, the PROSIM simulated signal gives good statistical agreement with the measured signal. The propagation constants of each measured signal are stored into PROSIM. Hence, every time the user chooses one of the AGC XM Radio scenarios, a signal is simulated with the stored propagation constants, and the statistics of the measured and simulated signals are displayed for Roll and Rock satellite. The data processing relative to the AGC measurements, and the description of each PROSIM scenario are detailed in Chapters 4, 5 and 6.

3.4.4.2 non-AGC XM Radio Scenarios

In the case of non-AGC XM Radio scenarios, the PROSIM signal simulated from the stored extracted propagation constants is not in good agreement with the measured signal. So, the non-AGC measurements display a comparative study of the statistics of the signals received from both satellites. Also, the fading correlation is investigated. The data processing relative to the non-AGC measurements, the description of the correlation study and explanations for the failure of PROSIM in the non-AGC case are detailed in Chapters 4, 5 and 6.

Chapter 4

Validation of PROSIM: XM Radio Propagation Measurements Campaign

4.1 Introduction

The PROSIM simulator was validated by Suh and Stutzman [15] based on data from a measurement campaign conducted by Goldhirsh and Vogel [18] at the UHF frequency band. However, no study has been conducted to validate PROSIM at S-band. To extend the validity of PROSIM to S-band, the Virginia Tech Antenna Group conducted a measurement campaign based on the XM Radio signals. The measurement campaign is described in the following sections.

4.2 Description of the XM Radio System

4.2.1 *The Digital Audio Radio Satellite (DARS) Service*

The Digital Audio Radio Satellite (DARS) service proposes to provide nationwide radio programming with compact disc quality sound via satellite. DARS is the solution to expand radio choice for rural population which is often underserved by terrestrial broadcasters, and to target niche audience with specialized programming. The Federal Communications Commission (FCC) allocated 25 MHz of spectrum to DARS, between 2320 and 2345 MHz. On April 1, 1997, the Commission conducted auctions for two DARS licenses [19]. The first license, from 2320 to 2332.5 MHz was won by Sirius Satellite Radio [20], and the second one from 2332.5 to 2345 MHz was won by XM Radio [21]. In this study, we will focus on to the XM Radio DARS system.

4.2.2 *Overview of the XM Radio System*

The XM Radio DARS (Digital Audio Radio Satellite) system employs two geostationary satellites to cover the North American subcontinent. The first satellite, referred as 'Roll' is positioned 85º W ±0.1º longitude, and the second satellite, referred as 'Rock' is positioned at 115º W ±0.1º longitude. The XM DARS satellites 'Rock' and

'Roll' are observed respectively at elevation angles of 34º and 47º from the horizon when viewed from Blacksburg, Virginia, located at 80.41º W and 37.22º N.

The XM Radio system broadcasts in the S-band frequency spectrum, from 2332.5 to 2345 MHz. Table 4.2-1 summarizes the frequency bands and the center frequencies dedicated to the XM DARS satellite-to-ground transmissions. The specifications of the system are described in the "XM Radio DARS (Digital Audio Radio Satellite) Specifications" provided by General Motors under a nondisclosure agreement. The XM Radio frequency spectrum is divided into six frequency slots: four slots have 1.84 MHz bandwidth and are dedicated to satellite-to-ground transmission, and the remaining two slots have 2.53 MHz bandwidth and are dedicated to terrestrial transmission. The measurement campaign focuses on the four satellite-to-ground frequency slots.

Table 4.2-1 Frequency bands and center frequencies for the satellite-to-ground transmission in the XM Radio DARS system.

Frequency Slot in DARS Spectrum	Frequency Band (MHz)	Center Frequency (MHz)
Satellite 1 (Roll) A	2332.545 – 2334.385	2333.465
Satellite 2 (Rock) A	2334.385 – 2336.225	2335.305
Satellite 2 (Rock) B	2341.285 – 2343.125	2342.205
Satellite 1 (Roll) B	2343.125 – 2344.965	2344.045

4.2.3 *The XM Radio Receiver*

The XM Radio DARS satellite signals (specified in Table 4.2-2) are received using an antenna module with omni-directional coverage over all azimuth angles and 20º to 60º coverage for satellite reception in elevation. The G/T specifications for the antenna are –20 dB/K in clear sky and –22 dB/K in shadowed environment. The LNA in the antenna module offers a gain of 22 dB. The general specifications of the XM Radio receiver are shown in Table 4.2-2.

Table 4.2-2 General specifications of the XM Radio receiver. For the purpose of the study, only the satellite channels performance requirements are listed.

Antenna G/T specifications	• -20 dB/K (clear sky) • -22 dB/K (shadowed environment)
RF Tuner processing loss	1 dB
Channel decoder processing loss	1.5 dB
Receiver gain	3.1 dB (antenna gain)
LNA gain (antenna module)	22 dB
Satellite Minimum RF signal level into tuner	-85 dBm
Satellite Maximum RF signal level into tuner	-55 dBm
Antenna coverage	• Omni-directional over the azimuth • 20° to 60° for satellite reception in elevation
Switching time performance	< 6 ms
Quality of Service	Excellent
Operating Temperature range	-40 to 85 °C
Eb/No (dB) – High SNR, Single and Dual satellite channels	15 dB
Eb/No (dB) – Low SNR, Single and Dual satellite channels	6.2 dB
Eb/No (dB) – Low SNR with diversity combining, Dual satellite channels	1.9 dB
Modulation	QPSK

In the XM Radio receiver, the signals received from the satellites are first downconverted to the IF center frequency of 114.655 MHz. Then, as shown in Figure 4.2-1, they are further downconverted to a second IF center frequency of 6.095 MHz. Note that the IF center frequencies shown on Figure 4.2-1 are calculated as the center frequencies of the two adjacent 1.84 MHz wide bands (center frequency of Block A slots or Block B slots). Table 4.2-3 summarizes the downconversion of the Block A signals received from XM DARS satellites ‘Rock’ and ‘Roll’. Similarly, Table 4.2-4 summarizes

the downconversion of the Block B signals received from XM DARS satellites 'Rock' and 'Roll'.

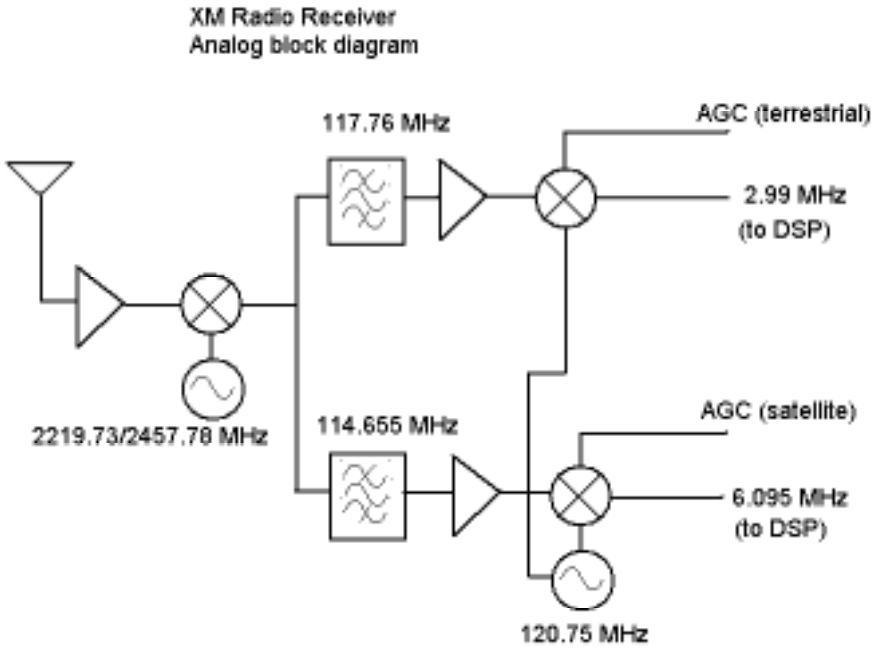

Figure 4.2-1 Block diagram of the front-end of XM Radio receiver.

Table 4.2-3 Block A received signal frequency bands and IF center frequencies for signals transmitted by XM DARS satellites 'Rock' and 'Roll'.

Signal Frequency slot Block A	**Satellite 1: Roll**	**Satellite 2: Rock**
Received signal Frequency Band (MHz)	2332.545 – 2334.385	2334.385 – 2336.225
Received signal Center Frequency (MHz)	2333.465	2335.305
First IF Signal Band (MHz) LO = 2219.73 MHz	112.815 – 114.655	114.655 – 116.495
First IF Center Frequency (MHz)	113.735	115.575
Second IF Signal Band (MHz) LO = 120.75 MHz	6.095 – 7.935	4.255 – 6.095
Second IF Center Frequency (MHz)	7.015	5.175

Table 4.2-4 Block B received signal frequency bands and IF center frequencies for signals transmitted by XM DARS satellites 'Rock' and 'Roll'.

Signal Frequency slot Block B	**Satellite 1: Roll**	**Satellite 2: Rock**
Received signal Frequency Band (MHz)	2343.125 – 2344.965	2341.285 – 2343.125
Received signal Center Frequency (MHz)	2344.045	2342.205
First IF Signal Band (MHz) LO = 2457.78 MHz	112.815 – 114.655	114.655 – 116.495
First IF Center Frequency (MHz)	113.735	115.575
Second IF Signal Band (MHz) LO = 120.75 MHz	6.095 – 7.935	4.255 – 6.095
Second IF Center Frequency (MHz)	7.015	5.175

For the measurement campaign, a commercial XM Radio receiver was modified and the second IF output of the XM receiver connected to a Spectrum Analyzer to observe distinct 1.84 MHz bands. However, no guard band between the satellite signals was discernible. In addition, since the DSP inside the XM Radio receiver is unknown, it is not possible to determine which slots between Block A and Block B are observed: the DSP algorithm implemented in the receiver selects the stronger signal for each satellite between Block A and Block B, and no indication is given about which block is selected.

The gain of the IF amplifiers is controlled by an AGC loop imbedded in the DSP board of the XM Radio receiver. To perform propagation measurements, it becomes necessary to either break the AGC loop in receiver (preferred) or record the AGC voltages to correct for the effects of the AGC on the gain of the system. AGC voltages ranges from 0.5 V to 2.0 V corresponding to XM Radio receiver IF gain of respectively 80 dB and 30 dB. Figure 4.2-2 summarizes the signal power at the output of XM Radio receiver IF satellite port at 5.175 MHz (Rock satellite) for a -75 dBm signal level at the input to the receiver at 2335.305 MHz. Note that the AGC response is quite linear in the range of its operation. For the propagation analysis, measurements are performed with and without AGC. In the case where measurements are performed 'without AGC', the AGC pin in the XM Radio receiver is disconnected and a fixed voltage of 1.57 Volts is

provided to achieve optimum performance in clear sky conditions at Blacksburg, Virginia. The results of these measurements will be further detailed in Chapter 6.

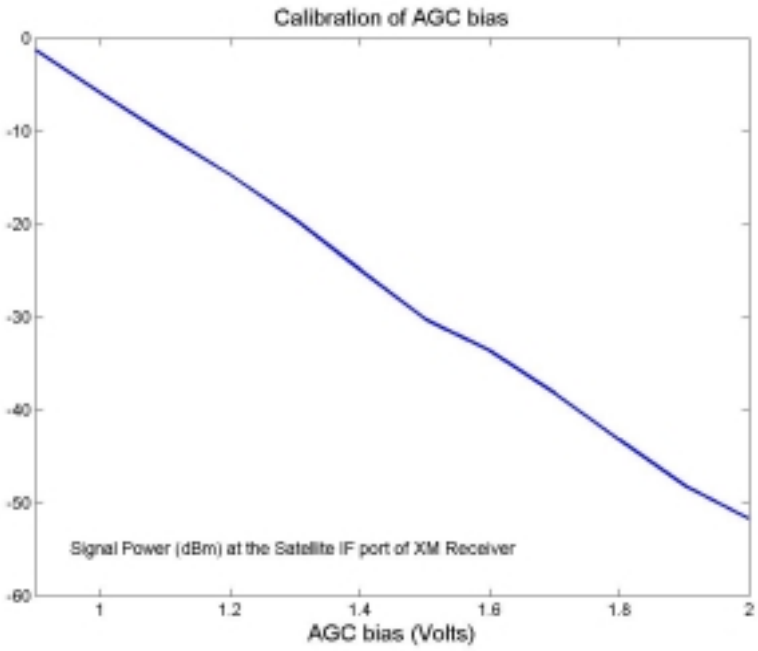

Figure 4.2-2 Signal power at the output of XM Radio receiver IF Satellite port at 5.175 MHz (Rock satellite) for –75 dBm input to the receiver at 2335.305 MHz with resolution BW = 30 kHz.

The output of the second IF from the XM Radio receiver, centered at 5.175 MHz for Rock satellite and 7.025 MHz for Roll satellite, is used as an input to the Virginia Tech Antenna Group IF Propagation receiver, VIPR. The VIPR was designed and built at Virginia Tech Antenna Group to investigate the satellite-to-ground propagation characteristics and is explained in details in the next section.

4.2.4 *The Virginia Tech Antenna Group IF Propagation Receiver (VIPR)*

The Virginia Tech Antenna Group IF Propagation Receiver (VIPR) was designed and built to investigate the satellite-to-ground propagation characteristics of the XM Radio signals. First, the XM signals centered at 5.175 MHz and 7.025 MHz at the output of the second IF XM receiver are buffered and split using a 3 dB power divider. Then, two band pass filters (BPF) built using passive L/C components are used to separate the two satellite signals at the output of the buffer as shown in Fig.4.2-3. Once filtered, the power from each satellite channel is measured using a power detector. The power detector consists of a logarithmic amplifier (Analog Devices AD 8361) and a DC buffer amplifier. The output is a DC voltage proportional to the input power in dBm.

The S_{21} parameters of the band pass filters were measured using a network analyzer. Since there is no guard band between the slots of the satellites signals, the band pass filters require steep skirts (i.e. high order filters) to separate the power between the two channels. Figure 4.2-4 shows the S_{21} filter response of the band pass filter with center frequency 5.175 ~ 5.22 MHz (Rock satellite). Note that this band pass filter has 7.2 dB insertion loss at center frequency and a BW_{3dB} = 675 kHz. Similarly, the S_{21} filter response of the band pass filter with center frequency 7.025 ~ 7.000 MHz (Roll satellite) is shown in Figure 4.2-5. This filter has narrow 3 dB bandwidth of BW_{3dB} = 528 kHz. The insertion loss at the center frequency of 7.00 MHz was recorded to be 11.5 dB.

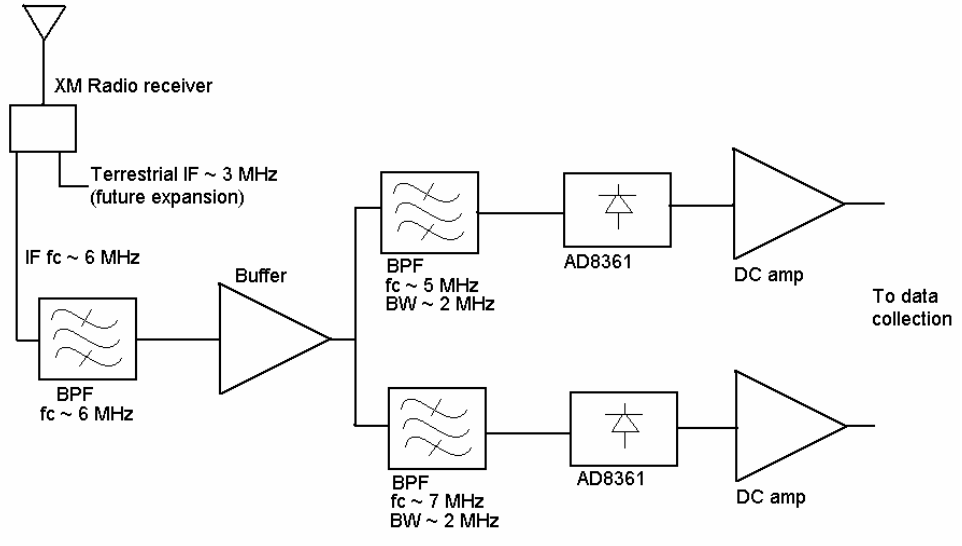

Figure 4.2-3 Block diagram of VTAG IF Propagation Receiver (VIPR).

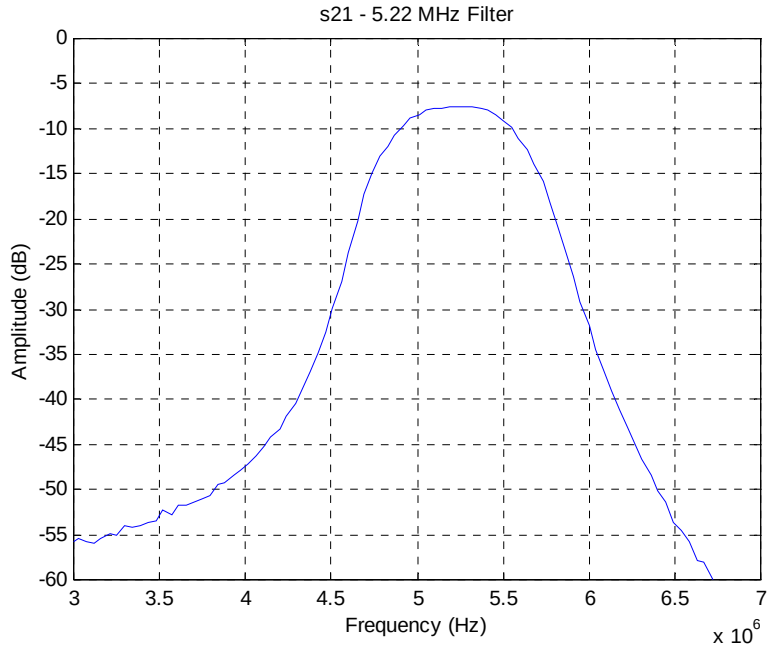

Figure 4.2-4 Band Pass Filter Characterization with center frequency 5.22 MHz. Measured 3 dB beamwidth is 675 kHz . Insertion loss at center frequency is –7.2 dB.

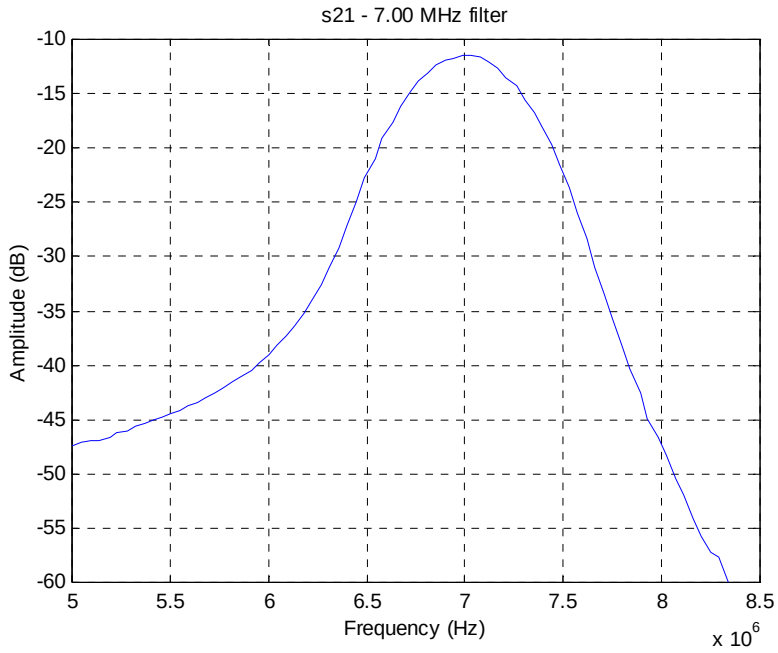

Figure 4.2-5 Band Pass Filter Characterization with center frequency 7.00 MHz. Measured 3 dB beamwidth is 528 kHz . Insertion loss at center frequency is –11.5 dB .

The AD8361 log amplifier power detector is not well characterized below 10 MHz. In order to insure the accuracy of the measurements, the combination of band pass filters centered at 5.175 MHz and 7.025 MHz and AD8361 power detectors were calibrated as a system to evaluate their performance. The calibration of the BPF with f_c = 5.22 MHz combined with the power detector is shown by solid line in Figure 4.2-6. Note that the band pass filter with f_c = 7.00 MHz offered an insertion loss of 4.3 dB more than the BPF with f_c = 5.22 MHz. Compensating for this offset of 4.3 dB, a new curve for the response of BPF with f_c = 7.00 MHz is shown in Figure 4.2-6.

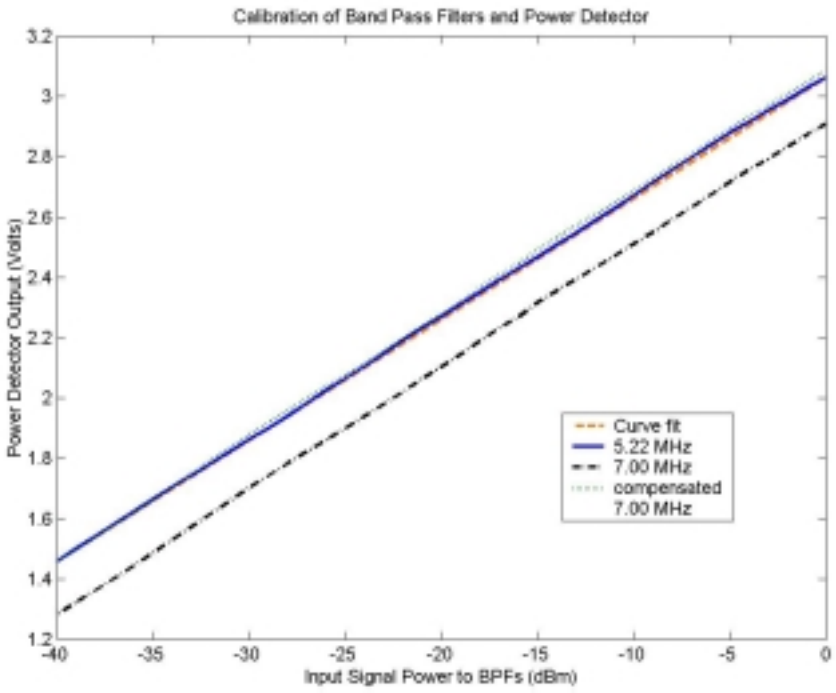

Figure 4.2-6 Calibration of the BPFs combined with the power detectors. The response of the BPF with f_c = 7.00 MHz is compensated for its high insertion loss and a curve fit is displayed.

4.2.5 *The Data Acquisition Interface*

The output of the log amplifier/power detectors provides us with a measure of the signal level from each satellite. The signal level measurement from the power detectors is captured every 0.5 millisecond using a 12-bit PCMCIA data acquisition card. Some features of the data acquisition card are summarized in Table 4.2-5.

Table 4.2-5 Salient features of 12-Bit data acquisition PCMCIA card.

Sampling over all Channels	100 kilo samples/sec (maximum)
Analog input Resolution	12-Bit
Analog Inputs	16 single-ended, 8 differential
Programmable Gain	0 dB, 3 dB, 6 dB and 9 dB
External clock source	24 Bit pacer clock

The output of each of the two power detectors is scanned at 2 kHz (every 0.5 millisecond) to instantaneously capture the signal power. The measured signal strength available from each of the two channels is stored in a binary file that is read later to analyze the fade behavior. Calibration of the complete system from the antenna module to the data acquisition system was performed. Results of this calibration are given in Table 4.2-6.

Table 4.2-6 Calibration of the complete system from the antenna module to the data acquisition system with AGC = 1.57 V.

Signal Gen. to the I/P of XM Receiver (dBm)	Estimated Signal Power at the O/P Antenna Module (dBm)	Receiver IF O/P at 5.22 MHz (dBm)	Receiver IF O/P at 7.00 MHz (dBm)	Power Detector O/P for 5.22 MHz (V)	Power Detector O/P for 7.00 MHz (V)
-51	-73	5.0	5.7	3.5	3.43
-56	-78	0.4	0.7	3.29	3.23
-61	-83	-5.2	-4.0	3.08	3.03
-66	-88	-9.3	-9.0	2.89	2.83
-71	-93	-14.5	-14.2	2.66	2.61
-76	-98	-19.5	-19.2	2.47	2.41
-81	-103	-24.1	-23.8	2.25	2.20
-86	-108	-29.2	-28.6	2.05	2.00
-91	-113	-34.6	-33.9	1.83	1.79
-96	-118	-39.2	-38.6	1.69	1.64
-101	-123	-43.6	-42.9	1.61	1.56
-106	-128	-47.6	-47.2	1.58	1.52
-111	-133	noise	noise	1.57	1.51

4.3 The Measurement Campaign

4.3.1 *Description of the Measurement Procedure*

For each vehicle course, the vehicle speed was kept constant. The XM Radio antenna was positioned in the center of the car's roof, and the VTAG measurement system was operated from within the car. Each measurement was conducted with AGC and then the same vehicle course was repeated without AGC. The measurement system operator ensured that the acquisition of the signals started and stopped at the same spatial reference to ensure further comparison of the measurements courses.

4.3.2 *Description of the Measurement Sites*

Table 4.3-1 Summary of measurement scenarios and road characteristics.

Route designator	**Environment description**
Route114WEST1 Route114EAST3	Straight road. Mostly unshadowed. Isolated single tree lines. Open fields (yards+houses)
Route114WEST2 Route114EAST2	Straight road. Discontinuous parallel tree lines (2 to 4). Moderate tree height. Some yards and houses. Rare overhanging branches
Route114WEST3 Route114EAST1	Long continuous dense vegetation events with occasional overhanging branches. Some high trees.
Route11NORTH1 Route11SOUTH2 Route11NORTH2 Route11SOUTH1	Multiple curve road. Hills with forests. Cliff (Route11NORTH1 and Route11SOUTH2). Vegetation on opposite sides non proportional
Route11bisNORTH1 Route11bisSOUTH2 Route11bisNORTH2 Route11bisSOUTH2	Straight road. Very regular continuous forest on both side of the road. Moderate height.
Route460EAST Route460WEST	Line of sight. Two bridges. 4-lane (2 lanes in each direction)
Route723NORTH Route723SOUTH	Multiple curve road. Hills with moderate height vegetation. Vegetation on opposite sides non proportional
SALEMStr FRANKLINStr CHURCHStr	Downtown Roanoke. Urban environment (2 to 3 story buildings). Speed of 15 mph. No AGC. One to two blocks long

Table 4.3-1 summarizes the environment description for each PROSIM scenario in the measurement campaign. The XM Radio measurement campaign was conducted in the Blacksburg/Christiansburg/Radford VA area. The focus was performed on two routes, Route 114 and Route 11, going East/West from Radford to Christiansburg. These roads are highlighted on the map of this area in Figure 4.3-1. These two routes have several measurements advantages:

- Light traffic load and low speed limit ensure an easier and safer way to keep a constant vehicle speed

- Diversity of the driving environment with multiple shadowing scenarios

- East/West orientation for fading correlation study between the two satellites

Additional measurements were taken along Route 460 and Route 723, two North/South oriented roads shown on the map in Figure 4.3-2. Also, some measurements were taken in downtown Roanoke, VA, for examples of urban propagation.

The reader should notice that Route 11 is referred to as Route 11 North or South, because of the official highway designation but for the section where the measurements were performed, the road is actually East/West oriented. The measurement campaign uses the North/South description, where North designated direction is actually East and South direction is actually West. In the same way, Route 460 is referred to as Route 460 East or West, although it is North/South oriented. Here again, the East/West description is used, where East designated direction is actually South and West is actually North.

For analysis purpose, the measurement runs along each road were divided into approximately one-minute long PROSIM scenarios. This way, each scenario presents a typical environment that can be studied statistically. Also, the data processing time is reduced.

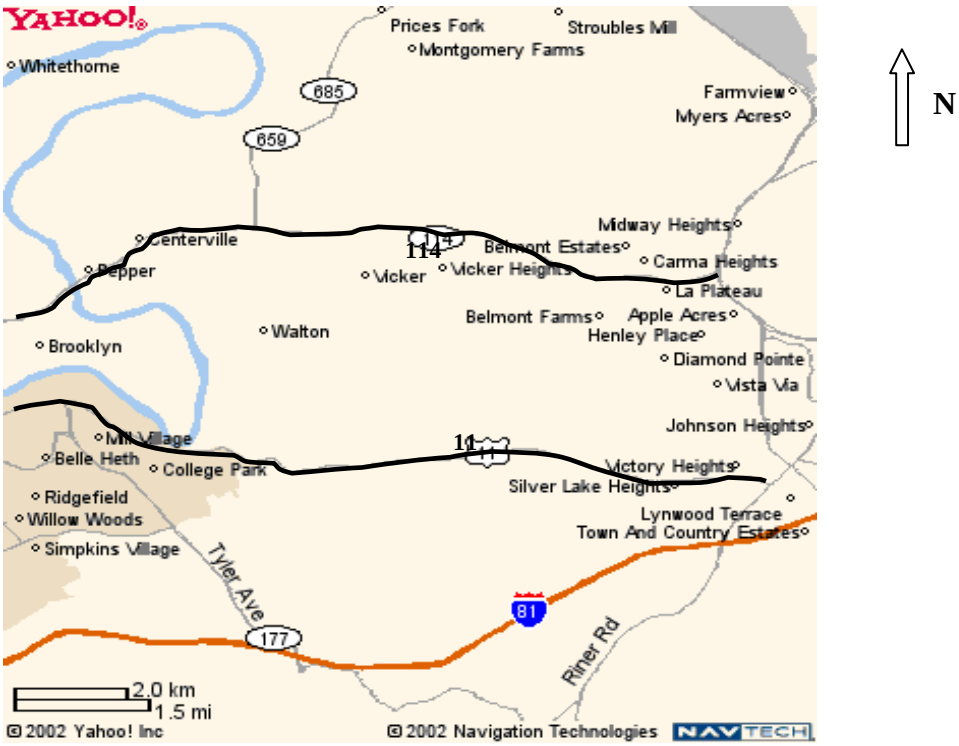

Figure 4.3-1 Map of the measurement routes: Route 114 and Route 11, between Christiansburg and Radford, VA. For Route 11, the North designated direction is actually East and the South designated direction is actually West.

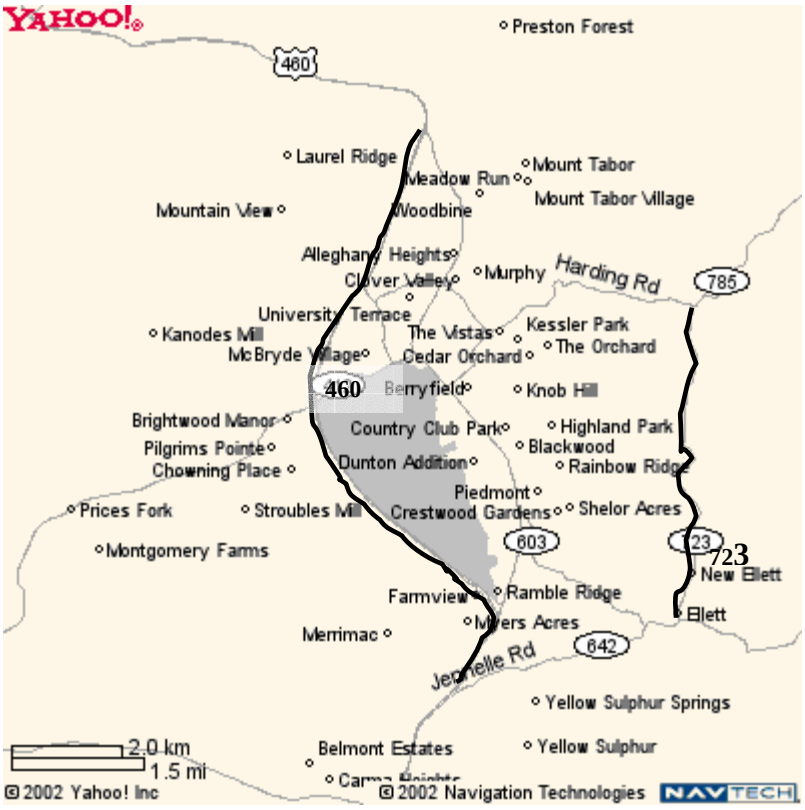

Figure 4.3-2 Map of the measurements routes: Route 460 from Blacksburg to Christiansburg, VA, and Route 723. For Route 460, the East designated direction is actually South and the West designated direction is actually North.

4.3.2.2 The Route 114 Course

Route 114 is an East/West two-lane connection between the New River Valley Mall and the town of Radford. Measurements were taken in both directions (West and East), with AGC, and then without AGC. For analysis purposes, the measurement courses along the road were divided into three PROSIM scenarios, corresponding to approximately one minute of the total travel time for each: Route114EAST1, Route114EAST2 and Route114EAST3.

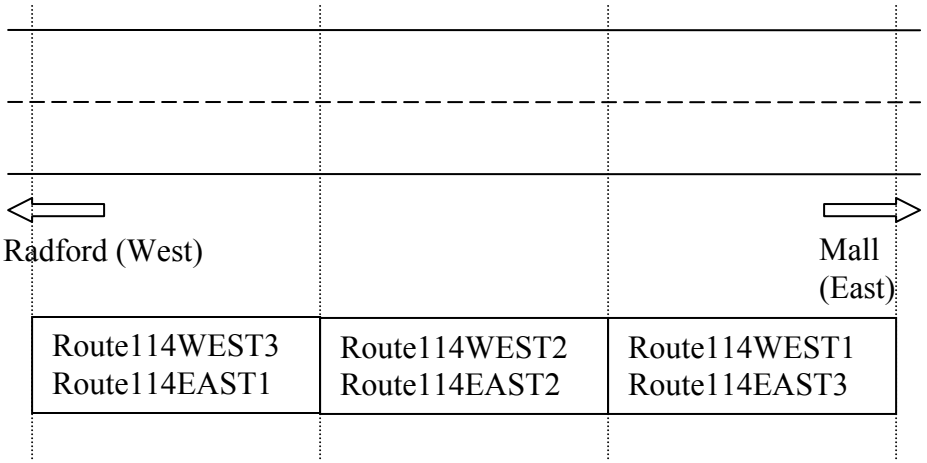

Figure 4.3-3 Diagram of a portion of Route 114 PROSIM scenarios showing the data sets.

Since the measurements were conducted in both East and West directions, the PROSIM user also has access to the West scenarios: Route114WEST1, Route114WEST2 and Route114WEST3. One should notice that Route114WEST1 approximately corresponds to the same portion of Route 114 than Route114EAST3, as well as Route114WEST2 corresponds to Route114EAST2 and Route114WEST3 corresponds to Route114EAST1. However, the propagation results for corresponding scenarios can be different since the vehicle was traveling on different sides of the road and hence the satellite signals undergo different shadowing events. Figure 4.3-3 summarizes the portion of the road for the different scenarios.

4.3.2.1.1 The Route114WEST1 and Route114EAST3 Courses

Route114WEST1 and Route114EAST3 scenarios are mainly line-of-sight scenarios. This portion of the road is straight, and mostly unshadowed. There are some yards and houses bordering the road, as well as isolated single tree lines. Figure 4.3-4 shows a typical clear LOS measurement environment on this road, while Figure 4.3-5 shows a shadowed portion along this route. A typical shadowing event for these scenarios is showed on Figure 4.3-6.

Figure 4.3-4 Photo taken eastward towards the New River Valley mall, close to the mall. A typical LOS environment for Route114WEST1 and Route114EAST3 scenarios.

Figure 4.3-5 Route114WEST1 and Route114EAST3 scenarios: typical shadowed portion of the road. The photo is taken westward towards Radford, at a point located at the end of Route114WEST1 course.

Figure 4.3-6 Route114WEST1 and Route114EAST3 scenarios: the typical shadowing events are single isolated tree lines.

4.3.2.1.2 The Route114WEST2 and Route114EAST2 Courses

Route114WEST2 and Route114EAST2 courses correspond to moderately shadowed environments. Here, the road is also straight, and is bordered with discontinuous parallel tree lines (2 to 4 lines) of moderate height. In rare instances, some branches slightly overhang on the road. There are still some unshadowed portions, with houses and yards. Figure 4.3-7 represents a typical environment for this portion of the road, while Figure 4.3-8 shows a typical shadowing event, with slight overhanging branches.

Figure 4.3-7 Route114WEST2 and Route114EAST2 scenarios: typical measurement environment. The photo is taken eastward towards the New River Valley mall, at a point approximately in the middle of the courses.

Figure 4.3-8 Route114WEST2 and Route114EAST2 scenarios: the typical shadowing events are discontinuous parallel tree lines (2 to 4) with moderate tree height and rare overhanging branches.

4.3.2.1.3 The Route114WEST3 and Route114EAST1 Courses

In Route14WEST3 and Route14EAST1 courses, the roadside is lined by long continuous dense tree lines of moderate height. From time to time, higher shadowing event occur, along with branches overhanging up to the middle of the lane. Figure 4.3-9 represents a typical environment for this portion of the road. Figure 4.3-10 shows a typical shadowing event, with overhanging branches.

Figure 4.3-9 Route114WEST3 and Route114EAST1 scenarios: typical measurement environment. The photo is taken westward towards Radford, at a point approximately in the middle of the courses.

Figure 4.3-10 Route114WEST3 and Route114EAST1 scenarios: the typical shadowing events are long continuous dense vegetation events with occasional overhanging branches.

4.3.2.2 The Route 11 Course

Two sets of measurements were conducted on Route 11, corresponding to completely different environments. The first portion of Route 11 from Radford to Christiansburg presents has several curves and is referred as Route11 in PROSIM scenarios, whereas the second portion of the road is straight and is referred as Route11bis. As with Route 114, measurements were conducted in both East and West direction, with and then without AGC.

4.3.2.2.1 The Route11 Scenarios: Route11NORTH1, Route11NORTH2, Route11SOUTH1, Route11SOUTH2

Route11 scenarios correspond to the meandering section of Route 11. For PROSIM analysis, the measurements were divided in two portions: the first portion gives Route11NORTH1 course and Route11SOUTH2 course, whereas the second portion of the road is studied in Route11NORTH2 and Route11SOUTH1courses.

For all these courses, the environment is predominately shadowed, since the road is in a mountainous landscape; hills are covered with dense and high vegetation border both sides of the road. At the beginning of the route, corresponding to Route11NORTH1 and Route11SOUTH2 PROSIM scenarios, the main shadowing event is a cliff, topped with trees. An interesting characteristic of these scenarios is the diversity of shadowing events: there can be excessive shadowing on the South side of the road, and minimal shadowing on the North side (and vice-versa). Figure 4.3-11 shows the cliff for Route11NORTH1 and RouteSOUTH2, while Figure 4.3-12 shows a typical environment for Route 11 scenarios. Figures 4.3-13 and 4.3-14 are examples of two typical shadowing events for Route 11.

Figure 4.3-11 Route11NORTH1 and RouteSOUTH2 scenarios: the typical shadowing event for these scenarios is a cliff on the North side of the road. The photo is taken eastwards towards Christiansburg, at the beginning of the Route11NORTH1 course.

Figure 4.3-12 Route11 scenarios: the typical environment for the Route11 scenarios is a multiple curve road that travels in the middle of hills covered with forest. The photo is taken eastward towards Christiansburg, at a point approximately in the middle of the Route11NORTH2 course.

Figure 4.3-13 Route11 scenarios: The typical shadowing event is dense forest covering hills. The vegetation on opposite side of the road is sometimes non proportional.

Figure 4.3-14 Route11 scenarios: another example of shadowing event. The typical shadowing event is dense forest covering hills. The vegetation on opposite side of the road is sometimes non proportional.

4.3.2.2.2 The Route11bis Scenarios: Route11bisNORTH1, Route11bisNORTH2, Route11bisSOUTH1, Route11bisSOUTH2

A second set of measurements was conducted on Route11, and is referred to as Route11bis in PROSIM scenarios. Once again, the runs were divided in two portions for analysis purposes. Since the road was traveled in both directions, 4 PROSIM scenarios are obtained: Route11bisNORTH1, Route11bisNORTH2, Route11bisSOUTH1, and Route11bisSOUTH2. For all scenarios, the road was straight, with dense forest of moderate height on both sides. The vegetation was very uniform all along the road, except for some fields and houses for scenarios Route11bisNORTH2 and Route11bisSOUTH1. Figure 4.3-15 shows a typical environment for Route11bis scenarios.

Figure 4.3-15 Route11bis scenarios: The typical environment is a straight road with very continuous forest on both sides of the road. The vegetation height is moderate. The photo is taken westwards towards Radford, at the end of the Route11bisNORTH2 course.

4.3.2.3 The Route 460 Course

Route 460 travels North/South between Blacksburg and Christiansburg. There are few shadowing events along this route. Two bridges cross it, providing some fading events typical of high capacity roads in urban and suburban areas. The measurements for this route were relatively short, thus there are only two PROSIM scenarios: Route460EAST and Route460WEST. Figure 4.3-16 shows a typical environment for the Route 460 course.

Figure 4.3-16 Route 460 scenarios: the typical environment is a four-lane straight highway with light and low vegetation on the side. Thus, the propagation along this course is typically unshadowed. The photo was taken southward towards Christiansburg, at the beginning of the Route460EAST scenario.

4.3.2.4 Additional Measurements: The Route 723 Course and Downtown Roanoke Measurements

Additional measurements were taken along the middle section of Route 723, to study the near-far effect of roadside tree attenuation. As shown in Figure 4.3-2, Route 723 is North/South oriented. The section of the road presents large curves, with more vegetation on the South side of the road than on the North side of it. The typical shadowing event is hills covered with moderate height vegetation. A constant speed of 30 mph was maintained for each measurement run. Since the measurement runs for this route were relatively short, there are only two corresponding PROSIM scenarios: Route723NORTH and Route723SOUTH.

Then, measurements were taken in a downtown Roanoke, VA, urban environment. For those measurements, the speed was maintained constant at 15 mph, and the AGC was turned off. Because of traffic lights, each measurement run is only one or

two blocks long. Three streets were chosen for measurements, all East/West oriented: Franklin St., Church St. and Salem St. The corresponding PROSIM scenarios are FRANKLINStr, CHURCHStr and SALEMStr.

4.4 Data Processing

4.4.1 *Reading the Binary Files*

Once a data record is acquired, it is converted to a binary file. The format for the binary file name was 'road_direction_agc option_date.bin'. Since each record contains a large number of data points, reflecting different successive shadowing event scenarios, it was decided to divide the records is smaller segments, as discussed in Section 4.3.2. Most segments correspond to approximately one minute of recording time. However, the downtown Roanoke measurements are shorter due to the urban traffic and traffic lights. Since the vehicle speed can be different from one scenario to the other, the distance traveled for each scenario varies. Table 4.4-1 gives the name of the original binary files for the different VTAG PROSIM propagation scenarios, with AGC, and the distance traveled for each scenario. Table 4.4-2 gives the same results for the measurements without AGC.

Table 4.4-1 VTAG PROSIM scenarios, distance traveled and initial binary file names for AGC measurements.

VTAG PROSIM propagation scenario (AGC measurements)	**Speed in mph/ Distance traveled in meters/Distance traveled in wavelength**	**Initial binary file**
Route114EAST1	40 / 1697.2 / 9886	Route114_east_agc_sep1.bin
Route114EAST2		
Route114EAST3		
Route114WEST1	40 / 1716.2 / 13330	Route114_west_agc_sep1.bin
Route114WEST2		
Route114WEST3		
Route11NORTH1	40 / 1158.5 / 8997	Route11_north_agc_sep1.bin
Route11NORTH2		
Route11SOUTH1	40 / 1305.1 / 10136	Route11_south_agc_sep1.bin
Route11SOUTH2		
Route11bisNORTH1	40 / 1106.6 / 8594.5	Route11_north_straight_agc_sep1.bin
Route11bisNORTH2		
Route11bisSOUTH1	40 / 1138.8 / 8844.5	Route11_south_straight_agc_sep1.bin
Route1bisSOUTH2		
Route460EAST	40 / 3543.3 / 27519	Route460_east_agc_sep13.bin
Route460WEST	40 / 3561.2 / 27659	Route460_west_agc_sep13.bin
Route723NORTH	30 / 1252.3 / 9726	Route723_north_agc_oct14.bin
Route723SOUTH	30 / 1137 / 8830.5	Route723_south_agc_oct14.bin

Table 4.4-2 VTAG PROSIM scenarios, distance traveled and initial binary file names for non-AGC measurements.

VTAG PROSIM propagation scenario (AGC removed)	Speed in mph/ Distance traveled in meters/Distance traveled in wavelength	Initial binary file
Route114EAST1	40 / 1725.8 / 13404	Route114_east_sep1.bin
Route114EAST2		
Route114EAST3		
Route114WEST1	40 / 1743.6 / 13542	Route114_west_sep1.bin
Route114WEST2		
Route114WEST3		
Route11NORTH1	40 / 1283.6 / 9969.5	Route11_north_sep1.bin
Route11NORTH2		
Route11SOUTH1	40 / 1303.3 / 10122	Route11_south_sep1.bin
Route11SOUTH2		
Route11bisNORTH1	40/ 1169.2 / 9080.5	Route11_north_straight_sep1.bin
Route11bisNORTH2		
Route11bisSOUTH1	40 / 1097.7 / 8525.5	Route11_south_straight_sep1.bin
Route1bisSOUTH2		
Route460EAST	40 / 3554 / 27603	Route460_east_sep13.bin
Route460WEST	40 / 3571.9 / 27742	Route460_west_sep13.bin
Route723NORTH	30 / 1187.9 / 9226	Route723_north_oct14.bin
Route723SOUTH	30 / 1134.3 / 8809	Route723_south_oct14.bin
SALEMStr	15 / 174.27 / 1353.5	SalemJeff2firstsept2502.bin
FRANKLINStr	15 / 341.84 / 2655	Franklinfirsttothirdsept2502.bin
CHURCHStr	15 / 132.68 / 1030.5	Churchwest2Jeffsept2502.bin

The binary files contain the value of the amplitude of the signal received at the output of the VTAG measurement system (that is, at the output of the power detector). These values are encoded with 16 bits. Since we acquire two channels simultaneously (Roll and Rock signals), the binary record contains a Roll sample coded with 16 bits followed by the simultaneous Rock sample coded with 16 bits. During all the measurement campaign, the sampling rate was set to 2 samples/ms. Hence, each channel is sampled every 0.5 ms, which correspond to one sample every 0.0684 wavelength at a vehicle speed of 40 mph, one sample every 0.0521 wavelength for a vehicle speed of 30 mph, and one sample every 0.026 wavelength for a vehicle speed of 15 mph.

4.4.2 *Conversion to LOS Power Level*

The acquisition software does not store the real values of the received voltage, but encoded values of this voltage, depending on the calibration of the acquisition system, and the digitalization of the analog signal. In the XM Radio measurement campaign, the values read from the binary files are scaled to obtain the received signal voltage by a factor of 32767/5, using equation:

$$A\_exp1=A\_m/(32767/5) \tag{4.4-1}$$

where A_m is the value stored in the binary file and A_ exp1 is the corresponding output voltage level. The scaling factor was provided by the designers of the acquisition card, and depends on the acquisition parameters (number of channels, and calibration of each channel).

The restored voltage is the received voltage level at the output of the power detector of the VTAG IF receiver. However, the propagation modeling should not take into account the receiving system, and the different power losses and gains that it induces. The relevant signal level is the one at the input of the receiving system at the output of the antenna module: the signal strength at this point corresponds to the strength of the signal received by an XM Radio. By calibrating the receiver, we obtained the signal power at the output of the antenna module in dBm for various voltage levels at the output of the power detector for each satellite. These results are summarized in Table 4.4-3. The calibration reveals that an almost linear relation exists between the input and output signal levels. Applying a linear regression for each satellite gives

$$\begin{aligned} &A\_dBm=24.3931*A\_exp1-156.6636, \text{ for Roll satellite} \\ &B\_dBm=24.1565*B\_exp1-157.2064, \text{ for Rock satellite,} \end{aligned} \tag{4.4-2}$$

where A_dBm is the input power level in dBm for Roll, and A_exp1 is the acquired signal voltage at the output of the receiver. From this calibration curve and formula, we can obtain both the amplitude and the power of the received signal in dB.

Table 4.4-3 Estimated signal power received at the input of the antenna module for various values of the VTAG IF receiver power detector output, for each satellite.

Estimated Signal Power at the O/P Antenna Module (dBm)	Power Detector O/P for 5.22 MHz (V) Rock satellite	Power Detector O/P for 7.00 MHz (V) Roll satellite
-73	3.5	3.43
-78	3.29	3.23
-83	3.08	3.03
-88	2.89	2.83
-93	2.66	2.61
-98	2.47	2.41
-103	2.25	2.20
-108	2.05	2.00
-113	1.83	1.79
-118	1.69	1.64
-123	1.61	1.56
-128	1.58	1.52
-133	1.57	1.51

The next step of the data processing is the normalization of the signal to the LOS signal; the LOS component is assumed to be the mean of the received signal. Hence, the total signal is divided by its mean so that we have a final signal with amplitude relative to a 0 dB LOS, compatible with PROSIM simulations.

Chapter 5

Validation of the Experiment Procedure and Extraction of the Propagation Constants

5.1 Validation of the Experiment Procedure

After the experiment hardware and software were developed, experiments were conducted to validate the operation of the system and to verify its calibration. The tests focused on the sampling rate of the signals, and the repeatability of the measurements.

5.1.1 *Sampling Rate Influence*

The first aspect of validation of the data collected is to ensure the adequacy of the sampling rate. The sampling rate is based on the signals spectral content. From a spectral point of view, the bandwidth of the signal is determined by the maximum Doppler shift frequency. The signal, including all the multipath components, is contained in a bandwidth

$$B = f_d = \frac{v}{\lambda} = \frac{(40*1609/3600)}{\left(3*10^8/(2.33*10^9)\right)} = \frac{17.8778}{0.1288} = 138.8 \text{ Hz} \qquad (5.1\text{-}1)$$

where the following experiment parameter were used: v = 40 mph or 17.8778 m/s, and λ = 0.1288 m.

Therefore, the sampling rate has to be at least 2*138.8= 277.6 Hz in order to meet the Nyquist criteria of twice the highest frequency component of the signal. For the measurement campaign, the sample rate 2 samples/ms, or 2 kHz, was used which should be fast enough to capture all the spectrum of the fading signals.

The influence of the sampling rate was tested with the preliminary measurements conducted on July 11. For this particular measurement session, the signals were sampled at two different rates: 1 kHz and 10 kHz, to make sure that the signals were not undersampled, leading to an undersampling of the fading events. Figure 5.1-1 presents an example of comparison of the envelope of the signals at both sampling rates. Figure 5.1-2 is a comparative plot of the CDF of these signals. As Figure 5.2-2 shows, there is

excellent agreement between the curves. Thus, we conclude that a sample rate as low as 1 kHz is adequate and will not lead to data processing errors.

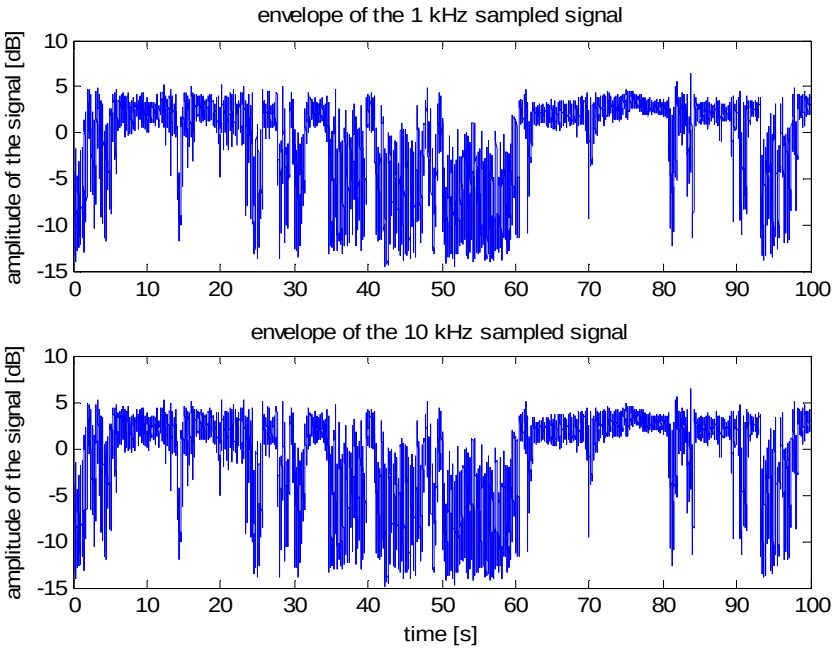

Figure 5.1-1 Envelope of sampled signal for Route 114 East measurements without AGC, Roll satellite, July 11 data collection for (a) 1 kHz sample rate, and (b) 10 kHz sample rate.

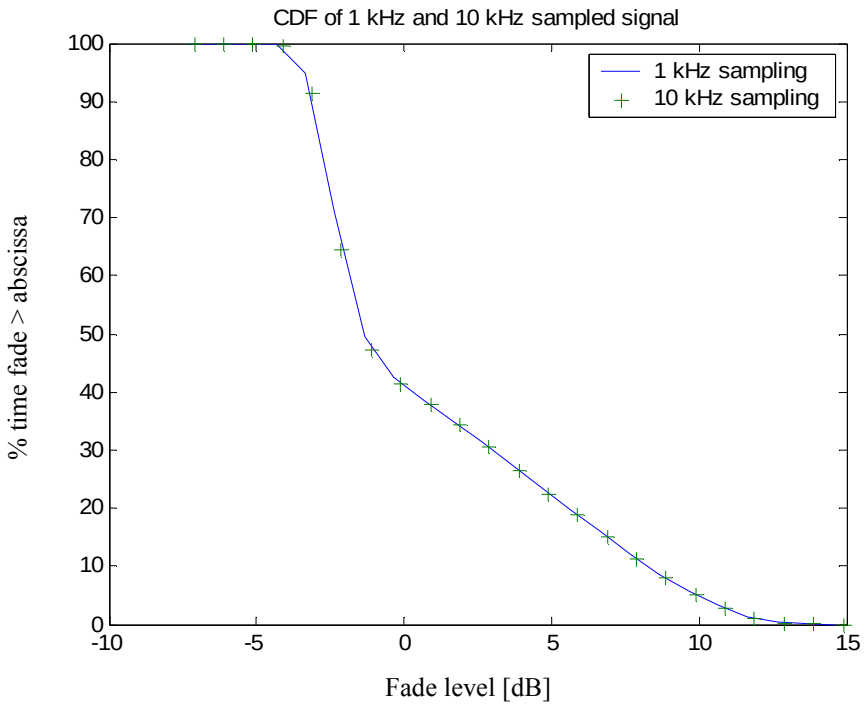

Figure 5.1-2 CDF of sampled signal for Route 114 East measurements without AGC, Roll satellite, July 11 data collection, for sample rates of 1 kHz and 10 kHz.

In the real time PROSIM data processing, the reading rate of the files is set to one sample every 2 ms, or f_r = 500 Hz. Since this value is close to the Nyquist limit value of 277.6 Hz, it has to be validated as well. Figure 5.1-3 compares the envelope of the signals sampled at 1 kHz and at the reading rate f_r = 500 Hz. Figure 5.1-4 is a comparative plot of the CDF of the signals for the two sample rates. Here again, the curves match, indicating that a reading rate of 500 Hz for real-time data processing is adequate and will not lead to data processing errors.

In summary, the different sampling rates used in PROSIM measurements campaign seem to be adequate: whether the signal is sampled at 500 Hz for real-time data processing or at 2 kHz for constants extraction, the Nyquist criteria is validated, and no propagation information is lost.

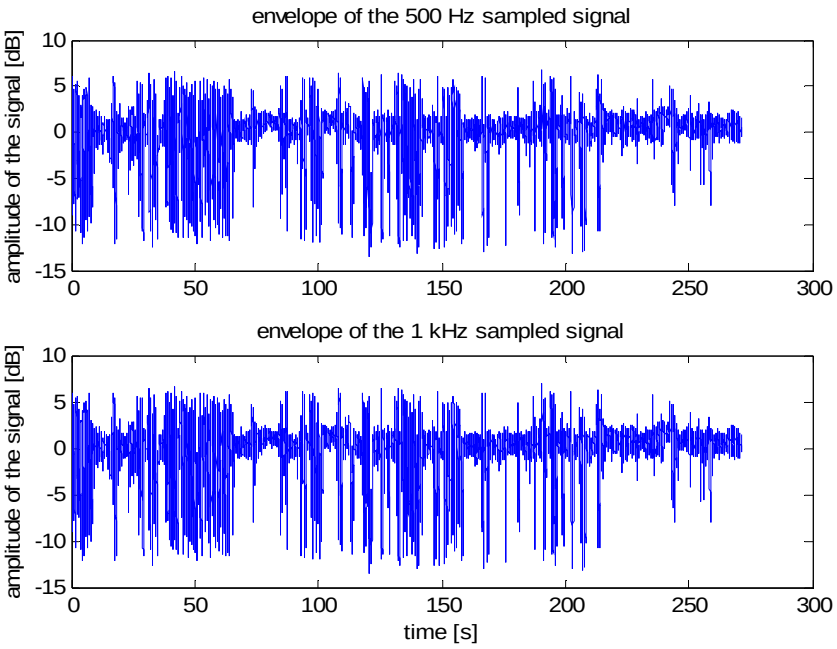

(a)

(b)

Figure 5.1-3 Envelope of sampled signal for Route 114 East measurements, with AGC, Roll satellite, July 11 data collection, for (a) 500 Hz sample rate, and (b) 1 kHz sample rate.

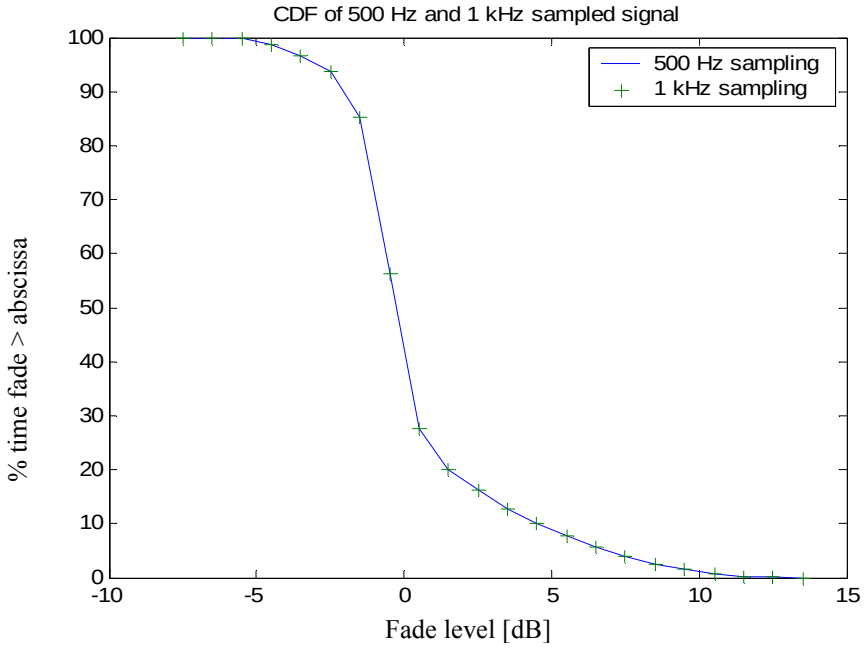

Figure 5.1-4 CDF of sampled signal for Route 114 East measurements with AGC, Roll satellite, July 11 data collection for sample rates of 500 Hz and 1 kHz.

5.1.2 *Measurement Repeatability*

Another measurement concern is the reliability of the experiment system; that is, different runs in the same shadowing scenario should produce similar statistical results. The repeatability of the measurements was validated for several runs. In each case, the vehicle speed was maintained constant at 40 mph and the data recording was started and stopped at the same locations along the route. Figures 5.1-5 to 5.1-8 show examples of the repeatability tests, for different roads, with or without AGC. The Figures show that the signal amplitude and CDF of successive runs match very well in each case. Thus, the experiment system can be considered reliable for data acquisition and compatible with the further propagation analysis of these data.

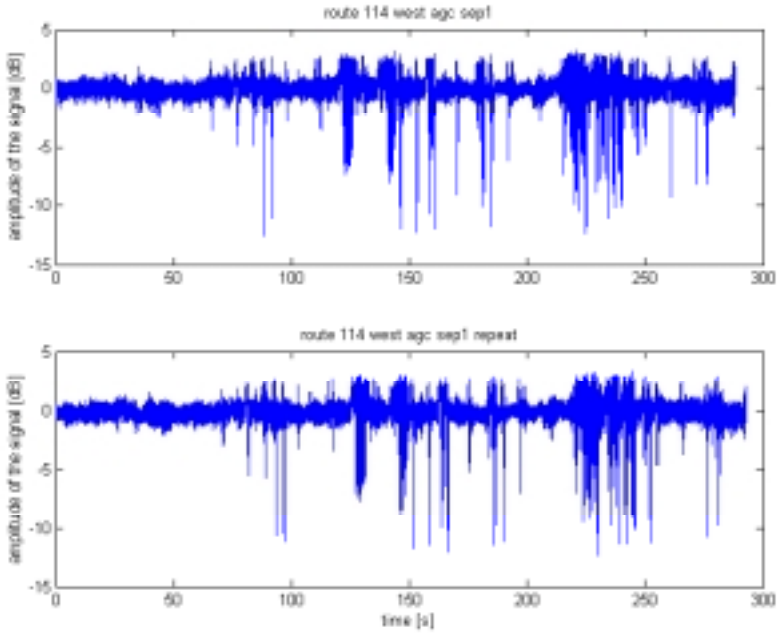

Figure 5.1-5 Envelope of the received signals for successive runs for Route 114 East, with AGC, Roll satellite, September 1 data collection.

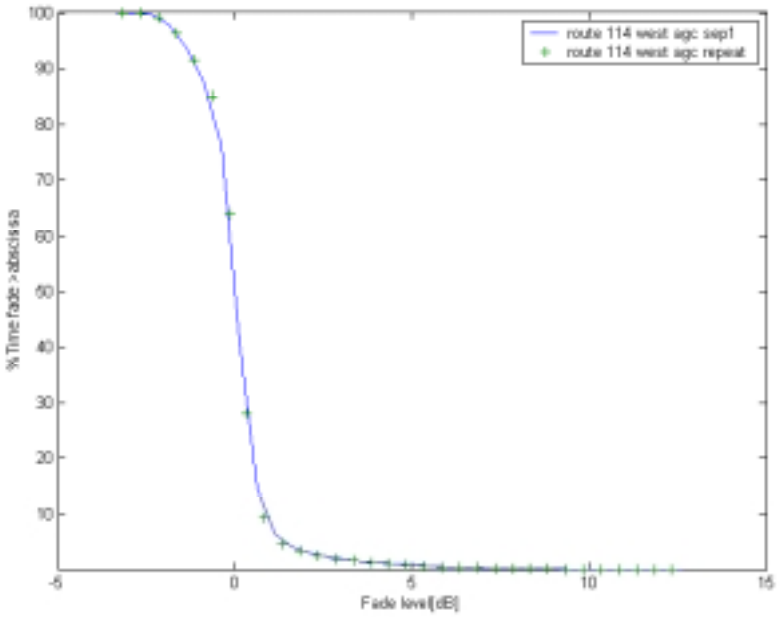

Figure 5.1-6 Plot of the CDF of two successive runs of the data in Figure 5.1-5 for Route 114 East, with AGC, Roll satellite, September 1 data collection.

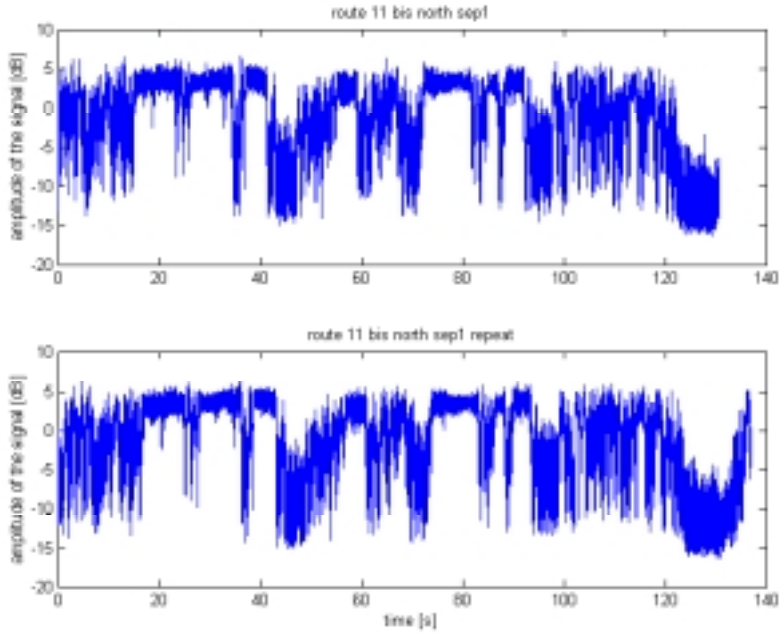

Figure 5.1-7 Envelope of the received signals for successive runs for Route 11bis North, without AGC, Rock satellite, September 1 data collection.

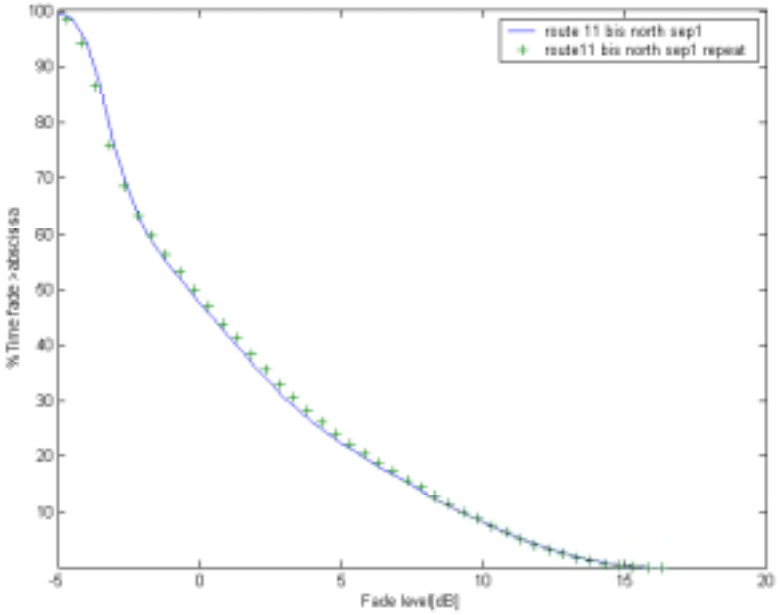

Figure 5.1-8 Plot of the CDF of two successive runs of the data in Figure 5.1-7 for Route 11bis North, without AGC, Rock satellite, September 1 data collection.

5.2 Extraction of Propagation Constants

To validate the signals simulated by PROSIM, real data must be analyzed and compared to a corresponding simulated signal. In order to do this, one of the first tasks is to extract the propagation constants from the measured data. This set of constants can be used as inputs to PROSIM, and the resulting simulated signal can be compared to the measured data.

The data used for parameter determination was signals received from the XM Radio satellites at 2.33 GHz. The signals were measured in September in the Blacksburg/Christiansburg/Radford area. They were sampled at a 2 kHz rate and processed as described in Section 4.4 and their amplitude was relative to the LOS signal power level.

5.2.1 *Original Propagation Constants Extraction: the Threshold Method*

The first constant extraction technique that was investigated is based on the data processing techniques used by Schmier [14] and Barts [13] to generate the universal data sets for the VT propagation simulator LMSSMOD. These techniques were originally implemented in FORTRAN and used to analyze the Vogel data [18]. They have been adapted to the new measured data and implemented using MATLAB; by doing so, the data are processed faster and the unity of the computational environment is preserved.

5.2.1.1 Conversion to the Spatial Domain

After the data processing described in Section 4.4, the received signals are still time sequenced, with one data point every 2 milliseconds. During the test runs, the vehicle speed was maintained at constant speed of 40 mph, 30 mph or 15 mph, depending on the experiment. Real world driving conditions lead to small variations in vehicle speed. Small variations in the vehicle speed should have little effect on primary statistics, but it can significantly affect the secondary statistics. Consequently, in order to avoid the distortions due to vehicle speed variations in the statistical analysis, the data are converted to a new format of one sample every 0.5 wavelength traveled. For a speed of 40 mph and a signal frequency of 2.33 GHz, one sample every 0.5 wavelength corresponds to approximately one sample every 3.6 milliseconds. So, after setting the new time intervals, the values of the signal at the new points are obtained with a linear interpolation of the 2-millisecond measured signal values. The MATLAB function used to compute the interpolation is ‘interp1’.

One should note that the conversion is only used to obtain wavelength-distance normalized values of the statistics of the signals. However, the time information is necessary to extract the propagation constants. In addition, the 2-millisecond signals are used for all the statistical comparison with measured data, as it saves computational time. But, for the constant extraction, the more data points we have, the more accurate the extraction. That is why all the constant extraction programs are run on the initial 1-millisecond data points signals. Doing this increases the computation time, but increases

the precision in the constant extraction, which is required since the constant extraction is the base of all the further comparisons between measurements and simulation.

5.2.1.2 Calculation of the Running Average

The total received signal, whether shadowed or unshadowed, is the sum of a rapidly varying multipath component and a slowly varying direct component. An approximation of the slow-varying signal can be obtained by low-pass filtering the signal, referred as a "running average". MATLAB was used to compute this running average because it has a whole set of filtering algorithms already implemented and using one of them can save a lot of computing time. The most appropriate MATLAB filter seems to be 'fir1', which is a first impulse response digital filter using a Hamming window. The size of the window is set to 200 points, or 0.2 second, and the order of the filter is set to 199, since the window length must be the same as the filter length. The cutoff frequency of the filter has to be chosen very small. Since the multipath signal frequencies are in the order of the Doppler shift frequencies, the cutoff frequency has to be smaller than the maximum Doppler shift frequency, $fd = mean(v)/\lambda$. The cutoff frequency $fc = fd/4 = 34.7Hz$ was determined empirically by trial and errors. The frequency response of the MATLAB 'fir1' filter is given Figure 5.2-1. Then, when filtering the signal one should be aware that the window filtering induces an offset of a half-window size between the input and output signals. Once this offset is eliminated, it can be observed that the filtered signal follows the mean of the total signal. Figure 5.2-2 shows an example of a raw signal together with the same signal after filtering with the 'fir1' MATLAB filter of Figure 5.2-1.

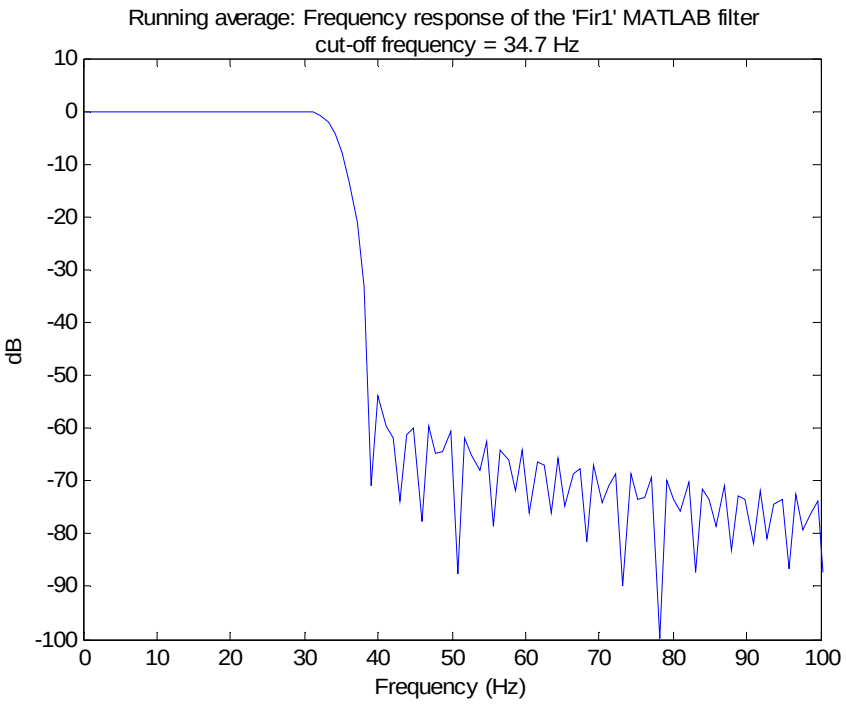

Figure 5.2-1 Frequency response of the 'fir1' MATLAB filter used to compute the running average of the signals. The cut-off frequency of 34.7 Hz was chosen empirically.

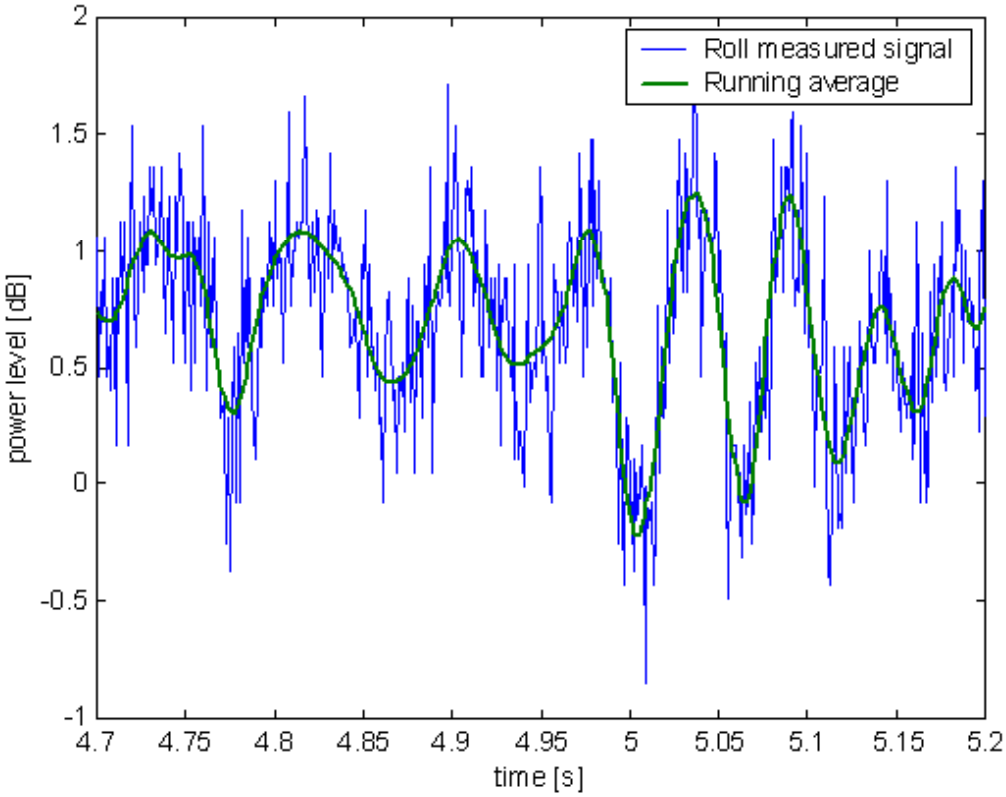

Figure 5.2-2 Example of the running average procedure for a signal with and without the MATLAB 'fir1' filter of Figure 5.2-1 applied for a data set collected on Route 114 West, without AGC, on September 1, for Roll satellite.

5.2.1.3 Extraction of the Percentage of Shadowing S

So far we have discussed measured signals composed of both shadowed and unshadowed data points. To extract the propagation constants, the data points are sorted and separated into shadowed and unshadowed data points. Then, their statistical behavior can be compared with the propagation models for each distribution, to determine the appropriate constants.

The running average signal level discussed in Section 5.1.2.2 is used to separate the data into shadowed and unshadowed groups. For our processing, we normalized the signals to a 0 dB LOS power level, as described in Section 4.4.2 and we used a running

average threshold of $S_t = -1$ dB; that is, when the running average of the signal, S_a, is below –1 dB, the corresponding data point is considered shadowed:

$$S_a < S_t = \text{-1 dB, then the point is shadowed} \qquad (5.2\text{-}1)$$

$$S_a \geq S_t = \text{-1 dB, then the point is unshadowed}$$

The –1 dB threshold is somewhat empirical but produces good results. The percentage of shadowing, S, is simply the ratio of the number of sorted shadowed data points, Ns, to the total number of points in the signa,l N_{tot}:

$$S = \frac{Ns}{N_{tot}} * 100 \qquad (5.2\text{-}2)$$

The remainder of this section gives details on the propagation constants extraction process for the signals collected during the measurement campaign.

5.2.1.4 Constant Extraction: Comparison with Analytical Model

The final step in the constant extraction process is to use the separated data subsets to compare with analytical distributions from which the distribution parameter values can be determined. The MATLAB routine used to extract the propagation constants with the threshold method is ‘extraction2’. The extraction method that is used here is an improvement over that used by Schmier [14] and Bart [13], and is enabled by the large computation capacity of MATLAB, which was not available at the time when Schmier and Barts did their experiments. The new technique is based on a comparison between the statistics of the measured data set and the corresponding analytical model. For each measured data set, the best fitting analytical model, whether Ricean distributed for unshadowed propagation or VS distributed for shadowed propagation, determines the appropriate propagation constants. We now discuss how the extraction is performed in each of these cases.

5.2.1.4.1 Extraction of K for Unshadowed Data Set (Rician)

The unshadowed data set is completely described statistically by its carrier-to-multipath ratio, K. As seen in Section 2.3.1.2, with a LOS signal of 0 dB, the probability density function of the Ricean unshadowed signal is

$$p(r) = 2r \exp\left[-10^{-K/10}(r^2+1)\right] I_0\left(2r^{-K/10}\right) \quad , \mathrm{r} > 0$$

$$p(r) = 0, \quad \mathrm{r} < 0 \tag{5.2-3}$$

and its cumulative fade duration is

$$CFD(R) = 1 - G(R \mid \overline{VS}), \tag{5.2-4}$$

where $G\left(R \mid \overline{VS}\right) = \int_R^\infty p_{unshadowed}(r)dr$ is the probability that the unshadowed signal exceeds a given level R. Specifically, the procedure used to extract K is to compute the analytical CFD for values of K from 0 to 30 dB in 0.1 dB steps and to compare it with the CFD of the measured data set using a mean-square error test. The selected value of K is the one that minimizes the mean-square error between the analytical and the measured CFD. The MATLAB routine designed to extract K with the threshold method is 'Riceextraction'.

5.2.1.4.2 Extraction of μ, σ and $\overline{K}$ for the Shadowed Data Set (VS)

As seen in Section 5.2.1.2, the running average of the signal provides a good approximation to the slow-varying component of the shadowed signal. This component can be modeled with a lognormal distribution, which is completely defined by the propagation constants μ and σ, as described in Section 2.3.1.3. The extraction of μ and σ is quite straightforward, because they correspond to the mean and the standard deviation of the running average of the shadowed data set:

$$\begin{aligned} \mu(dB) &= 20 * \log(e) * mean(\ln(avshad)) \\ \sigma(dB) &= 20 * \log(e) * std(\ln(avshad)) \end{aligned} \tag{5.2-5}$$

where 'avshad' refers to the running average of the shadowed data points.

Once μ and σ are extracted, the only remaining unknown of the shadowed distribution is $\overline{K}$, the carrier-to-multipath ratio for the rapidly-varying component of the shadowed distribution. From Section 2.3.1.4, with a LOS signal of 0 dB, the probability density function of the shadowed distribution is

$$p(r) = \frac{2r}{\sqrt{2\pi}\alpha\sigma} \int_0^\infty \frac{1}{z} I_0\left(\frac{2rz}{\alpha}\right) \exp\left[-\frac{(\ln z - \mu)^2}{2\sigma^2} - \frac{(r^2+z^2)}{\alpha}\right] dz, \tag{5.2-6}$$

where $$\overline{K} = 10 \log \frac{1}{\alpha}, \text{ in dB} \quad (5.2\text{-}7)$$

The associated cumulative fade duration is

$$CFD(R) = 1 - G(R \mid VS), \quad (5.2\text{-}8)$$

where $G(R \mid VS) = \int_{R}^{\infty} p_{VS}(r)dr$ is the probability that the shadowed signal exceeds a given threshold R. Specifically, the procedure used to extract $\overline{K}$ is to compute the analytical CFD for values of $\overline{K}$ from 0 to 30 dB in 0.1 dB steps and to compare it with the CFD of the measured data set using a mean-square error test. The selected value of $\overline{K}$ is the one that minimizes the mean-square error between the analytical and measured CFD. The MATLAB routine designed to extract μ, σ and $\overline{K}$ with the threshold method is 'shadextraction'.

5.2.1.5 Results of the Constant Extraction Using the Threshold Method

The threshold method described in Sections 5.2.1.1 to 5.2.1.4 was used to extract the propagation constants of the XM Radio measured signals. Then, the constants were used as inputs to PROSIM. The PROSIM simulated signals showed a good agreement with the measured signals for the XM Radio AGC measurements. That is, the statistics of the signal simulated with PROSIM using the set of extracted constants provides a good match to the statistics of the measured signal.

However, in most cases, it appears that the extracted percentage of shadowing does not represent the real percentage of shadowing of the measured data set in spite of the statistics agreeing. In a real-time measured signal, the shadowing events are characterized by large variations of the signal amplitude around the mean of the signal, whereas the unshadowed events correspond to much smaller variations of the signal amplitude. Thus, it is easy to obtain a visual estimate of the percentage of shadowing, S, by examining the envelope of the measured signal. In the case of the threshold method, it has been found that the extracted percentage of shadowing is often low compared to the visual estimate of shadowing. This may indicate that the sorting of the data points using the –1 dB threshold does not lead to an accurate estimate of the percentage of shadowing.

But, the mean goal is to predict the signal statistics, not the vegetation parameters and the combination of S and the other propagation constants do give valid signal statistics. Generally speaking, a set of constants can be considered statistically 'good' and at the same time, the associated real-time signal may not have an envelope profile that matches the simulated signal amplitude characteristics. In the same way, various combinations of constant sets can yield good statistical matches to the measured signal statistics.

The problem with the percentage of shadowing can be observed in the example data set RouteNORTH2 shown in Figure 5.2-3. The threshold method yields a percentage of shadowing of 17.9%. The faded (i.e. shadowed) portion of the signal that appears as wide vertical traces in Figure 5.2-3 is a much larger percentage of the time than 17.9%. A visual estimate of the shadowing is from 50 to 70 %. Figures 5.2-4 and 5.2-5 are CDF plots of the measured signal for the shadowed and unshadowed data that show good matches with the best fit analytical CDF. The constants extracted with the Threshold method for the Route 114 measurements are summarized in Table 5.2-1 for the signals received from Roll satellite. Table 5.2.2 gives the extracted constants for the same runs for the signals received from Rock.

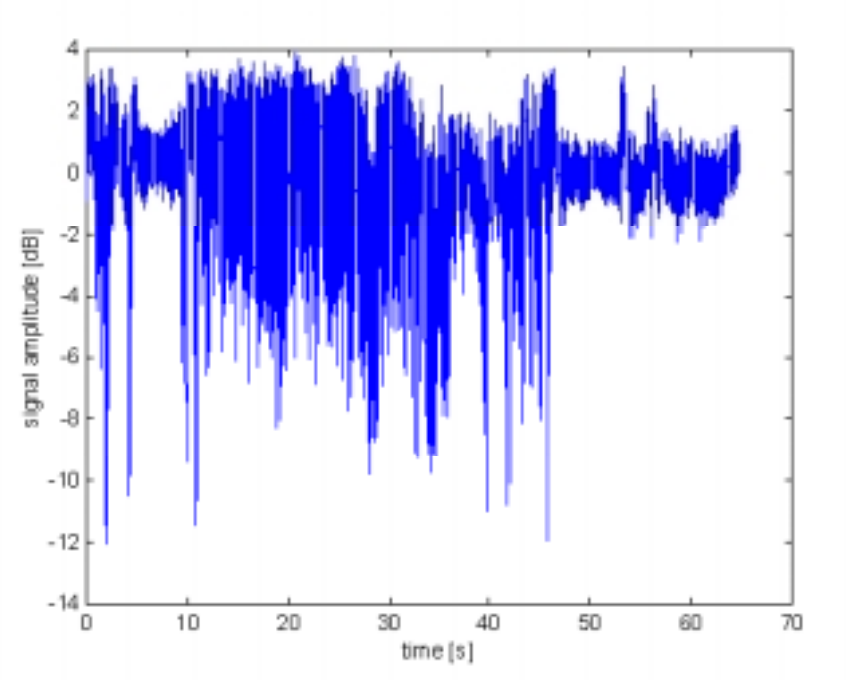

Figure 5.2-3 Measured signal amplitude for Route11NORTH2 with AGC, September 1, Roll satellite.

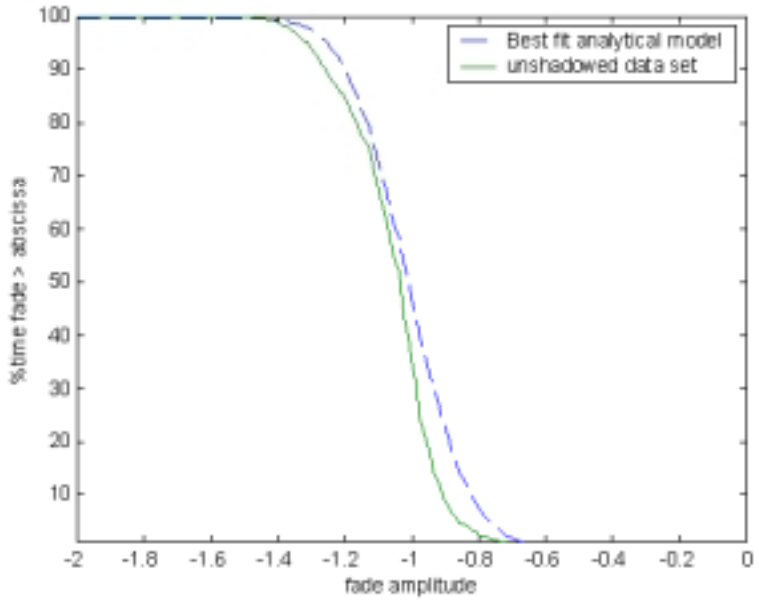

Figure 5.2-4 CDF of measured signal and best fit analytical CDF for the unshadowed portion of the data set Route11NORTH2 with AGC, September 1, Roll satellite, shown in Figure 5.2-3. Note that the fade is in amplitude, not in dB values.

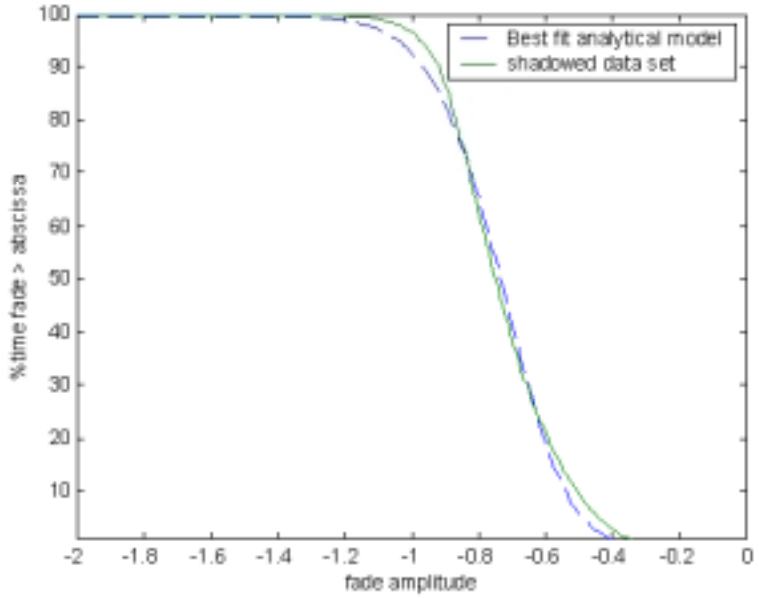

Figure 5.2-5 CDF of measured signal and best fit analytical CDF for the shadowed portion of the data set Route11NORTH2 with AGC, September 1, Roll satellite, shown in Figure 5.2-3. Note that the fade is in amplitude, not in dB values.

Table 5.2-1 Propagation constants for Route 114 measurement runs described in Section 4.3.2.2 for Roll satellite, September 1 data collection, extracted with the Threshold method.

		S (%)	K (dB)	$\overline{K}$ (dB)	μ(dB)	σ(dB)
With AGC	Route114EAST1	13.799	16.7	17.3	-2.9337	1.7701
	Route114EAST2	11.8709	17.9	18.2	-3.3617	2.1848
	Route114EAST3	4.9317	22.3	19	-3.2554	2.2162
	Route114WEST1	1.8424	22.7	24.7	-2.5587	1.9905
	Route114WEST2	6.8464	19.3	19.7	-2.9906	2.1033
	Route114WEST3	8.4017	18.5	19.2	-2.5077	1.6101
Without AGC	Route114EAST1	32.7517	6.3	18.1	-5.537	3.1263
	Route114EAST2	24.1353	9.1	20.7	-6.8421	3.7706
	Route114EAST3	9.3611	19.1	17.6	-4.5599	3.2833
	Route114WEST1	4.1219	21.6	23.4	-3.0844	2.4148
	Route114WEST2	14.5455	15.2	18.7	-5.9837	3.9305
	Route114WEST3	20.3257	12.6	17.9	-4.8364	2.9619

Table 5.2-2 Propagation constants for Route 114 measurement runs described in Section 4.3.2.2 for Rock satellite, September 1 data collection, extracted with the Threshold method.

		S (%)	K (dB)	$\overline{K}$ (dB)	μ(dB)	σ(dB)
With AGC	Route114EAST1	26.8563	10.5	17.6	-4.0133	2.3452
	Route114EAST2	23.7692	11.5	18.6	-4.8749	2.7531
	Route114EAST3	11.2587	18.4	17.6	-3.83	2.6725
	Route114WEST1	8.4164	19	18	-3.3132	2.4827
	Route114WEST2	21.8743	12.3	18.2	-4.7592	2.6759
	Route114WEST3	22.3889	12.4	17.8	-4.0584	2.3285
Without AGC	Route114EAST1	38.4278	3.9	18.7	-5.8443	2.8330
	Route114EAST2	33.2316	5.2	20.5	-6.5861	3.1517
	Route114EAST3	13.6461	15.8	17.6	-4.8666	3.2754
	Route114WEST1	8.5849	18.5	17.4	-4.0996	3.1107
	Route114WEST2	26.0644	8.2	20.2	-6.5643	3.2940
	Route114WEST3	29.1611	7.3	18.8	-5.7508	3.0672

5.2.2 *New Constant Extraction: the MinMax Method*

5.2.2.1 Presentation of the MinMax Method

To solve the problem of the unrealistic percentage of shadowing, a new method was developed to separate the data points into shadowed and unshadowed subsets. This new method is based on a more sophisticated sorting of the total signal. The shadowing event creates large variations in the signal amplitude that are much larger than for the non-shadowed portion of the signal. The new method, called 'MinMax Method', uses this fact to distinguish shadowed and unshadowed data points.

The idea is to examine the minimum and the maximum values of the signal, and the range between them. To build the 'max' signal, a 200-point sliding window is used; the value of the 'max' signal for each data point is the maximum of the signal within the 200-point window around this point. The same technique is applied to create a 'min' signal that follows the minimum values of the signal. Hence, the equations used to derive the 'max' and 'min' signals are

$$\text{Max\_signal}(i)=\max(\text{A\_dB}(i-w/2:i+w/2))$$
$$\text{Min\_signal}(i)=\min(\text{A\_dB}(i-w/2:i+w/2)) \quad (5.2\text{-}9)$$

where Max_signal(i) is the value of the 'max' signal for point i, Min_dB(i) is the value of the 'min'signal for point i, A_dB is the signal amplitude in dB, and w is the window size. An example of the 'max' and 'min' sliding window signals is given Figure 5.2-6, where the 'min' and 'max' signals are superimposed on the total signal for the Route11NORTH2 measurements (with AGC, September 1, Roll Satellite).

Then, the range between the 'max' and 'min' signal, is computed using

$$\text{Range} = |\text{Max\_signal} - \text{Min\_signal}| \quad (5.2\text{-}10)$$

Whenever the difference between the 'max' and 'min' signals is greater than 4 dB, the corresponding data point of the measured signal is considered shadowed, and unshadowed in the other case; that is

$$\text{if Range (i)} \geq 4 \text{ dB, then i is shadowed}$$
$$\text{if Range (i)} < 4 \text{ dB, then i is unshadowed} \quad (5.2\text{-}11)$$

The 4 dB threshold was determined empirically by examining the sliding range between the 'max' and 'min' signal. An example of the sliding range is shown in Figure 5.2-7, which represents the sliding range for the Route11NORTH2 data (with AGC, September 1, Roll satellite). The reader can compare the signal amplitude in Figure 5.2-6 with its sliding range in Figure 5.2-7 to check the validity of the 4-dB threshold. The MATLAB routine corresponding to the MinMax extraction is 'testminmax'.

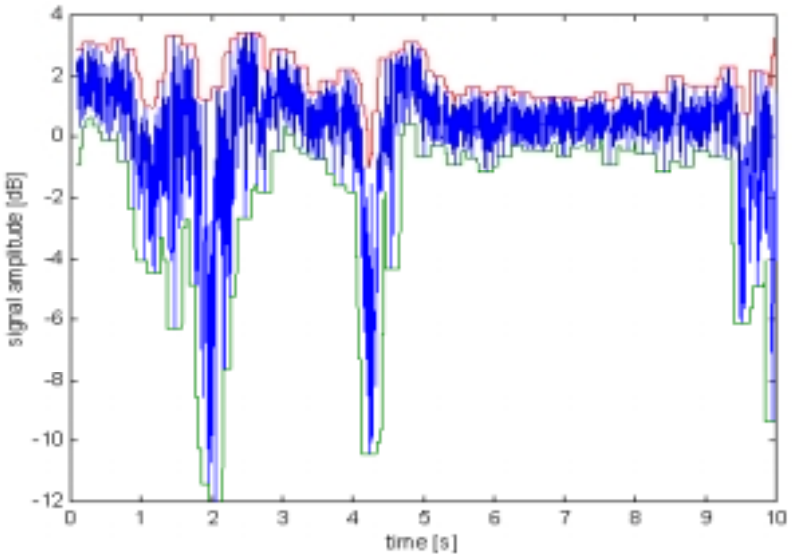

Figure 5.2-6 Measured signal amplitude for Route11NORTH2 with AGC, September 1, Roll satellite: the maximum and minimum sliding window signals are superimposed on the signal.

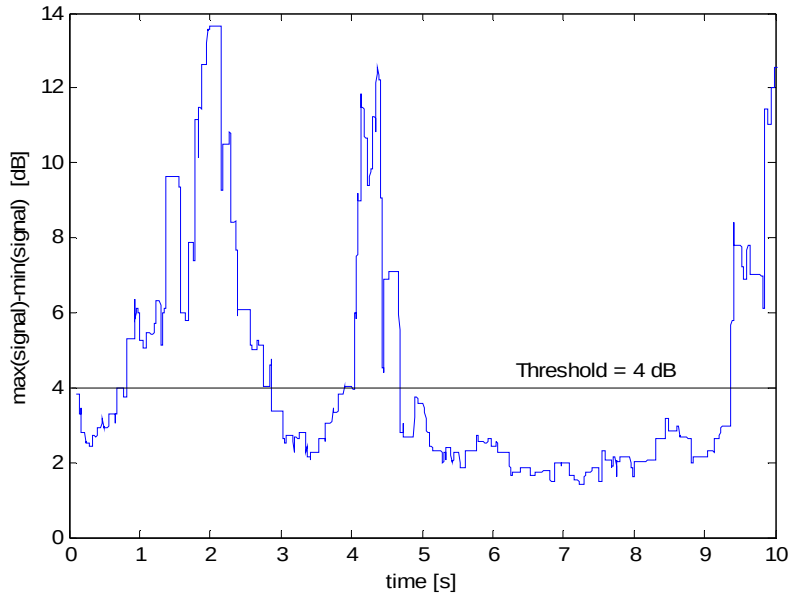

Figure 5.2-7 Route11NORTH2 with AGC, September 1, Roll satellite: difference between the 'max' and 'min' sliding window signals for the data set of Figure 5.2-6. According to the MinMax Method, if a point is above the 4 dB threshold, the corresponding data point is considered to be shadowed; see (5.2-11).

5.2.2.2 Comparison of the Threshold and the MinMax Method

The MinMax method generates propagation constant sets for the measurements with AGC that agree well with the PROSIM simulations, as will be presented in Section 6.1. Because the sorting of the signal is more precise, the data sets are more accurate, and the probability for a data point to be assigned to the wrong data set is reduced. Hence, the percentage of shadowing obtained with the MinMax method is much more realistic than the one obtained with the Threshold method. For example, the percentage of shadowing extracted with the MinMax method for the data set Route11NORTH2 of Section 5.2.1.5 is 55.6%, which agrees with the visual estimate of 50 to 70%.

The MinMax method always provides a good matching between the CDF of the measured data sets and the best fit analytical CDF, in both shadowed and unshadowed cases, for AGC measurements. Figure 5.2-8 presents a comparison of the analytical and measured CFD for the two methods, for Route11NORTH2 (with AGC, September 1 data collection, Roll satellite measurement), for the unshadowed data set. Figure 5.2-9 presents the same results for the shadowed data set. Note that for each shadowed or unshadowed sets, both the Threshold and MinMax methods yields good agreement between the analytical and measured CFD. The reader can refer to Table 5.2-3 for a summary of the propagation constants extracted with both methods for Route11NORTH2 with AGC, Roll satellite.

From the comparison, it appears that in the AGC measurements case, both methods yields good sets of propagation constants. However, the MinMax method gives a more realistic percentage of shadowing, and therefore more realistic simulated signals. Consequently, all the propagation constants used for further work are extracted with the MinMax method. All the constants extracted with the MinMax method for the AGC measurements are listed in Table 5.2-4 (Roll satellite) and 5.2-5 (Rock satellite).

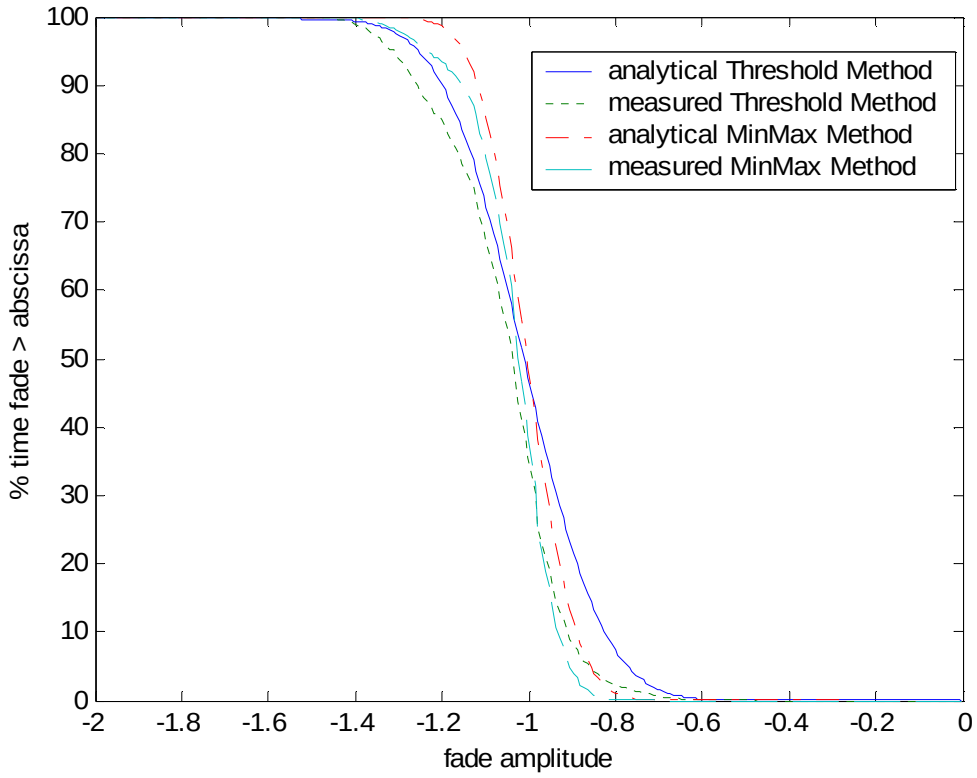

Figure 5.2-8 Comparison of the Threshold and MinMax method: analytical and measured CDF for Route11NORTH2, with AGC, September 1, Roll satellite, unshadowed data set.

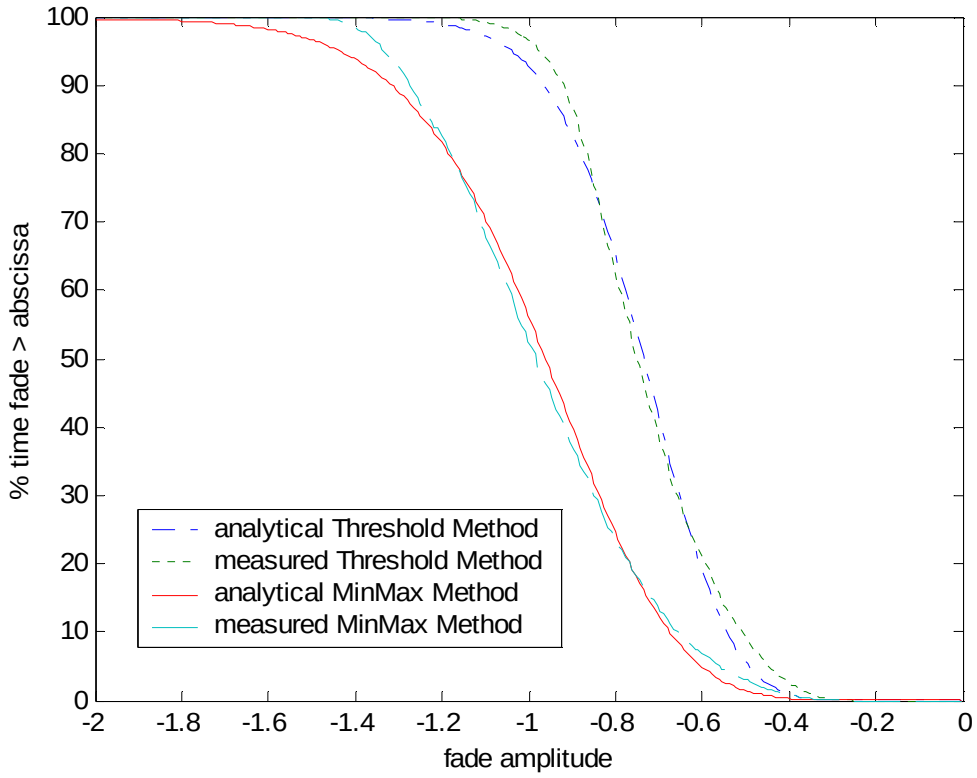

Figure 5.2-9 Comparison of the Threshold and MinMax method: analytical and measured CDF for Route11NORTH2, with AGC, September 1, Roll satellite, shadowed data set.

Table 5.2-3 Comparison of extracted propagation constants for the Threshold and MinMax method, Route11NORTH2 with AGC, September 1, Roll satellite.

	Threshold Method	MinMax Method
S (%)	17.9685	55.5834
K	13.7	18
$\overline{K}$	19.2	15.6
μ	-2.7664	-0.4687
σ	1.7198	1.9996

Table 5.2-4 Propagation constants for AGC measurements, Roll satellite, extracted with the MinMax method.

	S (%)	K (dB)	$\overline{K}$ (dB)	μ (dB)	σ (dB)
Route114EAST1	60.4883	14.8	15.2	-1.0216	3.3010
Route114EAST2	49.2622	15.1	15.9	-1.5307	3.9249
Route114EAST3	25.5629	19.8	18.8	-1.0045	3.2026
Route114WEST1	13.6502	19.2	17.1	-1.5092	2.9774
Route114WEST2	42.7945	13.7	15.1	-1.9064	3.6291
Route114WEST3	46.1974	14.1	15.4	-1.4514	3.1556
Route11NORTH1	81.1303	11.6	17.5	-0.4916	2.9524
Route11NORTH2	68.9948	10.5	14.3	-1.1393	3.3657
Route11SOUTH1	61.4016	12.3	14.2	-1.1607	3.2778
Route11SOUTH2	72.7384	10.9	21.2	-0.7916	2.8681
Route11bisNORTH1	71.9291	16	16	-0.7273	3.1128
Route11bisNORTH2	77.7349	10.2	16	-0.8828	3.1417
Route11bisSOUTH1	51.0102	15.5	17.9	-0.8304	2.4332
Route11bisSOUTH2	42.5483	19	30	-0.1891	2.0233
Route460EAST	2.4712	24.2	19.1	-1.2272	3.2112
Route460WEST	1.7492	24.8	15.3	-2.1365	3.6246
Route723NORTH	7.6802	16.8	23.7	-0.4841	1.5581
Route723SOUTH	7.1110	15.1	17.6	-0.1174	1.2409

Table 5.2-5 Propagation constants for AGC measurements, Rock satellite, extracted with the MinMax method

	S (%)	K (dB)	$\overline{K}$ (dB)	μ (dB)	σ (dB)
Route114EAST1	40.2453	20.10	15.3	-0.6828	2.0310
Route114EAST2	27.3286	19.8	15.5	-1.237	2.4241
Route114EAST3	8.6124	22.6	16.9	-1.5901	2.5565
Route114WEST1	2.9916	22.8	30	-0.9484	2.3977
Route114WEST2	16.1468	20.2	26	-0.7733	2.3482
Route114WEST3	24.7187	20.3	18.7	-0.3724	1.8554
Route11NORTH1	50.9791	12.7	17.4	-0.4826	1.5870
Route11NORTH2	55.5834	18	15.6	-0.4687	1.9996
Route11SOUTH1	35.4665	19.3	17.4	-0.4133	1.9307
Route11SOUTH2	47.8009	14.7	18.7	-0.6293	1.6909
Route11bisNORTH1	50.5859	15.9	17.1	-0.8379	2.2889
Route11bisNORTH2	59.8117	16.5	16.5	-0.5453	2.0533
Route11bisSOUTH1	18.9194	19.4	30	-0.4897	1.7269
Route11bisSOUTH2	14.5334	19.7	21.1	-1.6078	2.5274
Route460EAST	8.1777	20.7	18.2	-2.1893	3.2781
Route460WEST	3.2588	20.5	24.9	-1.1538	2.5734
Route723NORTH	47.2988	10.6	14.9	-1.9357	3.2013
Route723SOUTH	54.2807	5.9	15	-2.6832	3.8674

Chapter 6

Results from the PROSIM Simulator and the Measurement Campaign

6.1 AGC/non-AGC Measurement Analysis

6.1.1 *Comparison of Signals Measured With or Without AGC*

Measurements were taken for each shadowing scenario with and without automatic gain control (AGC), as described in Section 4.3. An example of the measured results is given in Figure 6.1-2 and 6.1-2, which represent the envelope of the signal for the Rock satellite on Route 11 South in both AGC and non-AGC cases.

It can be observed that the signals in the AGC and non-AGC cases match. Despite a small time offset of a few seconds due to a slightly different measurement starting time, the fading events occur at approximately the same time. However, it should be noticed that the use of the AGC reduces the depth of the fading. The signal experiences fades as large as 16 dB in the non-AGC case, but only 13 dB in the AGC case. Also, the AGC enhances part of the shadowed data points amplitudes. Instead of a fade where the signal amplitudes are roughly below -1 dB in Figure 6.1-1 (non-AGC case), certain shadowed amplitudes are enhanced up to 5 dB in Figure 6.1-2 (AGC case). So, as expected, the AGC seems to compensate, in part, for the shadowing.

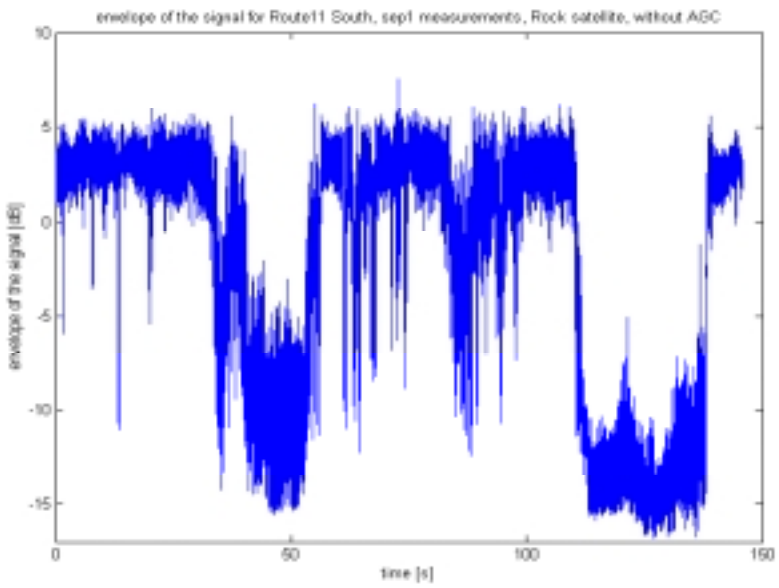

Figure 6.1-1 Envelope of the signal for Route11 South, September 1, Rock satellite, without AGC; see Section 4.3.2.2.1 and Figures 4.3-11 to 4.3-13 for a description of the measurement run and the associated shadowing environment.

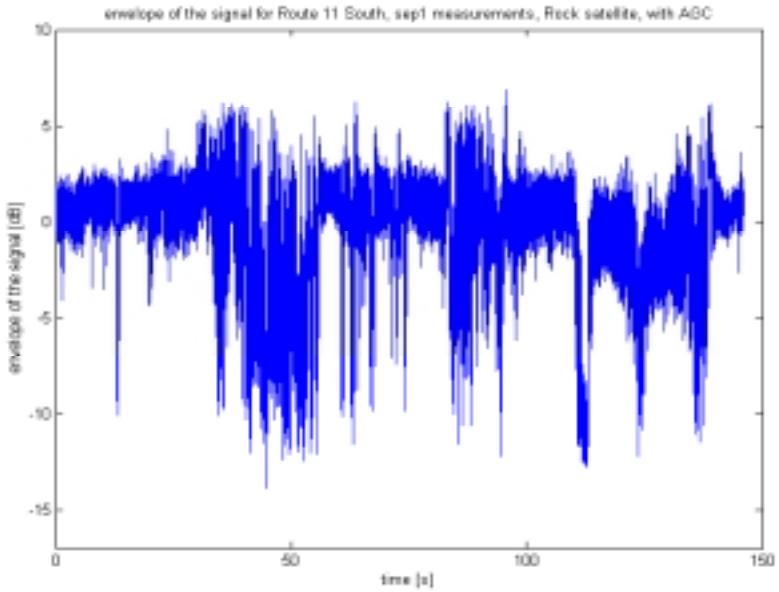

Figure 6.1-2 Envelope of the signal for Route11 South, September 1, Rock satellite, with AGC; see Section 4.3.2.2.1 and Figures 4.3-11 to 4.3-13 for a description of the measurement run and the associated shadowing environment.

6.1.2 *Comparison with PROSIM Simulation*

6.1.2.1 Results with AGC

Once the propagation constants are extracted for each propagation scenario with the MinMax method described in Section 5.2.2, they are used as the input to PROSIM, and the resulting simulated signals are compared with the measured signal. Comparisons to be described in this subsection show that for the case of AGC measurements, the statistics of the measured and simulated signals presents a good match. However, in the non-AGC case, the simulated signal does not give the expected statistical behavior, as will be further explained in Section 6.1.2.2.

First, it is important to note that PROSIM, and all the previous VTAG propagation work is based on Vogel's measurements [18]. Vogel's measurements were conducted at 870 MHz during October 1985 and March 1986 in Central Maryland, in order to study the impact of the foliage on the fade distribution. Vogel and Goldhirsh [18] used a helicopter carrying a transmitting source, instead of a satellite. The transmitter was pointing at a 45° depression angle relative to the horizontal. They used a van equipped with a receiver as the mobile vehicle and mounted a receiving antenna on the top of the roof. The van was equipped with the receiver system and data acquisition instrumentation. Data were sampled and stored at a rate of 1024 samples per second. One example of the measured signal is given Figure 6.1-3. Obviously, this signal has large enhancements during shadowing events. We must remember that Vogel removed the mean from his raw signals, using the phase information. In the XM Radio measurement campaign, phase information was not collected. Hence, the mean removal processing could not be performed. However, the presence of an AGC and the normalization of the signals to their means gives measured signals with overall characteristics similar to the Vogel's measured signals after the mean is removed. Consequently, it was expected that PROSIM simulator, validated in the past with Vogel's measurements, would give good statistical results for the AGC measurements at 2.33 GHz.

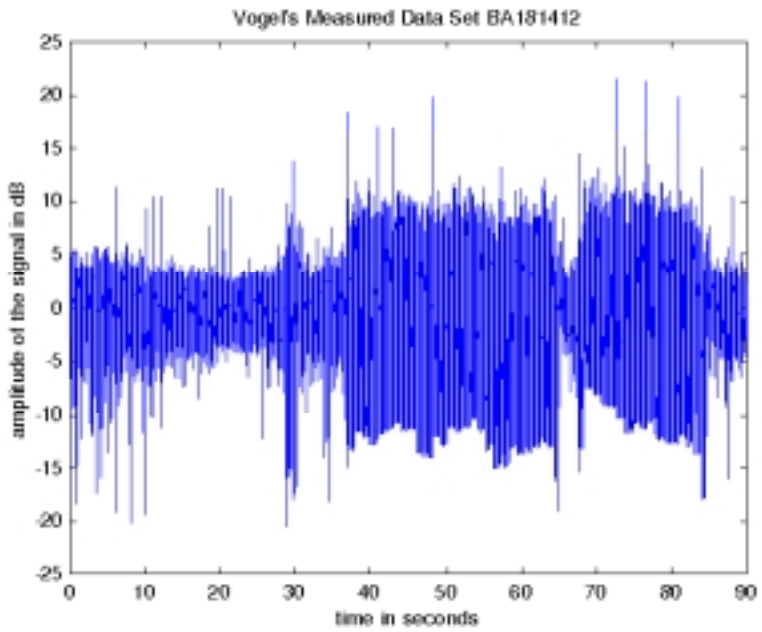

Figure 6.1-3 Envelope of a Vogel signal; data set BA181412.

Examples of the statistical comparison between measured signal with AGC and PROSIM simulated signal are given Figures 6.1-4 through 6.1-6. After observations of all the different scenarios, it can be noticed that the matching is consistently better for Roll than for Rock. Generally speaking, it seems that the Rock signal suffers more shadowing, and deeper fades. This impression is confirmed by the comparison of the extracted percentage of shadowing for each satellite, summarized in Table 6.1-2; for each data set, the percentage of shadowing for the Rock signal is always at least 20% higher than the percentage of shadowing for the Roll signal. An explanation for the fact that the Rock signals are more shadowed than the Roll signals is the difference in elevation angle for the two satellites. As summarized in Table 6.1-1, the Rock satellite has an elevation angle of 34° when viewed from Blacksburg, Virginia, whereas Roll has an elevation angle of 47°. Consequently, the signals received from Rock are expected to experience more fading, since their path through the vegetation is longer, as shown in Figure 6.1-7. This is consistent with the results of Goldhirsh and Vogel [18]; after measuring the signals received from their source through vegetation for different elevation angles, they

found that the elevation angle of the satellite has a large impact on the depth of the fades, and the smaller the elevation angle, the deeper the fades.

Another quantity of interest is the width of the LCR curve. For Rock, as shown in Figure 6.1-6, the LCR curve is always wider, which indicates that high levels of shadowing are attained with a non-negligible probability. One should also notice that the AFD is always higher for Rock than for Roll, as shown in Figure 6.1-5. This confirms the fact that the signals received from Rock experience more fading than the signals from Roll. One can also note that the simulator reflects the measured shadowing characteristics of the signals: the secondary statistics of the simulated signals are in agreement with the secondary statistics of the measured signals, and reflects the fact that the Rock signals are more shadowed than the Roll signals; see Figures 6.1-5 and 6.1-6. The simulated signals are different for the satellites because the extracted propagation constants, used as inputs to PROSIM, are different, leading to distinct simulated signals.

Table 6.1-1 Elevation angles of Rock and Roll satellites when viewed from Blacksburg, VA, located at 80.41º W and 37.22º N.

	Roll satellite	**Rock satellite**
Position	85º W ±0.1º longitude	115º W ±0.1º longitude
Elevation angle	47°	34°

Table 6.1-2 Extracted percentage of shadowing for each measurement data set, and each satellite, with AGC.

	% shadowing Roll	**% shadowing Rock**
Route114EAST1	40.2453	60.4883
Route114EAST2	27.3286	49.2622
Route114EAST3	8.6124	25.5629
Route114WEST1	2.9916	13.6502
Route114WEST2	16.1468	42.7945
Route114WEST3	24.7187	46.1974
Route11NORTH1	50.9791	81.1303
Route11NORTH2	55.5834	68.9948
Route11SOUTH1	35.4665	61.4016
Route11SOUTH2	47.8009	72.7384
Route11bisNORTH1	50.5859	71.9291
Route11bisNORTH2	59.8117	77.7349
Route11bisSOUTH1	18.9194	51.0102
Route1bisSOUTH2	14.5334	42.5483
Route460EAST	2.4712	8.1777
Route460WEST	1.7492	3.2588
Route723NORTH	1.5581	3.2013
Route723SOUTH	1.2409	3.8674

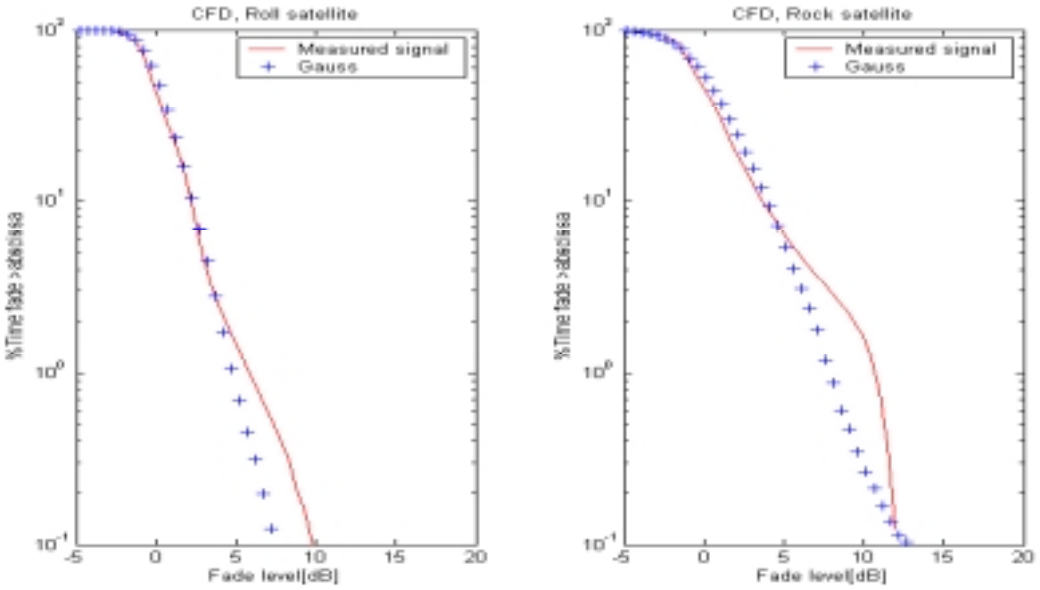

Figure 6.1-4 Cumulative Fade Distribution CFD of simulated (referred as 'Gauss') and measured signal for Route11SOUTH2, with AGC on, for Roll and Rock satellite.

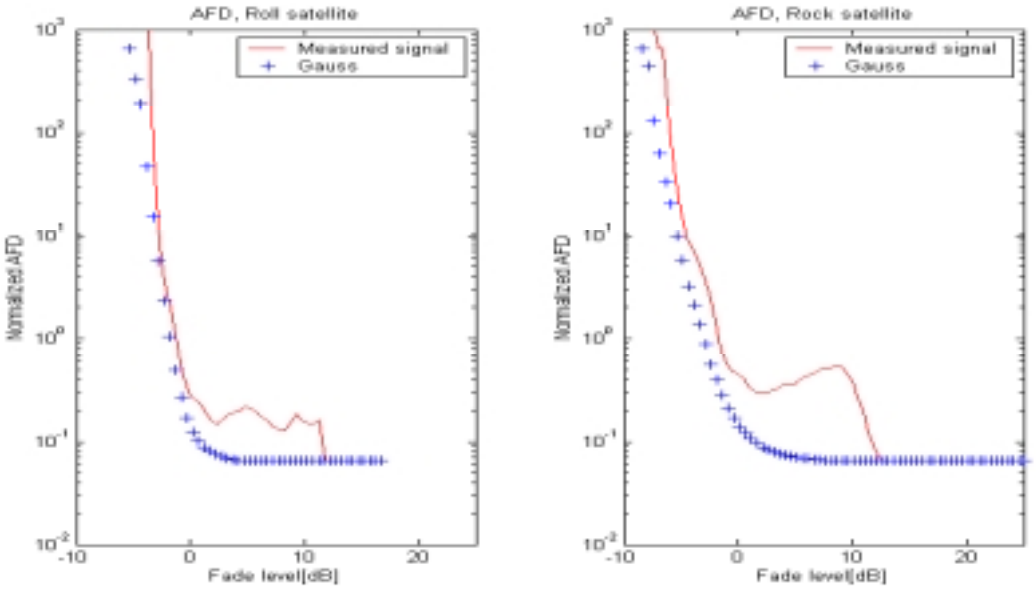

Figure 6.1-5 AFD of simulated (referred as 'Gauss') and measured signal for Route11SOUTH2, with AGC on, for Roll and Rock satellite.

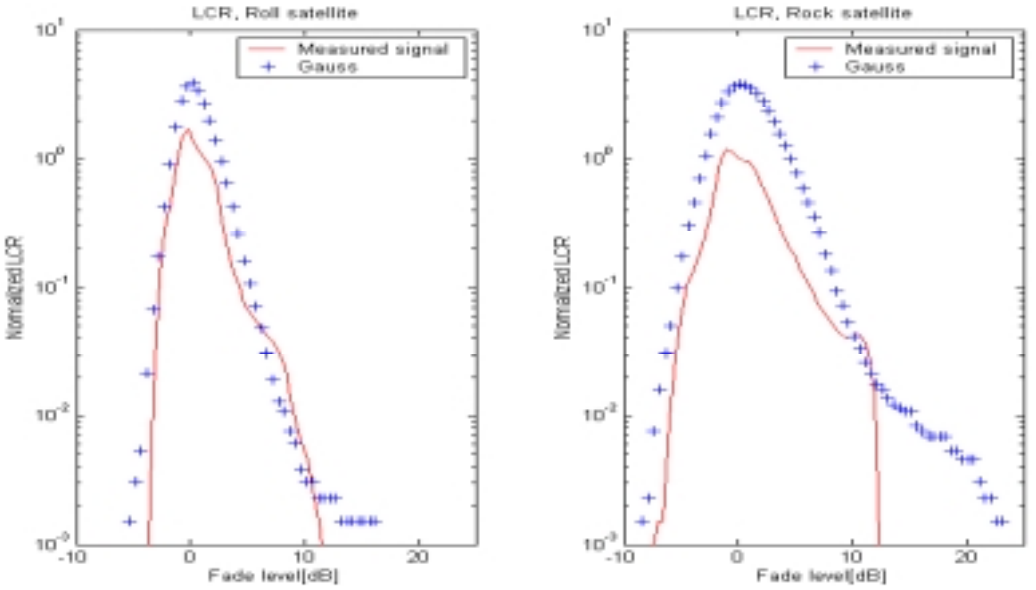

Figure 6.1-6 LCR of simulated (referred as 'Gauss') and measured signal for Route11SOUTH2, with AGC on, for Roll and Rock satellite.

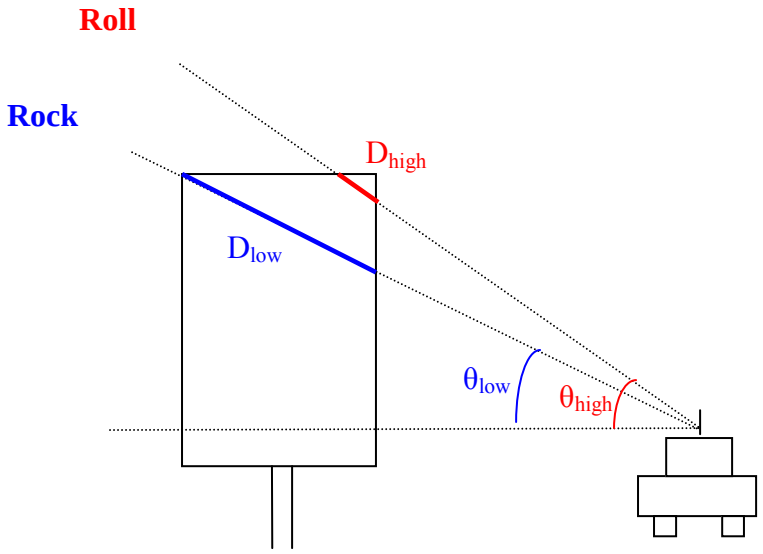

Figure 6.1-7 Path length through the vegetation for different elevation angles. It can be seen that for a low elevation angle θ_{low}, the path through the vegetation D_{low} is longer than the path through the vegetation D_{high} for a high elevation angle θ_{high}.

To discuss the fact that the Rock signals present a higher percentage of shadowing, S, than the Roll signals, one could question the extraction process of S, and especially the validity of the 4 dB threshold in the MinMax method for the Rock signals. However, the plot of the Rock signal in Figure 6.1-8, along with the range of the signal amplitude |max(signal)-min(signal)| seems to indicate that the 4 dB range threshold is still appropriate to differentiate shadowed and unshadowed data points. Every time the range is larger than 4 dB, the corresponding data point is considered shadowed.

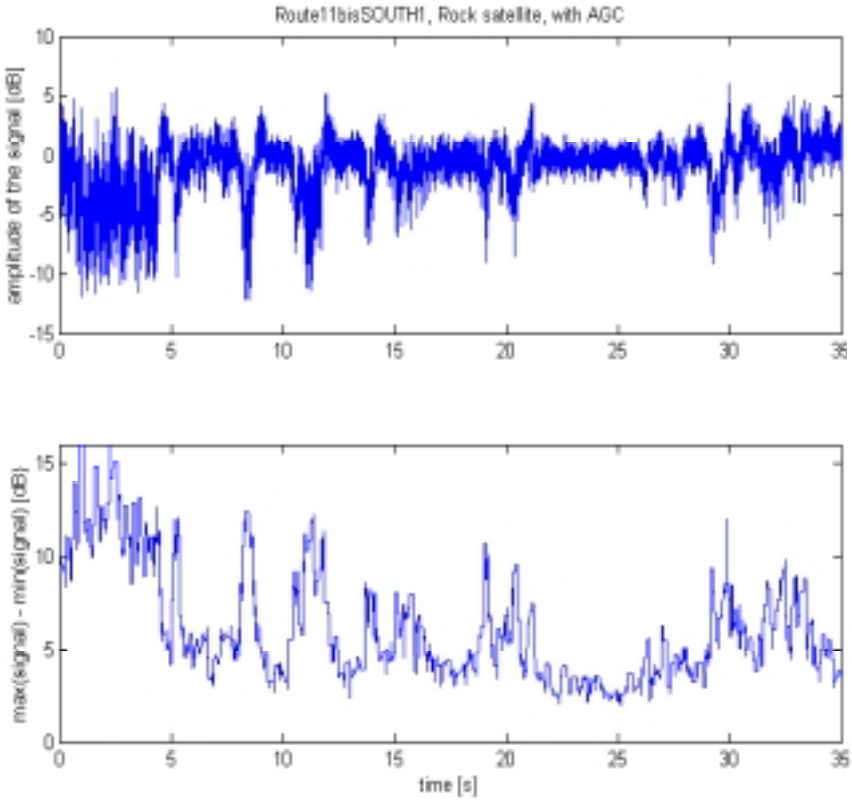

Figure 6.1-8 Signals received from the Rock satellite for the Route11bisSOUTH1 measurement, with AGC on: (a) Amplitude of the signal versus time,

(b) |max(signal) – min(signal)| with a 200 point sliding window for the signal of (a).

6.1.2.2 Non-AGC Results

In the case of non-AGC measurements, there is a consistently poor match between the propagation statistics of the measured signal, and those of the PROSIM simulated signals using the extracted propagation constants. Even though the Cumulative Fade Duration CFD sometimes agree, as in Figure 6.1-9, the secondary statistics AFD and LCR do not match between measured and simulated signals, as shown in Figure 6.1-10 and 6.1-11.

When examining the extraction process, it becomes obvious that the unshadowed data set cannot be modeled by a Ricean distribution in the case of the non-AGC

measurements. Figure 6.1-12 shows an example of the comparative plot of the measured CDF and best fit analytical CDF for the unshadowed data set of Route11bisNORTH2, Roll satellite. The two CDFs do not match, which indicates that the Ricean distribution may not be appropriate to model the unshadowed distribution for the non-AGC measurements. The extracted Ricean carrier-to-multipath ratio K does not have an acceptable value, and the statistics of the simulated signal do not reflect the statistics of the real signal. To explain the failure of the Ricean model, one should remember that the Ricean model assumes a constant LOS signal of 0 dB. Practically, when the AGC is turned off, it does not compensate for the variation of the received signal. Thus, a constant LOS does not exist anymore. It seems that one contribution of the AGC is to maintain a 0 dB constant LOS component in the unshadowed data set, by compensating for variations of the signal.

Since the extraction process does not work for the non-AGC measurements, the user will not be able to compare measured and simulated signal without AGC under PROSIM. Instead, he/she can access comparative plots of the statistics of the signal received from both satellites, and a study of the fading correlation between the two satellites.

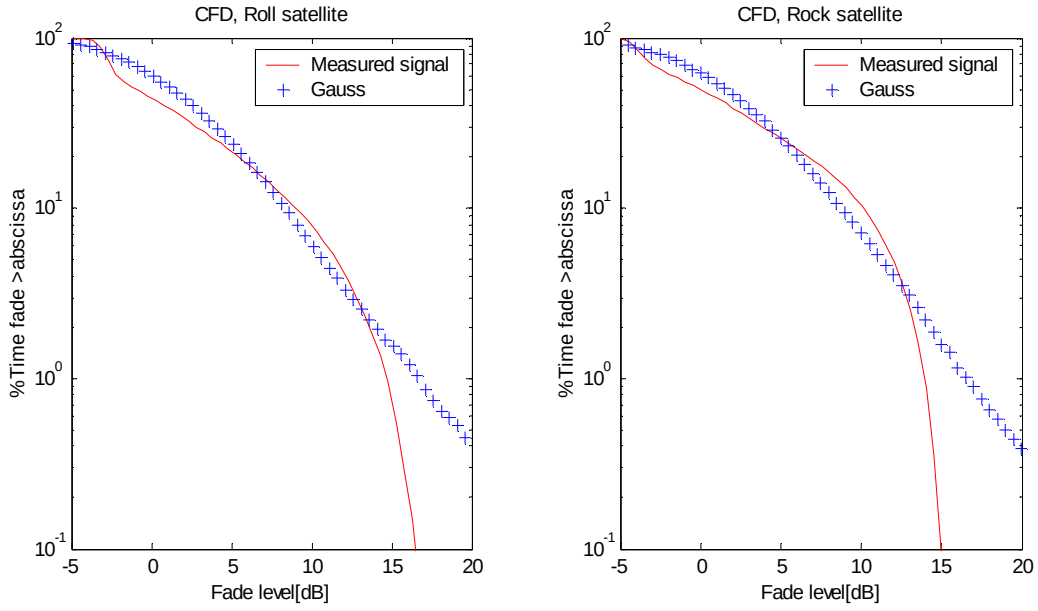

Figure 6.1-9 Cumulative Fade Distribution CFD of simulated (referred as 'Gauss') and measured signal for Route11bisNORTH2, without AGC, for Roll and Rock satellite

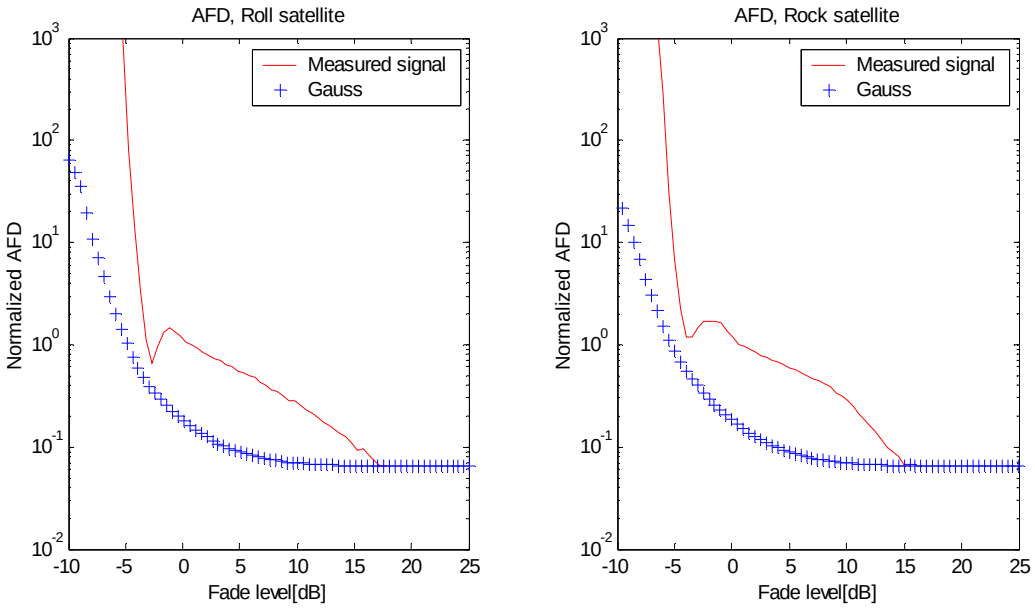

Figure 6.1-10 AFD of simulated (referred as 'Gauss') and measured signal for Route11bisNORTH2, without AGC, for Roll and Rock satellite

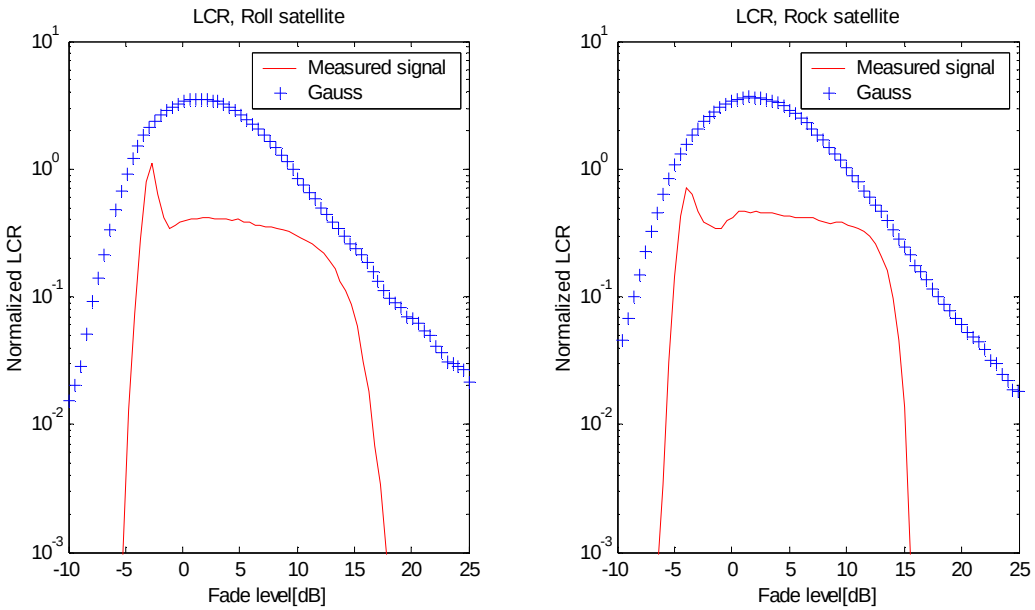

Figure 6.1-11 LCR of simulated (referred as 'Gauss') and measured signal for Route11bisNORTH2, without AGC, for Roll and Rock satellite

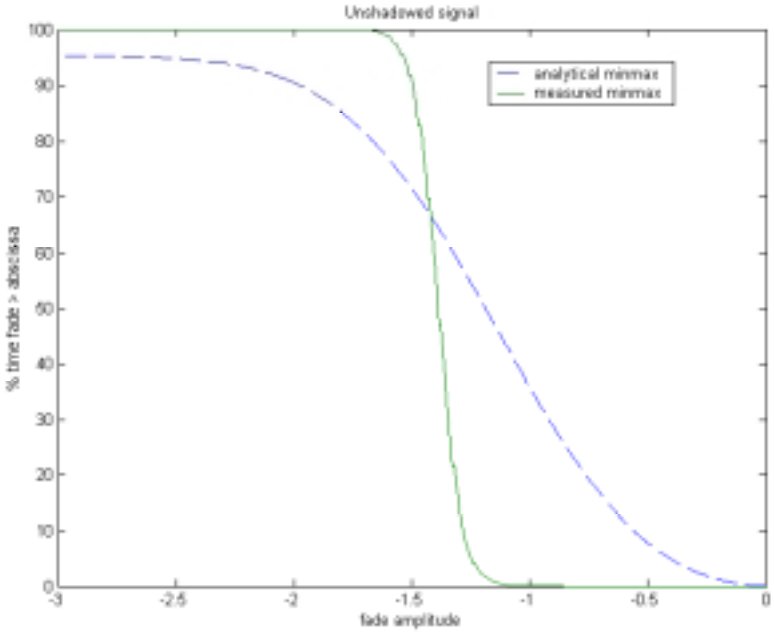

Figure 6.1-12 CDF of the measured signal and best fit analytical CDF using the MinMax constant extraction method for Route11bisNORTH2, Roll satellite, without AGC, for the unshadowed data set.

6.1.2.3 New Model for the Unshadowed Data Set for the non-AGC Measurements

As seen in Section 6.1.2.2, the Ricean model does not yield predictions that agree with measurements for unshadowed propagation in the non-AGC case. Because the AGC is turned off, and we do not have the phase information to remove the mean of the signals, the measured signals behave as if the 0 dB LOS was removed. Consequently, a new model was developed to represent the unshadowed signal. The idea of the new model is to model the unshadowed data set with another VS distribution. Essentially, the new VS model treats the unshadowed signal as a very slightly vegetatively shadowed signal. Hence, the mean of the lognormal distribution is expected to be positive, since the unshadowed signal experiences less fading than the shadowed data set. Also, its standard deviation is expected to be much smaller than in the shadowed case, since the unshadowed propagation is characterized by small variations of the signal amplitude.

This new model is based on two different VS distributions for shadowed and unshadowed data sets. The MATLAB routine designed to extract the constants for this

new VS model is 'Testminmax2'. It was tested on the Route 114 measurements, without AGC. The constants extracted with the MinMax method for each data set are summarized in Table 6.1-3 for Roll satellite and Table 6.1-4 for Rock satellite. In Figure 6.1-13, one can see that for Route114EAST1, the best-fit analytical CDF corresponding to the new VS model matches the CDF of the measured unshadowed signal much better than the best-fit analytical CDF derived with the Ricean model. At the same time, the statistics of the simulated signal are improved, as can be seen in Figures 6.1-14 to 6.1-16. The combination of the new VS model and the Gaussian repartition of the signal (see Section 3.3.2.2) gives secondary statistics that are closer to the statistics of the measured signal, as shown in Figures 6.1-15 and 6.1-16. However, the statistics of the signal simulated with the new VS model remain unsatisfying. Consequently, this new model was not further investigated, and not implemented into PROSIM.

Table 6.1-3 Propagation constants for Route 114 measurements, without AGC, Roll satellite, extracted with the MinMax method, for the new model.

	S (%)	**Unshadowed data set**			**Shadowed data set**		
		$\overline{K}$ (dB)	μ (dB)	σ (dB)	$\overline{K}$ (dB)	μ (dB)	σ (dB)
Route114EAST1	49.4280	26.3	1.8633	0.4476	16.6	-3.3310	4.0561
Route114EAST2	35.5693	27.2	1.3584	0.3981	19	-4.4014	4.7454
Route114EAST3	14.8285	28.7	0.3040	0.4651	17.1	-2.7072	3.5587
Route114WEST1	3.6856	27.8	0.0822	0.4182	30	-1.9523	2.6712
Route114WEST2	23.5853	25.9	0.6628	0.3612	15.8	-3.5720	4.3675
Route114WEST3	35.4456	24.6	0.8759	0.4869	15.6	-2.5317	3.5285

Table 6.1-4 Propagation constants for Route 114 measurements, without AGC, Rock satellite, extracted with the MinMax method, for the new model.

	S (%)	**Unshadowed data set**			**Shadowed data set**		
		$\overline{K}$ (dB)	μ(dB)	σ(dB)	$\overline{K}$ (dB)	μ(dB)	σ(dB)
Route114EAST1	60.8331	22.5	2.5228	0.6223	17.1	-3.1473	4.2597
Route114EAST2	49.0886	22.7	2.0746	0.4561	19.3	-4.0351	4.5587
Route114EAST3	25.6771	25.3	0.5008	0.5725	15.1	-2.3572	3.6116
Route114WEST1	13.8502	25.4	0.2457	0.5335	15.9	-2.3538	3.3007
Route114WEST2	41.2961	23	1.4769	0.4646	17.5	-3.7829	4.5204
Route114WEST3	48.6331	23.5	1.6024	0.6409	16	-3.0295	4.1407

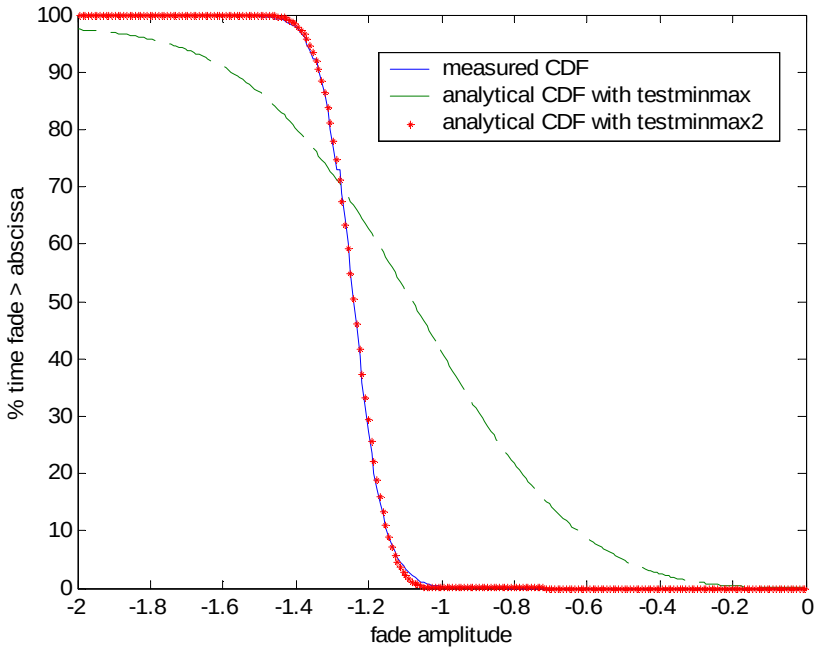

Figure 6.1-13 CDF of the measured signal, best fit analytical Ricean model CDF and best fit analytical VS model CDF for Route114EAST1, Roll satellite, without AGC, unshadowed data set. The new VS model fits better to the unshadowed propagation data than the Ricean model.

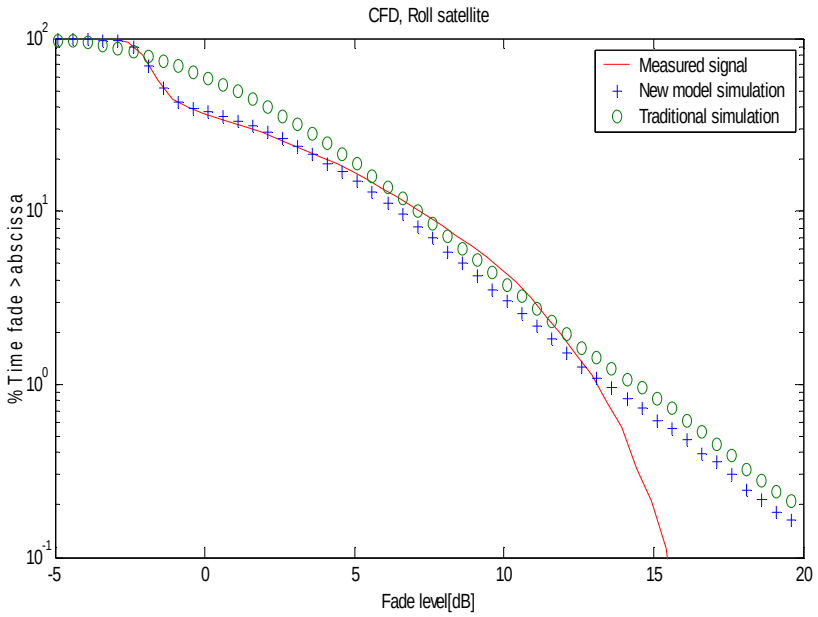

Figure 6.1-14 Cumulative Fade Duration CFD of measured signal, traditional PROSIM simulated signal and new VS model PROSIM simulated signal for Route114EAST1, September 1 measurements, without AGC, Roll satellite.

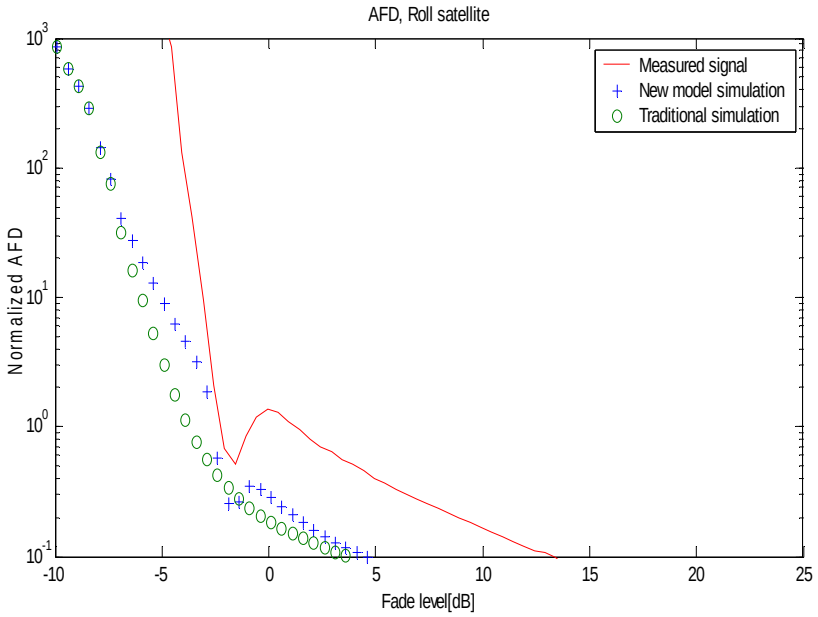

Figure 6.1-15 AFD of measured signal, traditional PROSIM simulated signal and new VS model PROSIM simulated signal for Route114EAST1, September 1 measurements, without AGC, Roll satellite.

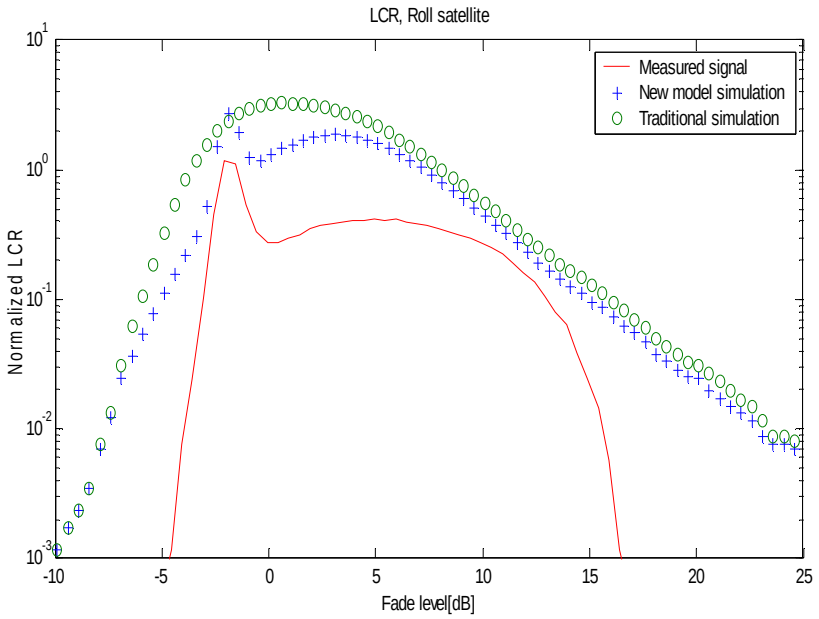

Figure 6.1-16 LCR of measured signal, traditional PROSIM simulated signal and new VS model PROSIM simulated signal for Route114EAST1, September 1 measurements, without AGC, Roll satellite.

6.2 Fade Correlation Study using Two Satellite Data

6.2.1 *Description of the Problem*

The objective of this section is to examine the correlation of the fading events between the signals received simultaneously from Roll and Rock. Roll covers the East coast while Rock is stationed over the West coast. The direction of the vehicle travel has an impact on the correlation of the shadowing events; when the vehicle is traveling in the East/West direction, then a shadowing event disturbing the signal received from Roll will also likely affect the signal received from Rock, as shown in Figure 6.2-1. In fact, the shadowing events are aligned with the satellite signals. On the other hand, when the vehicle is traveling in the North/South direction, the signals received from Rock and Roll may not undergo the same fading, since the signals may come from different sides of the road. Thus, no correlation is expected. Figure 6.2-2 illustrates the North/South case.

In case of the strong correlation, both signals are lost during the fading events. The XM Radio system uses information stored in a buffer to compensate for the loss of the signal. However, if the buffer size is too small, it will not be long enough to compensate for the signal loss. The information is lost and the XM Radio user loses his/her favorite channel, temporarily. Hence, it is important to make sure that the buffer is long enough to compensate for the correlation length of the fading.

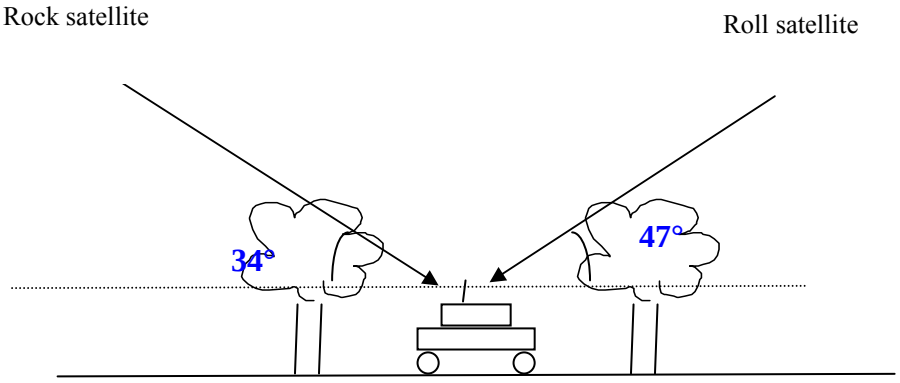

Figure 6.2-1 East/West traveling direction: the same shadowing events affect both Roll and Rock signals. High correlation is commonly encountered.

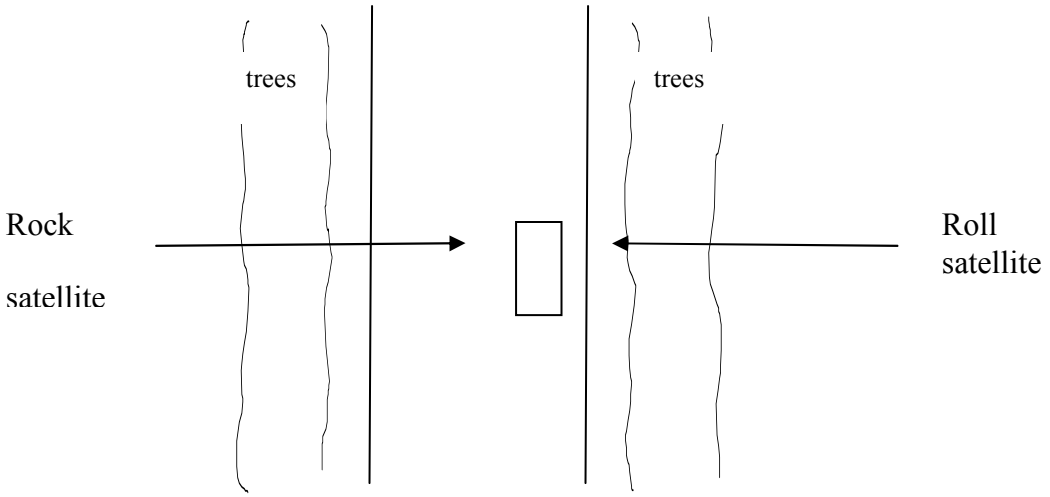

Figure 6.2-2 Diagram of top view of highway situation for North/South traveling direction. The shadowing events are different for the signals from the two satellites and no correlation is expected between the two signals.

6.2.2 *Results of the Fading Correlation Study*

In the East/West direction of travel, the shadowing events are expected to be correlated, which can lead to the loss of the signal for the XM Radio user. The study is performed using the different measurements conducted on Route 11 and Route 114, as well as the downtown Roanoke measurements, all East/West oriented. Moreover, the study is limited to the non-AGC measurement. Indeed, the AGC compensates for fading events; each time the signal goes below a certain threshold, it is enhanced. However, the procedure of enhancement is not clearly defined, so that the enhancements cannot be predicted. So, when looking at the amplitude of the signals for simultaneous received signals, it seems that some shadowing events are compensated differently from one satellite link to the other. In most cases, the simultaneous shadowed signals do not appear the same, since the AGC enhances the signal amplitudes more or less 'randomly'.

Hence, to obtain correlation results, the AGC is removed. The observation of the shadowing events then confirms the idea of a strong fading correlation for East/West

travel. In all cases, whenever the Roll signal undergoes a deep fade, Rock undergoes a fade with the same characteristics.

For each PROSIM scenario without AGC, a typical fading event was selected. It is important to remember that, for the whole correlation study, signal processing was performed on the real signal amplitude in volts, and not in dB values. Moreover, the shadowing events are converted to the space domain in order to remove the impact of the vehicle speed on the correlation length.

The first step in the data processing is to normalize the signal relative to the LOS component, so that the unshadowed portions of the signal have a mean of unity. Then, the unshadowed component of the signal is not relevant for the fading correlation study. Thus, unity is subtracted from the amplitude of the total normalized signals, so that the impact of the LOS component is limited.

Once the signals have been normalized and the LOS has been removed, they are correlated, and the correlation length is computed. In this study, the correlation length Lc is defined as the traveled distance for which the correlation falls to half its maximum value, according to

$$Lc = dist(\max(cor)/2) - dist(\max(cor)) \qquad (6.2\text{-}1)$$

where 'dist' is the array of the distance traveled and 'cor' is the correlation.

The MATLAB function created to compute the correlation length is 'correlation2'. The user can access the correlation study from PROSIM. Every time the user chooses to run a non-AGC scenario, the correlation is computed and the results presented in a MATLAB figure similar to Figure 6.2-3.

The results of the correlation study are given Table 6.2-1. For each PROSIM scenario, a shadowing event is selected and the corresponding correlation length is computed. It becomes then easy to deduce the buffer size required to compensate for the

fading. Since the car was traveling at 40 mph, 30 mph or 15 mph for each measurement, the buffer size in second is the ratio of the correlation length and the vehicle speed in m/s. Hence,

$$buff(s) = \frac{correlation(m)}{speed(m/s)} \tag{6.2-2}$$

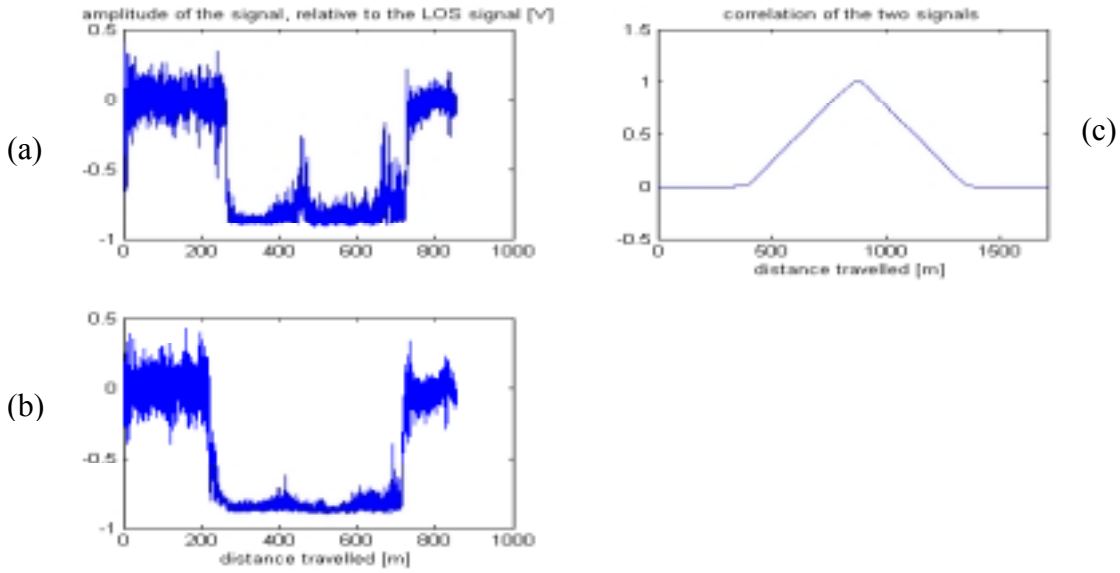

Figure 6.2-3 Correlation results for Route11SOUTH2, without AGC: (a) typical shadowing event for the signal received from Roll, (b) shadowing event for the signal received from Rock, simultaneous to the signal received from Roll in (a),

(c) Correlation of the simultaneous shadowing events of (a) and (b).

Table 6.2-1 non-AGC PROSIM scenarios with East/West direction of travel, correlation results: selected shadowing events, corresponding shadowing event length, correlation distance, and required buffer size to compensate for the loss of the signal.

	Typical shadowing interval	Typical shadowing event length (m)	Correlation distance (m)	Corresponding required buffer length (s)
Route114EAST1	200-400 m	200	72	4.0273
Route114EAST2	580-655 m	75	23.88	1.3357
Route114EAST3	350-380 m	30	9.46	0.5291
Route114WEST1	1455-1480 m	25	7.33	0.41
Route114WEST2	1150-1230 m	80	27.55	1.5410
Route114WEST3	680-780 m	100	42.55	2.38
Route11NORTH1	740-1000 m	260	111.63	6.2441
Route11NORTH2	1000-1160 m	1160	87.36	4.8865
Route11SOUTH1	110-145 m	35	261.63	14.6344
Route11SOUTH2	430-480 m	50	248.18	13.8820
Route11bisNORTH1	300-650 m	350	38.69	2.1641
Route11bisNORTH2	300-800 m	500	86.26	4.825
Route11bisSOUTH1	600-1000 m	400	12.87	0.7199
Route1bisSOUTH2	700-1200 m	500	15.97	0.8933
SALEMStr	20-80 m	60	14.55	2.1702
FRANKLINStr	250-320 m	70	11.20	1.6709
CHURCHStr	40-60 m	20	14.94	2.2278

In case of North/South direction of traveling, the signals received from the satellites are not expected to experience the same shadowing events, as shown in Figure 6.2-2. So, the signals should be uncorrelated and the statistics of the signals should be different for each satellite. These ideas are confirmed from the measurements along Route 723, North/South oriented. Figure 6.2-4 presents the amplitude of the signals received from both satellites for Route723NORTH, whereas Figures 6.2-5 to 6.2-7 show their statistics. It is obvious from Figure 6.2-4 that the two signals do not experience the

same shadowing events; the statistics of the signals Figure 6.2-5 to 6.2-7 confirms the idea that the two signals are received through two totally different propagation channels.

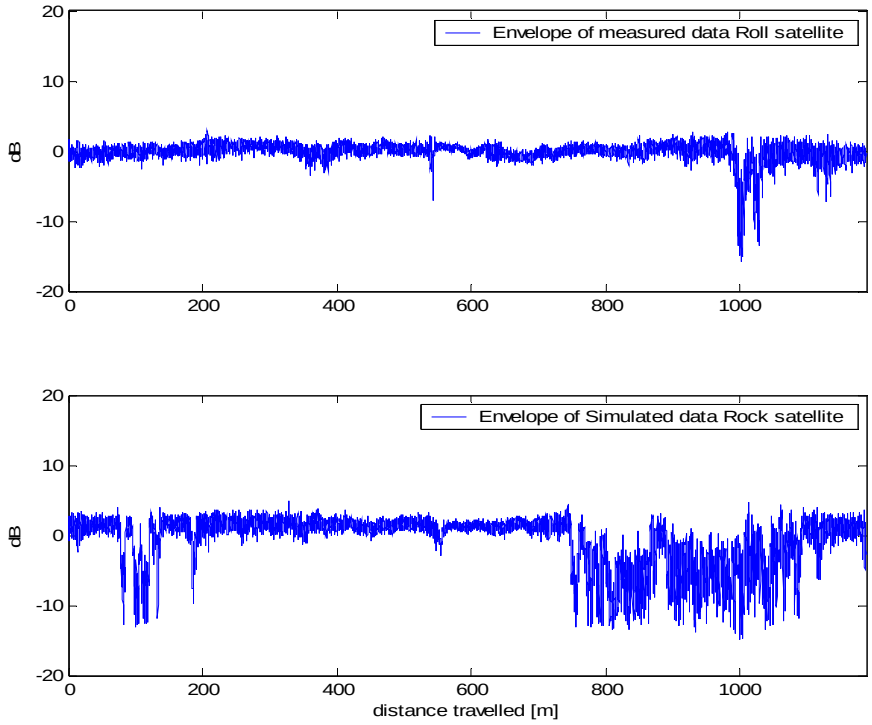

Figure 6.2-4 Route 723 measurements, North direction, without AGC: amplitude of the signals received from Roll and Rock satellites versus distance traveled.

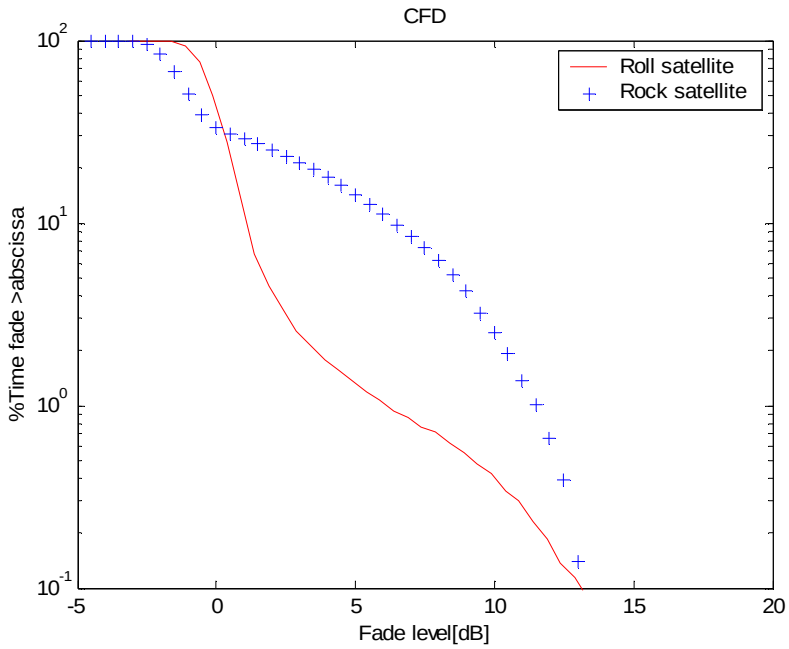

Figure 6.2-5 Cumulative Fade Duration CFD for Route 723 measurements, North direction, without AGC, for Roll and Rock satellite.

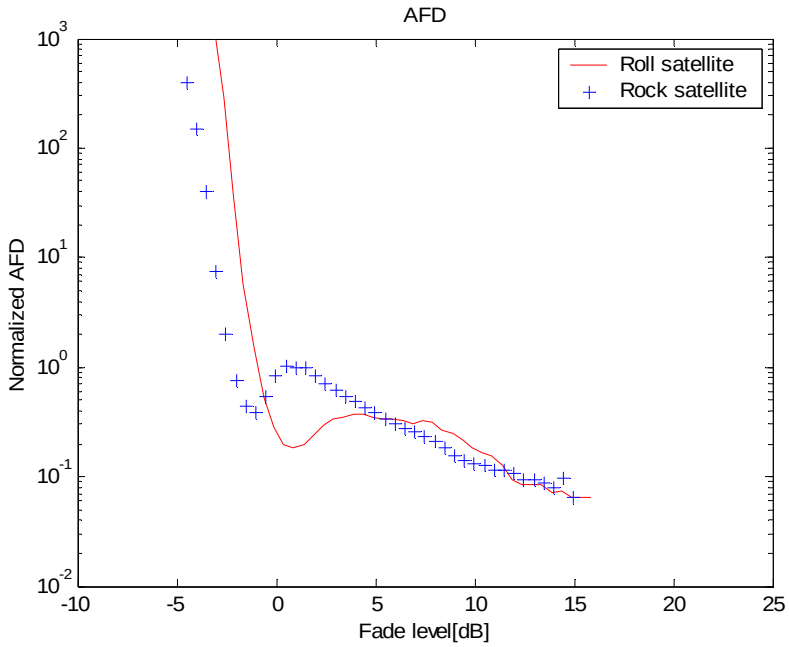

Figure 6.2-6 AFD for Route 723 measurements, North direction, without AGC, for Roll and Rock satellite.

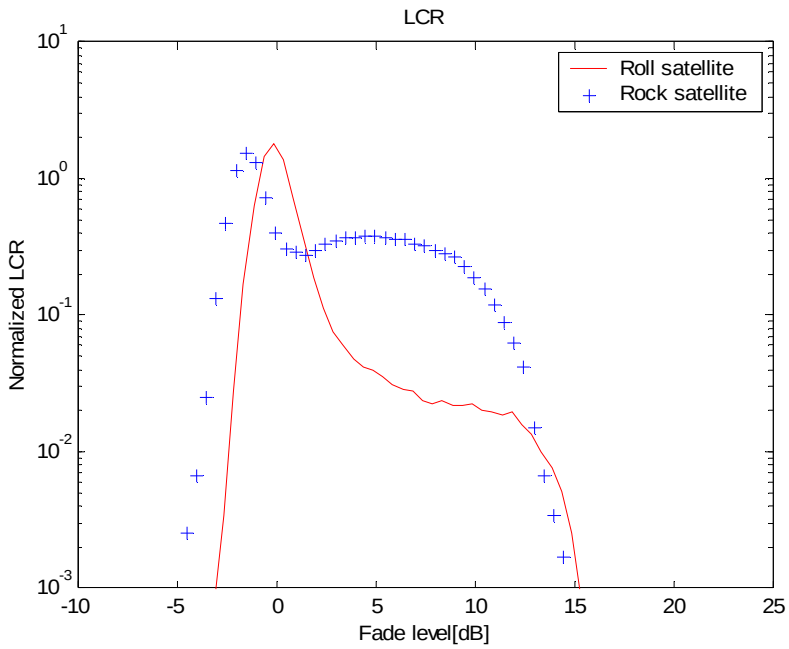

Figure 6.2-7 LCR for Route 723 measurements, North direction, without AGC, for Roll and Rock satellite.

6.3 Near-far effects of North/South Direction of Travel

The measurements for the North/South direction of travel on Route 460 and Route 723, described Section 4.3.2, are useful to study the near-far effect of the shadowing on the received signals. When the vehicle travels close to the tree lane, the received signal is expected to experience more tree attenuation than if the vehicle travels one-lane away from the tree line, as illustrated in Figure 6.3-1. For example, when the vehicle travels towards South, the signal received from Rock is a 'near' vegetation signal, whereas when the vehicle travels towards North, the Rock signal is a 'far' from vegetation signal, as shown in Figure 6.2-2 in the previous section.

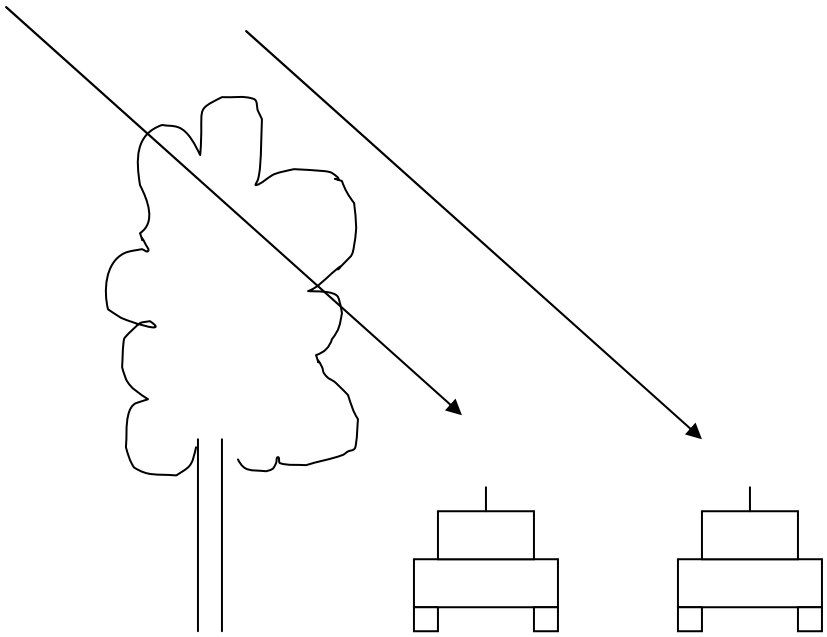

Figure 6.3-1 Example of the near-far roadside tree attenation: when the vehicle travels far from the tree line, the received signal is expected to experience less fading.

In order to study the near-far effects of tree attenuation, one should remember that measurements of the signals were performed in both North and South directions for the two satellites. Since the vehicle was traveling in opposite directions for each run along Route 723, the signals are not acquired in the same spatial order: the beginning of the record for Route723SOUTH corresponds to the end of the record for Route723SOUTH. Consequently, one of the records was read (and displayed in Figure 6.3-2 (b)) in reverse (that is from the end to the beginning) to ensure a spatial matching of the shadowing events. Figure 6.3-2 and 6.3-3 gives typical results for Route 723 measurements, for the Rock signal. As expected, the plot of the Cumulative Fade Duration shows that the 'South' signal, corresponding to the 'near' vegetation signal, experiences more fading than the 'North' signal. In the same way, the average fade duration of the 'South' signal is most of the time higher than for the 'North' signal, indicating longer shadowing events. Also, the level crossing rate for high level of shadowing is higher for the 'South' signal than for the 'North' signal. These results are confirmed by the plot of the amplitude of the

signals in Figure 6.3-2, where one can notice that the major fade in the first 500 meters of the records are deeper for the 'South' signal than for the 'North' signal. However, the statistics of the signals remain very similar. Since Route 723 is a 2-lane road, the 'far' from vegetation signals are still close to the tree line. The near-far effects analysis is limited by the absence of 4-lanes roads North/South oriented with significant shadowing events in the Blacksburg area.

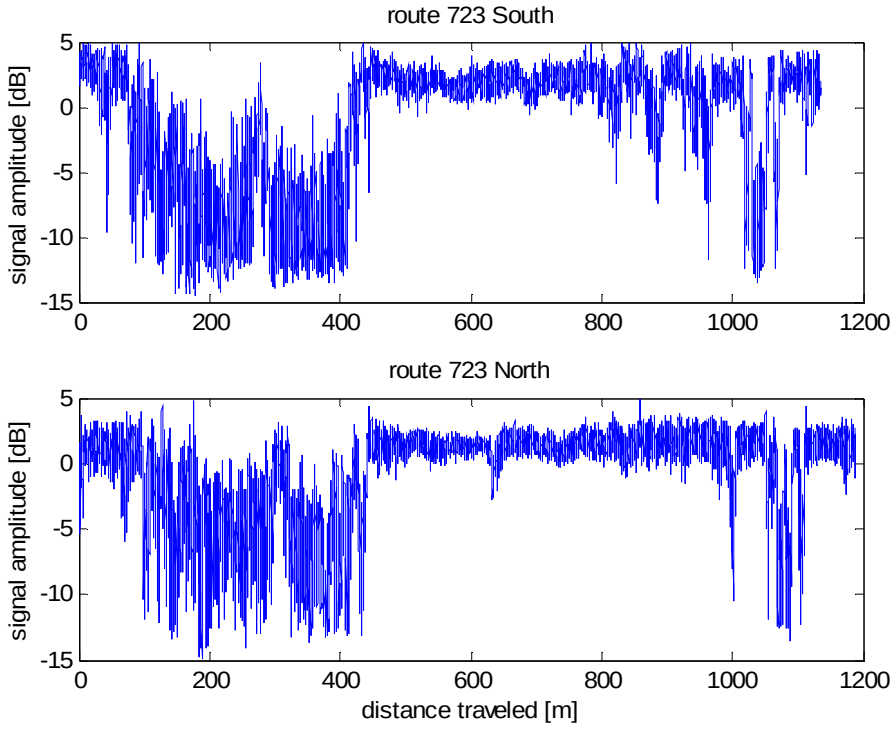

Figure 6.3-2 Route 723 measurements, without AGC: comparison of the signal amplitude when the vehicle travels (a) towards South (route 723 South signal, 'near' vegetation) or, (b) towards North (route723 North signal, 'far' from vegetation). Note that the route723 North signal is displayed in reverse.

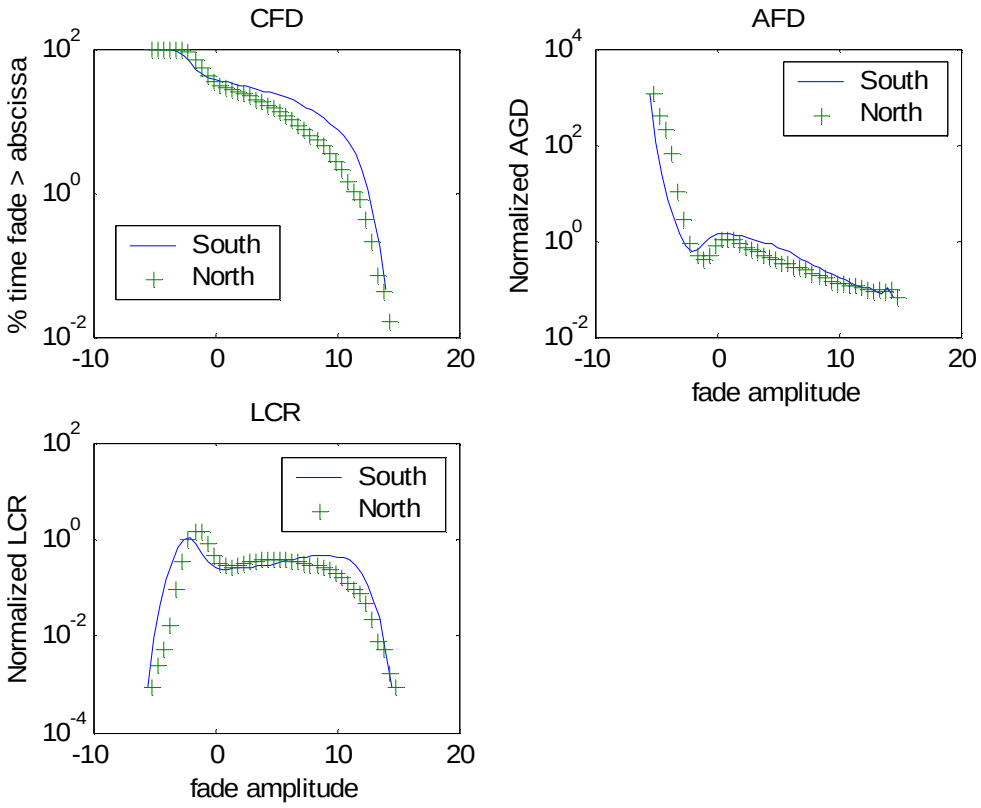

Figure 6.3-3 Statistics of the Rock signals for Route 723 measurements: comparison of the CDF, AFD and LCR when the vehicle travels towards South ('near' vegetation signal) or towards North ('far' from vegetation signal).

The measurements along Route 723 confirms the intuitive result that the received signal experiences more fading when the car travels close to the vegetation. However, additional measurements should be collected on 4-lane North/South oriented roads to further investigate the near-far propagation effects.

Chapter 7

Conclusion and Recommendations

A software propagation simulator for Land Mobile Satellite System, PROSIM, was described. PROSIM was developed in 1998 by Suh and Stutzman [15]. The original contribution to PROSIM from this research is the implementation of a new Gaussian method to combine the shadowed and unshadowed data sets into the total simulated signal. Initially validated for 870 MHz signals, PROSIM was adapted to the XM Radio Digital Audio Radio Satellite (DARS) system operating at 2.33 GHz, and validated using an analytical model and using measured XM Radio signals for various propagation environments. For those cases where the receiver AGC is applied, the simulator produces statistical results that agree well with the measured XM Radio signals, for both primary and secondary statistics. However, when the AGC is turned off, the secondary statistics do not match anymore and it appears that the Ricean model for unshadowed propagation may no longer be valid. The fact that the XM Radio system operates with two satellites permitted studies of signal correlation for the dual satellite system. The fading correlation between the two satellite signals was examined in the non-AGC case for East/West directions of travel. It was found that high levels of fading correlation exist in the case of East/West direction of travel. However, when the vehicle travels on a North/South oriented road, no correlation is expected, because the signals do not experience the same shadowing events. Finally, the near-far effects of road-side tree attenuation in the North/South direction of travel were studied and it was determined that the received signal experiences more fading when the car travels close to the vegetation.

Further investigation into the non-AGC case, and the unshadowed signal modeling could improve the accuracy of PROSIM for certain cases. Further investigation of the correlation issue could be also useful; maybe the case-by-case correlation study could be used to develop a model.

The measurement system could be improved by adding filters in the receiving system to ensure for the respect of the Nyquist criteria. The signal was sampled at 2 kHz; hence, filters with a 1 kHz bandwidth around the second IF frequencies should be added

to ensure that the acquired signals are free of noise. Then, additional measurements could be made to obtain extended results about the near-far effect of road-side tree attenuation. Specifically, some measurements in a shadowed environment for a 4-lane road North/South oriented would be helpful.

Finally, some efforts should be conducted to implement a third propagation state into PROSIM to account for urban environment propagation.

References

[1] W. L. Stutzman, “Polarization in Electromagnetic Systems,” Artech, Boston, 1992.

[2] W. J. Vogel and E. K. Smith, “Propagation Considerations in Land-mobile Satellite Transmission,” MSAT-X Report No. 105, NASA-JPL, Pasadena, CA.

[3] V. Jamnejad, “Ground Multipath in TOPEX’s Precision Orbit Determination Tracking System,” JPL Interoffice Memorandum 3365-84-003, Jet Propulsion Lab., Pasadena, CA, Jan. 9, 1985.

[4] P. Beckmann and A. Spizzichino, “The Scattering of Electromagnetic Waves From Rough Surfaces,” Pergamon Press, New York, 1963.

[5] R. L. Campbell and R. Estus, “Attenuated Direct and Scattered Wave Propagation on Simulated Land-mobile Satellite Service Paths in the Presence of Trees,” Proceedings of the Mobile Satellite Conference, JPL Publication 88-9, Pasadena, CA, May 3-5, 1988.

[6] P. Beckmann, “Probability in Communication Engineerings,” Harcourt, Brace & World, NY, 1967.

[7] C. Loo, “A Statistical Model for a Land Mobile Link,” IEEE Trans. Vech. Technol., vol VT-34, pp-122-127, Aug.1985.

[8] J. Aichison and J. A. C. Brown, “The lognormal distribution,” CambridgeUniversity press, London, 1957.

[9] W. T. Smith and W. L. Stutzman, “Statistical Modeling for Land Mobile Satellite Communications,” Virginia Tech Report EE Satcom 86-3

[10] E. Lutz, et al., “The Land Mobile Satellite Communication Channel-Recording, Statistics, and Channel Model,” IEEE Trans. On Vehicular Technology, vol. 40, no.2, pp.375-386, May 1991.

[11] W. S. Bradley and W. L. Stutzman, “Propagation Modeling For Land Mobile Satellite Communications,” Virginia Tech Report EE Satcom 85-3

[12] W. C. Jakes, “Microwave Mobile Communication,” John Wiley & Sons, NY, 1974.

[13] R. M. Barts and W. L. Stutzman, “Statistical Modeling and Simulation of Mobile Satellite Propagation,” Virginia Tech report EE Satcom No. 88-5

[14] R. G. Schmier and C. W. Bostian, “Fade Durations in Satellite-Path Mobile Radio Propagation,” Virginia Tech Report EE Satcom 86-5

[15] S. Y. Suh and W. L. Stuzman, "A land Mobile Satellite Communications Propagation Simulator," Space Communications 15 (1998), pp 33-53.

[16] Mathworks Inc., "MATLAB Manual," ver 4.2-c

[17] M. C. Jeruchim, P. Balaban and K. S. Shanmugan, "Simulation of Communication Systems," Plenum Press, New york

[18] J. Goldhirsh and W. J. Vogel, "Roadside tree attenuation measurements at UHF for land-mobile satellite systems," IEEE Trans. on Antennas and Propagation, vol. AP-86, Jan. 1987.

[19] Federal Communications Commission, Auction 15: Digital Audio Radio Satellite System. http://wireless.fcc.gov/auctions/15/factsheet.html

[20] Sirius Satellite Radio, www.siriusradio.com

[21] XM Radio, www.xmradio.com

Vita

Laure Mousselon was born in Clamart, France on October 26, 1980. She graduated in 1997 from Victor Hugo High School in Caen, France. She attended the preparatory classes program for French Engineering Schools at Ecole Privée Sainte Geneviève in Versailles, France, from 1997 to 1999. She did her undergraduate studies at Ecole Supérieure d'Electricité, Supélec, in Rennes, France. Then, in August 2001, she came to Virginia Tech, where she worked for 18 months as a research assistant for the Virginia Tech Antenna Group. In December 2002, she will receive the Master of Science in Electrical Engineering degree from Virginia Tech as well as her Engineering Diploma from Supélec.